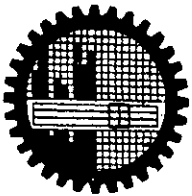


A NUMERICAL STUDY ON THE MIXING OF HYDROGEN IN SUPERSONIC AIR STREAM



SHAKIL AHMED



DEPARTMENT OF MECHANICAL ENGINEERING
BANGLADESH UNIVERSITY OF ENGINEERING & TECHNOLOGY
DHAKA, BANGLADESH



#94972#

at

A NUMERICAL STUDY ON THE MIXING OF HYDROGEN IN SUPERSONIC AIR STREAM

BY

SHAKIL AHMED

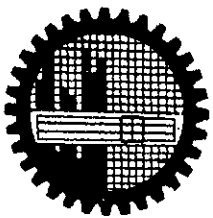
B.Sc. ENGG. (MECH.)

A Thesis

Submitted to the Department of mechanical Engineering in partial fulfillment
of the requirements

for

the degree of Master of Science in Mechanical Engineering



**DEPARTMENT OF MECHANICAL ENGINEERING
BANGLADESH UNIVERSITY OF ENGINEERING & TECHNOLOGY
DHAKA, BANGLADESH**

MARCH 2001

RECOMMENDATION OF THE BOARD OF EXAMINERS

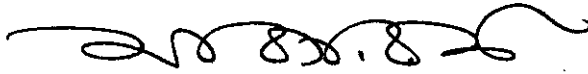
The board of examiners hereby recommends to the Department of Mechanical Engineering, BUET, Dhaka, the acceptance of this thesis, **“A NUMERICAL STUDY ON THE MIXING OF HYDROGEN IN SUPERSONIC AIR STREAM”**, submitted by Shakil Ahmed, in partial fulfillment of the requirements for the degree of Master of Science in Mechanical Engineering.

Chairman (Supervisor) :



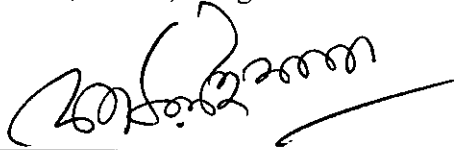
Dr. Mohammad Ali
Assistant Professor
Department of Mechanical Engineering
BUET, Dhaka, Bangladesh.

Member (Ex-officio) :



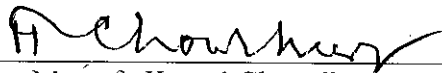
Dr. Md. Abdur Rashid Sarkar
Professor & Head
Department of Mechanical Engineering
BUET, Dhaka, Bangladesh.

Member :



Dr. A. K. M. Sadrul Islam
Professor
Department of Mechanical Engineering
BUET, Dhaka, Bangladesh.

Member (External) :



Dr. Mustafa Kamal Chowdhury
Professor
Department of Mathematics
BUET, Dhaka, Bangladesh.

CERTIFICATE OF RESEARCH

This is to certify that the work presented in this dissertation is the out come of the investigation carried out by the author under the supervision of Dr. Mohammad Ali, Assistant Professor, Department of Mechanical Engineering, Bangladesh University of Engineering & Technology (BUET), Dhaka, Bangladesh and that it has not been submitted anywhere for the award of any degree or diploma.



Dr. Mohammad Ali
Supervisor



Shakil Ahmed
Author



ACKNOWLEDGEMENT

The author would like to take this opportunity of expressing his heartfelt gratitude and indebtedness to his thesis supervisor Dr. Mohammad Ali, Assistant Professor, Department of Mechanical Engineering, BUET, Dhaka, for his valuable and continuous guidance, suggestions in the course of the present work; without which this entire project would be, but a failure.

The author feels grateful to Professor A. K. M. Sadrul Islam of Mechanical Engineering Department for his valuable suggestions from time to time, without which the thesis would be difficult.

Finally the author also thanks his colleagues, family and relatives, those who shared the troubles.

ABSTRACT

A numerical study on mixing of hydrogen injected into a supersonic air stream has been performed by solving Two-Dimensional full Navier-Stokes equations and a zero-equation algebraic turbulence model is used to calculate the eddy viscosity coefficient. The main objectives of this study are to increase the mixing efficiency and the flame holding capability of a supersonic combustor.

The mixing characteristics for several main flow (air) and side flow (injection of hydrogen) inlet parameters have been studied. The performance of combustor has been investigated by varying (i) the distance of injector position from left boundary (ii) the injector angle (iii) the air stream angle and (iv) the Mach number of the injecting hydrogen. For varying injector distance the results show that the configuration of small distance of injector position has high mixing efficiency but is not good for flame holding capability. The configuration for very long distance has lower mixing efficiency. The moderate distance of injector position can evolve large and elongated upstream recirculation which might be activated as a good flame holder.

For varying injecting angle investigation showed that small (30°) and large (120° & 150°) injecting angle have no significant upstream recirculation. Upstream recirculation is dominant for injecting angle 60° and 90° . Perpendicular injection increases both the mixing efficiency and flame holding capability. Small injecting angle and very large injecting angle have good flame holding capability but not mixing efficiency.

For the variation of air stream angle, investigation showed that small angle (60°) increases the mixing efficiency from injector position to downstream but in upstream mixing does not occur. Airstream angle (120°) has better mixing efficiency than (90°) but does not have good flame holding capability.

Lastly the Mach number of the injecting hydrogen was changed as 0.7, 1.0 and 1.3. The Mach number 1.3 increases both the mixing efficiency and flame holding capability. So injecting hydrogen having Mach number 1.3 might act as a good flame holder and become efficient in mixing.

CONTENTS

	Page
Title	II
Certificate of Approval	III
Certificate of Research	IV
Acknowledgement	V
Abstract	VI
Contents	VII
List of Figures	IX
List of Tables	XI
Nomenclature	XII

CHAPTER-I

INTRODUCTION

1.1	General	1
1.2	Background	2
1.3	Objectives	5

CHAPTER-II

FLOWFIELD MODEL OF SUPERSONIC MIXING

2.1	Governing Equations	6
2.2	Calculation of Temperature	9
2.3	Transport Coefficients	10
2.4	Numerical Scheme	12
2.5	Boundary Conditions and Convergence Criterion	13
2.6	Use of Turbulence Model	13

CHAPTER-III

RESULTS AND DISCUSSION

3.1	Introduction	15
3.2	Flow Field Description and Numerical Parameter	15
3.3	Effect of Injector Distance	16
3.4	Effect of Injecting Angle	20
3.5	Effect of Airstream Angle	23
3.6	Effect of Mach No. of the Injecting Hydrogen	26

CHAPTER-IV

CONCLUSION

4.1	Summary of the Study	30
4.2	Recommendations for Future Study	32



REFERENCES	76
-------------------	----

List of Publications (Related to this thesis)	80
--	----

LIST OF FIGURES

	Page
Fig. 3.1 (a~d) Schematic with Numerical Parameters	33
Fig. 3.1 (e) Grid System of the Calculation Flowfield	35
Fig. 3.2 (a~e) Velocity vector near injector (Case1~5)	36
Fig. 3.3 (a~e) Mole fraction contour of Hydrogen (Case1~5)	38
Fig. 3.4 Mixing efficiency along the length of physical model (Case1~5)	41
Fig. 3.5 Diffusion of Hydrogen at 0.08m from left wall (Case1~5)	41
Fig. 3.6 Pressure distribution at 0.08m from left wall (Case1~5)	42
Fig. 3.7 (a~e) Pressure (Pa) contour (Case1~5)	42
Fig. 3.8 (a~e) Temperature (K) contour (Case1~5)	45
Fig. 3.9 (a~e) Velocity vector near injector (Case6~10)	47
Fig. 3.10 (a~e) Mole fraction contour of Hydrogen (Case6~10)	50
Fig. 3.11 Mixing efficiency along the length of physical model (Case6~10)	52
Fig. 3.12 Diffusion of Hydrogen at 0.08m from left wall (Case6~10)	53
Fig. 3.13 Pressure distribution at 0.08m from left wall (Case6~10)	53
Fig. 3.14 (a~e) Pressure (Pa) contour (Case6~10)	54
Fig. 3.15 (a~e) Temperature (K) contour (Case6~10)	56
Fig. 3.16 (a~c) Velocity vector near injector (Case11~13)	59
Fig. 3.17 (a~c) Mole fraction contour of Hydrogen (Case11~13)	60
Fig. 3.18 Mixing efficiency along the length of physical model (Case11~13)	62
Fig. 3.19 Diffusion of Hydrogen at 0.08m from left wall (Case11~13)	62
Fig. 3.20 Pressure distribution at 0.08m from left wall (Case11~13)	63
Fig. 3.21 (a~c) Pressure (Pa) contour (Case11~13)	63
Fig. 3.22 (a~c) Temperature (K) contour (Case11~13)	65
Fig. 3.23 (a~c) Velocity vector near injector (Case14~16)	66
Fig. 3.24 (a~c) Mole fraction contour of Hydrogen (Case14~16)	68
Fig. 3.25 Mixing efficiency along the length of physical model (Case14~16)	69
Fig. 3.26 Diffusion of Hydrogen at 0.08m from left wall (Case14~16)	70
Fig. 3.27 Pressure distribution at 0.08m from left wall (Case14~16)	70

LIST OF FIGURES

	Page
Fig. 3.28 (a~c) Pressure (Pa) contour (Case14~16)	71
Fig. 3.29 (a~c) Temperature (K) contour (Case14~16)	72

LIST OF TABLES

		Page
Table 2.1	Coefficients of Thermodynamic Polynomials	74
Table 2.2	Constants used in Transport Equations	74
Table 3.1	Calculation Summary	75

NOMENCLATURE

<u>Symbol</u>	<u>Meaning</u>	<u>Unit</u>
b	width of injector	mm
h	height of backward-facing step	mm
C	molar concentration	Mole/m ³
c	sound speed	m/s
C_p	specific heat at constant pressure	J/(kg. K)
D_{iml}	molecular diffusion coefficient of i-th species	m ² /s
D_{it}	turbulent diffusion coefficient of i-th species	m ² /s
D_{ij}	binary-diffusion coefficient for species i and j	m ² /s
E	total energy	J/m ³
F	flux vector in x-direction	
F^\wedge	transformed flux vector in ξ -direction	
f_H	local mass fraction of hydrogen	
G	flux vector in y-direction	
G^\wedge	transformed flux vector in η -direction	
h	enthalpy	J/kg
J	transformation Jacobian	
J	number of grid points in x-direction	
JJ	maximum number of grid points in x-direction	
K	number of grid points in y-direction	
KK	maximum number of grid points in y-direction	
l	mixing length	m
M	Mach number	
m	mass flux of species	kg/s
p	pressure	Pa
q_c	energy flux by conduction	W/m ²
q_D	energy flux by diffusion	W/m ²
R	universal gas constant	J/(kg.mol.K)
S	Sutherland constant for viscosity	K
S'	Sutherland constant for thermal conductivity	K
T	temperature	K
T_ϵ	effective temperature	K
t	physical time	second
U	vector of conservative variables	
U^\wedge	transformed vector of conservative variables	
U	contravariant velocity in ξ -direction	
U_i	diffusion velocity of species i	m/s
u	horizontal velocity	m/s
V	contravariant velocity in η -direction	
v	Vertical velocity	m/s
W	molecular weight of species	gm/mol
x	horizontal Cartesian coordinate	m
Y	mass fraction of species	
y	vertical Cartesian coordinate	m

y	normal distance from bottom wall	m
z	mole fraction of species	
ξ	transformed coordinate in horizontal direction	
ψ	air stream angle	
η	Transformed coordinate in vertical direction	
η_m	mixing efficiency	
Φ	global equivalence ratio of fuel and oxidizer	
ϕ	local equivalence ratio of fuel and oxidizer	
θ	injecting angle	
ρ	mass density	kg/m ³
$\sigma_{x,y}$	normal stress	Pa
τ	shear stress	Pa
μ	coefficient of dynamic viscosity	kg/(m.s)
κ	thermal conductivity	W/(m. K)
Ω_D	diffusion collision integral	
$\sigma_{i,j}$	effective collision diameter	Å ^o
ω	vorticity	s ⁻¹

Superscript

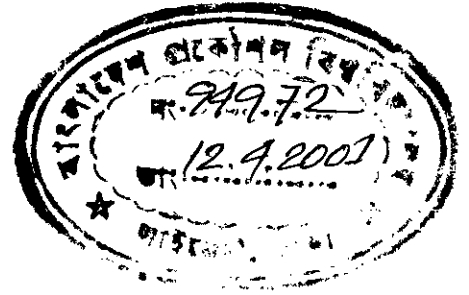
ns	number of species
0	standard state condition

Subscript

a	atmospheric condition
c	index for conduction
D	index for diffusion
i,j	index for species
l	laminar case
m	mixture
t	index for turbulence
v	viscous term
w	wall
x	horizontal direction
y	vertical direction
xy	reference plane
0	reference value, stagnation condition

CHAPTER-I

INTRODUCTION



1.1 General

Mixing of hydrogen in supersonic airstream and their combustion are very important in many engineering applications. Particularly, the fuel injection in both supersonic and hypersonic streams requires special attention for efficient mixing and stable combustion. Though a considerable number of researches have been carried out on mixing and combustion of fuel with supersonic air stream, still it faces many unsolved problems. The main problems that arise in this regard, concern mixing of reactants, ignition, flame holding, and completion of combustion. More investigations are required to overcome these problems. In fact, in supersonic combustion, high penetration and mixing of injectant with main stream is difficult due to their short residence time in combustor. In an experimental study, Brown et al. [1] showed that the spreading rate of a supersonic mixing layer decreased drastically with increasing free stream Mach number. A similar conclusion was drawn by Papamoschou et al. [2] on the basis of a theoretical analysis of shear-layers. Furthermore, they showed that the reduction in spreading rate correlated most closely with the convective Mach number, where convective Mach number is defined as the differential velocity normalized by the speed of sound. An independent linear stability theory analysis of Ragab et al. [3] reached the same conclusion. These investigations showed that difficulty exists in achieving a high degree of mixing in high Mach number flows. Therefore, it is necessary to investigate all the parameters that affect the mixing of hydrogen in supersonic airstream.

There exist several methods of fuel injection in the supersonic air stream. Perpendicular injection causes rapid mixing of injectant with main stream and is used to some degree at all flight Mach numbers to promote mixing and reaction, particularly in upstream portion of the combustor. Parallel injection is used when slow mixing process is desired, specially at lower speeds of space vehicles during which perpendicular injection may cause too rapid mixing

and combustion, and hence thermally choking the flow. I studied (i) the effect of change of injector position (ii) the effect of change of injecting angle (iii) the effect of change of air stream angle and (iv) the effect of change of mach number of the injector on mixing of hydrogen with air due to its wide application at the present stage.

1.2 Background

Both experimental and numerical investigations have been performed to analyze the mixing and combustion characteristics, and find out the means of increasing the mixing efficiency. In an experiment, Rogers [4] showed the effect of the ratio between jet dynamic pressure and free stream dynamic pressure on the penetration and mixing of a sonic hydrogen jet injected normal to a Mach 4 air stream. In similar flow arrangements, Kraemer et al. [5] found that the relative change in jet momentum (product of gap width, jet static pressure and injectants specific heat ratio) was directly proportional to the relative size between the flowfield disturbance and the upstream separation distance. The downstream injectant penetration height is directly proportional to the upstream separation distance, and, thus, the downstream mixing is dependent on the relative change in jet momentum. Similar conclusions were drawn by Holdeman [6] and Thayer III et al. [7]. Thayer III et al. [7] also found that the injectant concentration of the separated region was high at all conditions investigated. Heister et al. [8] conducted a calculation on the penetration and bow shock shape of a non-reacting liquid jet injected transversely into a supersonic cross flow. Mass and momentum balances were incorporated along the jet with and without the inclusion of mass loss due to droplet shedding. The predicted bow shock position agreed with the data and a correlation was obtained between mass loss, boundary layer thickness, recirculation and related parameters.

Catalano et al. [9] reported the measurements and computations for the turbulent jet discharging into a cross flow confined between two parallel plates. The authors concluded that the jet trajectory and the existence of opposite wall impingement were strongly dependent on the velocity ratio. Zakkay et al. [10] investigated experimentally the interactions of finite-span, transverse jet on a 7° cone with a Mach 5.8 stream. The authors

showed that along the plane of symmetry, the separated region upstream of the jet correlated well with the quasi 2-dimensional experiments in terms of the jet penetration height as the basic scale length. Thayer III [11] performed an experiment showing that the jet interaction flowfield depends markedly on the injectant molecular weight. About the effect of injectant molecular weight on mixing and penetration of normal jet, Torrence [12] performed an investigation and found that the decay of the maximum value of concentration with axial position was a strong function of injectant molecular weight and the effect on vertical penetration was small. The rate of decay in the far downstream of the injector was similar for all injectants.

Rodriguez et al. [13] showed by his experiment that the mixing zones created by the shock interaction with a discontinuous interface thickened due to turbulent diffusion and became wider than the continuous interface after the second reshock. The separation phenomena of a turbulent boundary layer ahead of a forward-facing were observed by Zukoshi [14] in an experiment without injection. With secondary injection of a gas normal to a supersonic stream, Zukoshi and Spaid [15] investigated the flowfield around the injection port, selected the penetration height as a scaling parameter for correlation of the data. The correlation had some lack of similarity with the observed pressure data in the laminar boundary layer separation region and at the lower mach numbers in the reattachment region downstream of the injector. Weidner et al. [16] conducted a parametric study using staged, perpendicular fuel injectors. They studied the mixing of hydrogen by varying the distance between injectors and the fuel split (percentage of fuel injected per injector). Another numerical investigation on the mixing of side jet into a supersonic flow was performed by Takahashi et al. [17]. The numerical results were compared against the published [16] experimental data, noting that the adoption of higher-class model like a two-equation model was necessary for better prediction. Considering different calculation parameters, a similar flow situation was given by Spaid and Zukoshi [18] with an attempt to correlate the parameters.

Yokota et al. searched the enhancement of mixing by varying (i) the angle of a finite length slit (when slit length is smaller than the width of computational domain) [19] and (ii) slit aspect ratios [20]. Besides, Yokota et al. examined the effects of injection methods [21] and

the existence of pressure wave in the flow with the injection [22] on mixing and total pressure loss. Yoshida et al. [23] found out that the ignition of hydrogen injected transversely into the supersonic air stream occurred in the upstream separated region, and the bulk flame produced for downstream of the test section was not essential to the supersonic combustion. Crabb et al. [24] provided an extensive review of earlier works and reported the measurements of the velocity characteristics of a jet in crossflow encompassing the entire mixing region. They confirmed the double vortex characteristics of the downstream flow and demonstrated that it was associated with fluid emanating from the jet. The injector position is another important factor for mixing and combustion. By the numerical investigation of two-dimensional reacting Scramjet engine flowfields, Drummond et al. [25] found that the insufficient penetration of hydrogen caused by locating the injector 6.0 cm from the engine minimum cross section reduced the overall reaction in the upstream portion of combustor. They tried to move the injector further upstream (1.3-cm from the engine minimum cross section) which made the engine thermally choked due to severe disturbances produced by injector.

By applying Direct Simulation Monte Carlo (DSMC) method several investigations [26, 27] can be found in literature where Nakae et al. [26] showed that the characteristics of the mixing field agreed with other computed results and Obata et al. [27] found that raising the temperature of the injected hydrogen not only contributed to rapid ignition but also accelerated mixing and diffusion. A numerical study has been performed by Kumar et al. [28] about the techniques for enhancement of turbulence, the ultimate goal of which was to increase the mixing. They found that the wall-region disturbances propagate along the shock, resulting in oscillating shock, which then enhanced turbulence in the main flow. The effect of convective Mach number on the mixing in supersonic shear layer was observed by Guirguis [29]. The result showed the enhancement of mixing when the convective Mach number was reduced. Orth et al. [30] studied in details the interaction and penetration of a supersonic side jet in supersonic external flow both experimentally and numerically. The shape of the side jet was varied. The authors showed that the penetration could be increased by supersonic injection and was weakly affected by injection hole shape.

In detailed experimental investigation on the near field (defined as the region of the flow from the jet exit a distance of a few diameters downstream of this exit), Moussa et al. [31] found that the geometric configuration of the boundaries of jet exit plays an important role in the mixing and development process. Some characteristics on boundary layer and turbulence in mixing field were investigated by Andreopoulos et al. [32] and Andreopoulos [33].

In detailed study, several side flow and main flow inlet parameters were adopted to study the mixing of hydrogen with supersonic air. Recirculation has an important role to enhance mixing. Therefore, backward-facing step was used which can assist to increase the recirculation region in upstream of injector. The interaction between the main flow and injector causes a bow shock in front of the injector. As an expectation, the bow shock increases the temperature and pressure of the flowfield. However, behind the shock the pressure decreases which causes expansion of injecting jet plume and increases penetration. If the shock is steeper and produced at further upstream, there is a possibility for more expansion of injecting jet plume, and higher penetration of injectant. In this study, both the main flow and side flow inlet parameters were changed to see how they effect to increase the mixing efficiency and flame holding capability.

1.3 Objectives

In this research attention has been made on the physics and mixing and found out the enhancement of mixing efficiency by using different main flow and side flow inlet parameters. Though, the researchers paid their attention to the injection method and shape of injector exit to get higher mixing, no information is available about the effect of main flow and side flow inlet parameters which I have done here. Most of investigations on mixing of supersonic air stream with hydrogen have been conducted for mixing in non-reacting flowfield. As I am interested to see the flowfield characteristics and mixing efficiency I also conducted my study in non-reacting flowfield.

CHAPTER-II

FLOWFIELD MODEL OF SUPERSONIC MIXING

2.1 Governing Equations

The flowfield is governed by the unsteady, two-dimensional full Navier-Stokes and species continuity equations. The body forces are neglected. With the conservation-law form, these equations can be expressed by

$$\frac{\partial U}{\partial t} + \frac{\partial F}{\partial x} + \frac{\partial G}{\partial y} = \frac{\partial F_v}{\partial x} + \frac{\partial G_v}{\partial y} \quad (2.1)$$

Where

$$U = \begin{pmatrix} \rho \\ \rho u \\ \rho v \\ E \\ \rho Y_i \end{pmatrix}, \quad F = \begin{pmatrix} \rho u \\ \rho u^2 + p \\ \rho uv \\ (E + p)u \\ \rho Y_i u \end{pmatrix}, \quad G = \begin{pmatrix} \rho v \\ \rho uv \\ \rho v^2 + p \\ (E + p)v \\ \rho Y_i v \end{pmatrix}$$

$$F_v = \begin{pmatrix} 0 \\ \sigma_x \\ \tau_{xy} \\ \sigma_x u + \tau_{yx} v - q_x \\ -\dot{m}_x \end{pmatrix}, \quad G_v = \begin{pmatrix} 0 \\ \tau_{yx} \\ \sigma_y \\ \tau_{xy} u + \sigma_{yv} - q_y \\ -\dot{m}_x \end{pmatrix}$$

$$p = \sum_{i=1}^{ns} \rho_i R_i T = \sum_{i=1}^{ns} \rho_i \frac{R}{W_i} T, \quad (2.2)$$

$$\begin{aligned}
E &= \sum_{i=1}^{ns} \rho_i h_i - \sum_{i=1}^{ns} \rho_i \frac{R}{W_i} T + \frac{\rho}{2} (u^2 + v^2) \\
&= \sum_{i=1}^{ns} \rho_i C_{pi} T - \sum_{i=1}^{ns} \rho_i \frac{R}{W_i} T + \frac{\rho}{2} (u^2 + v^2)
\end{aligned} \tag{2.3}$$

$$\begin{aligned}
\sigma_x &= \lambda \left(\frac{\partial u}{\partial x} + \frac{\partial v}{\partial y} \right) + 2\mu \left(\frac{\partial u}{\partial x} \right), & \sigma_y &= \lambda \left(\frac{\partial u}{\partial x} + \frac{\partial v}{\partial y} \right) + 2\mu \left(\frac{\partial v}{\partial y} \right), \\
\tau_{xy} = \tau_{yx} &= \mu \left(\frac{\partial u}{\partial y} + \frac{\partial v}{\partial x} \right), & \lambda &= -\frac{2}{3}\mu
\end{aligned} \tag{2.4}$$

Mass diffusion occurs whenever there exists a gradient in the proportions of the mixture, i.e. a concentration gradient. Because of this gradient, there is a mass motion of species i in the opposite direction. If the velocity of this mass motion is U_i , called the diffusion velocity, the mass flux of species i is $\rho_i U_i$. This mass flux is given approximately by Fick's law [34] as

$$\dot{m} = \rho_i U_i = -\rho D_{iml} \nabla Y_i \tag{2.5}$$

Where r is the mixture density and D_{iml} is the molecular diffusion coefficient of species i for diffusion into the mixture. The density of mixture is determined from

$$\rho = \sum_{i=1}^{ns} \rho_i \tag{2.6}$$

Due to heat conduction, the flux of energy

$$q_c = -\kappa \nabla T \tag{2.7}$$

And due to diffusion, energy flux of all species at the point,

$$q_D = \sum_{i=1}^{ns} \rho_i U_i h_i \tag{2.8}$$

Therefore, the total energy flux (radiation is neglected),

$$q = -\kappa \nabla T + \sum_{i=1}^{ns} \rho_i U_i h_i \quad (2.9)$$

Considering the flowfield with gradients of temperature and mass fractions in x- and y- directions, the total energy flux in x-direction can be obtained by Eq. (2.9) as

$$q_x = -\kappa \frac{\partial T}{\partial x} + \sum_{i=1}^{ns} \rho_i U_i h_i \quad (2.10)$$

Where U_{ix} is the component of diffusion velocity of species i in x-direction. From Eq. (2.5), we can write

$$\rho_i U_{ix} = -\rho D_{iml} \frac{\partial Y_i}{\partial x} \quad (2.11)$$

Combining Eq. (2.10) and (2.11), we get

$$q_x = -\kappa \frac{\partial T}{\partial x} - \rho \sum_{i=1}^{ns} D_{iml} h_i \frac{\partial Y_i}{\partial x} \quad (2.12)$$

Similarly, the total energy flux in y-direction

$$q_y = -\kappa \frac{\partial T}{\partial y} - \rho \sum_{i=1}^{ns} D_{iml} h_i \frac{\partial Y_i}{\partial y} \quad (2.13)$$

Moreover, from Eq. (2.5), we can write the mass flux of species i in x-direction caused by diffusion as

$$\dot{m}_x = -\rho D_{iml} \frac{\partial Y_i}{\partial x} \quad (2.14)$$

and in y-direction

$$\dot{m}_y = -\rho D_{iml} \frac{\partial Y_i}{\partial y} \quad (2.15)$$

The specific heat and enthalpy of the mixture are determined from the following expressions:

$$C_p = \sum_{i=1}^{ns} Y_i C_{pi} \quad (2.16)$$

$$C = \sum_{i=1}^{ns} Y_i h_i \quad (2.17)$$

Where C_{pi} and h_i are the specific heat and enthalpy of the i -th species.

The values of C_{pi} and h_i are considered as functions of temperature and are determined from the polynomial curve fitting developed by Moss [35]. They are as follows:

$$\frac{C_{pi}}{R_i} = a_{1i} + a_{2i}T + a_{3i}T^2 + a_{4i}T^3 + a_{5i}T^4 \quad (2.18)$$

$$\frac{h_i}{R_i T} = a_{1i} + \frac{a_{2i}T}{2} + \frac{a_{3i}T^2}{3} + \frac{a_{4i}T^3}{4} + \frac{a_{5i}T^4}{5} + \frac{a_{6i}}{T} \quad (2.19)$$

Where a_1 to a_6 are constants for different species. The coefficients for these curve fits are found in Table 2.1. Two sets of coefficients are available in the Table 2.1 of which one for temperature range 0 ~ 1000 K, the other set for 1000 ~ 5000 K.

2.2 Calculation of Temperature

Temperature at various grid points is calculated by Newton-Raphson method. By rearranging Eq. (2.3), a relation for temperature can be expressed as

$$F(T) = \sum_{i=1}^{ns} \rho_i h_i - \sum_{i=1}^{ns} \rho_i \frac{R}{W_i} T + \frac{\rho}{2}(u^2 + v^2) - E \quad (2.20)$$

Substituting the value of h_i from Eq. (2.19), Eq. (2.20) can be written as

$$F(T) = b_0 + b_1T + b_2T^2 + b_3T^3 + b_4T^4 + b_5T^5 \quad (2.21)$$

Where the coefficients are

$$\begin{aligned}
 b_0 &= \sum_{i=1}^{ns} \rho_i R_i a_{6i} + \frac{\rho}{2} (u^2 + v^2) - E, & b_1 &= \sum_{i=1}^{ns} \rho_i R_i a_{6i} - \sum_{i=1}^{ns} \rho_i R_i \\
 b_2 &= \frac{1}{2} \sum_{i=1}^{ns} \rho_i R_i a_{2i} & b_3 &= \frac{1}{3} \sum_{i=1}^{ns} \rho_i R_i a_{3i} \\
 b_4 &= \frac{1}{4} \sum_{i=1}^{ns} \rho_i R_i a_{4i} & b_5 &= \frac{1}{5} \sum_{i=1}^{ns} \rho_i R_i a_{5i}
 \end{aligned} \tag{2.22}$$

Differentiating Eq. (2.21) with respect to T, we get

$$F'(T) = b_1 + 2b_2T + 3b_3T^2 + 4b_4T^3 + 5b_5T^4 \tag{2.23}$$

Then the temperature is calculated by the following equation:

$$T_{\text{new}} = T_{\text{old}} - \frac{F(T_{\text{old}})}{F'(T_{\text{old}})} \tag{2.24}$$

The calculation of Eq. (2.24) is repeated until it fulfils the criterion for the temperature T_{new} .

The criterion for this calculation is $|(T_{\text{new}} - T_{\text{old}})| < 1.0$.

2.3 Transport Coefficients

The transport properties; the viscosity coefficient μ and thermal conductivity κ of individual species are determined from Sutherland formulae [36] as

$$\frac{\mu_i}{\mu_{i0}} = \left(\frac{T}{T_{i0}} \right)^{1.5} \frac{T_{i0} + S_i}{T + S_i} \tag{2.25}$$

$$\frac{\kappa_i}{\kappa_{i0}} = \left(\frac{T}{T_{i0}} \right)^{1.5} \frac{T_{i0} + S'_i}{T + S'_i} \tag{2.26}$$

Where S_i and S'_i are the Sutherland constants, while μ_{i0} , T_{i0} and κ_{i0} are the reference values of i -th species. These constants are taken from References 36 and 37 and are also tabulated in Table 2.2. Once the viscosity coefficient and thermal conductivity of each species are determined, the mixture viscosity and thermal conductivity are determined by Wilke's formula [36] and Wassiljewa's equation [38], respectively as

$$\mu_l = \sum_{i=1}^{ns} \frac{z_i \mu_i}{\sum_{j=1}^{ns} z_j \phi_{ij}} \quad (2.27)$$

$$\kappa_l = \sum_{i=1}^{ns} \frac{\kappa_i}{1 + \frac{1}{z_i} \sum_{\substack{j=1 \\ j \neq i}}^{ns-1} A_{ij} Z_j} \quad (2.28)$$

Where $\phi_{ij} = \frac{[1.0 + (\mu_i / \mu_j)^{0.5} (W_j / W_i)^{0.25}]^2}{(8 + 8W_i / W_j)^{0.5}}$, $A_{ij} = 1.065 \phi_{ij}$, z_i , and z_{ij} are the mole fractions of i-th and j-th species, respectively.

The molecular-binary-diffusion coefficient for i-th and j-th species, D_{ij} is determined from the empirical formula given by Chapman-Cowling [36] as

$$D_{ij} = \frac{0.002858 T^{1.5} \left(\frac{W_i + W_j}{W_i W_j} \right)^{0.5} \times 10^{-4}}{2 P \sigma_{ij} \Omega_D} \quad (2.29)$$

$$\text{Where } \Omega_D = \left(\frac{T}{T_{\epsilon i}} \right)^{-0.145} + \left(\frac{T}{T_{\epsilon i}} + 0.5 \right)^{-2.0} \quad (2.30)$$

$$T_{\epsilon ij} = (T_{\epsilon i} T_{\epsilon j})^{0.5} \quad (2.31)$$

$$\sigma_{ij} = \frac{1}{2} (\sigma_i + \sigma_j) \quad (2.32)$$

T = absolute temperature (K)

p = pressure (atm).

Values of the effective temperature T_{ei} and effective collision diameter, σ_i of i -th species are taken from References 36 and 38, are also tabulated in Table 2.2. Using the value of binary diffusion coefficient, the effective molecular diffusion coefficient for each species is determined by the following formula given in Reference 38 as

$$D_{iml} = \frac{1 - Z_i}{\sum_{\substack{j=1 \\ j \neq i}}^{ns-1} Z_j / D_{ij}} \quad (2.33)$$

2.4 Numerical Scheme

The system of governing equations has been solved, using an explicit Harten-Yee Non-MUSCL Modified-flux-type TVD scheme [39]. The scheme is second order accurate in time and space. The two-dimensional, rectangular physical coordinate system (x,y) is transformed into the computational coordinate system (ξ,η) in order to solve the problem on uniform grids. The details of the transformation procedure can be found in Reference 40. After applying the transformation, Eq. (2.1) can be expressed as

$$\frac{\partial \hat{U}}{\partial t} + \frac{\partial \hat{F}}{\partial \xi} + \frac{\partial \hat{G}}{\partial \eta} = \frac{\partial \hat{F}_v}{\partial \xi} + \frac{\partial \hat{G}_v}{\partial \eta} \quad (2.34)$$

Where $\hat{U} = J^{-1} U$

$$\begin{aligned} \hat{F} &= J^{-1} (\xi_x F + \xi_y G), & \hat{G} &= J^{-1} (\eta_x F + \eta_y G) \\ \hat{F}_v &= J^{-1} (\xi_x F_v + \xi_y G_v), & \hat{G}_v &= J^{-1} (\eta_x F_v + \eta_y G_v) \end{aligned} \quad (2.35)$$

The transformation Jacobian J and grid metric terms are

$$\begin{aligned} J^{-1} &= X_\xi Y_\eta - X_\eta Y_\xi, & \xi_x &= Jy_\eta, \quad \xi_y = Jx_\eta, \\ \eta_x &= -JY_\xi, & \eta_y &= -JX_\xi \end{aligned} \quad (2.36)$$

The time step for calculation is determined by

$$\Delta t = \frac{CFL}{\max\{|U|+|V|+a(\xi_x^2 + \xi_y^2)^{1/2} + c(\eta_x^2 + \eta_y^2)^{1/2}\}} \quad (2.37)$$

Where the Courant number CFL is chosen as 0.7 to obtain rapid convergence and avoid unsteadiness in calculation. The contravariant velocities are

$$U = \xi_x u + \xi_y v, \quad V = \eta_x u + \eta_y v \quad (2.38)$$

2.5 Boundary Conditions and Convergence Criterion

A Navier-Stokes analysis imposes that the normal and tangential velocity components are zero on the walls. The walls are assumed to be thermally adiabatic, so that $(\partial T / \partial n)_w = 0$. For non-catalytic walls, the normal derivative of species mass fraction also vanishes, and consequently the gradient of total density becomes zero. The pressure is determined from the equation of state. The temperature, pressure and density at inflow boundary are assumed steady. At the outflow boundary the variables are determined by first-order extrapolation due to supersonic character of flow. Throughout the present study, the following convergence criterion has been set on the variation of density:

$$\sqrt{\frac{\sum_{J=1, K=1}^{JJ, KK} \left(\frac{\rho_{new} - \rho_{old}}{\rho_{old}} \right)^2}{JJ.KK}} \leq 10^{-5} \quad (2.39)$$

Where JJ and KK are the total numbers of nodes in the horizontal and vertical directions respectively.

2.6 Use of Turbulence Model

Throughout the all investigation the backward -facing step makes the flowfield turbulent at the present Mach number. Particularly, the recirculations in both upstream and downstream of injector, shocks and expansion of both main stream and side jet leads us to use a

turbulence model. Therefore, to calculate eddy viscosity we selected the zero equation turbulence model.

CHAPTER-III

RESULTS AND DISCUSSION

3.1 Introduction

A numerical study on mixing of hydrogen injected into a supersonic air stream has been performed by solving Two-Dimensional full Navier-Stokes equations. An explicit Harten-Yee Non-MUSCL Modified-flux-type TVD scheme has been used to solve the system of equations, and a zero-equation algebraic turbulence model to calculate the eddy viscosity coefficient. The main objective of this study is to increase the mixing efficiency and the flame holding capability of a supersonic combustor. The performance of combustor has been investigated by varying (i) the distance of injector position from left boundary (ii) the injector angle (iii) the air stream angle and (iv) the Mach number of the injector through which hydrogen is entering. The results are discussed in the section 3.3.

3.2 Flow Field Description and Numerical Parameter

The geometric configuration of the calculation domain and the inlet conditions of main and injecting flows are shown in Fig. 3.1(a~d). In all cases, the left boundary of domain consists of a backward facing step of height 5 mm, a main flow inlet of height 1.35-cm and a solid wall of height 3.6-cm. The backward facing step of 5 mm was used because it was found most efficient in mixing investigated by Ali et al [41]. In the present study the variable parameters are injector distance, injecting angle, air stream angle and Mach number of the injecting hydrogen. All the numerical values of the variable parameters are tabulated in the table 3.1. The inlet conditions of air are used as Weidner et al [16] except the Mach number as shown in Fig 3.1(a~d). The Mach 5.0 was chosen for the main flow as the test program has been conducted over the flight Mach number range [42] from 3.0 to 7.0. The inlet widths of air and side jet are used as Ali et al [43], which showed good performance on mixing. Through out the study, the grid system consists of 194 nodes in the longitudinal direction and 121 in the transverse direction. The grid system of the calculation flowfield is shown in

Fig.3.1 (e). Results of four varying parameters are to be analyzed and discussed under the following contexts; (i) the physics of fluid dynamics in both upstream and downstream of the injector (ii) penetration and mixing of hydrogen under the variation of these parameters and (iii) the characteristics of the flow field.

3.3 Effect of Injector Distance

3.3.1 The Physics of Fluid Dynamics

The physics of flow is important to understand the penetration and mixing of hydrogen which is the special interest of this study. Figures 3.2(a~e) show the velocity vector in both upstream and downstream of injector. Strong interaction is occurring between the main and injecting flows in Case 1 shown in Fig. 3.2(a). The strength of interaction can be understood from the slope of vectors at the top of injector. For long distance of injector position both main and injecting flows lose their strength due to viscous action and upstream recirculations. Due to small space in upstream, two very small recirculations (one is primary and the other is secondary) exist. With the increase in distance of injector the recirculations are increasing in areas and the primary one expands towards the left though the pattern of expansion is different. In Case 2, recirculations are not strong and the upstream region is seemed to be stagnant, where as Cases 3 ~ 5 have strong recirculations due to wide space in upstream. In downstream two features are to be mentioned; (i) no strong recirculation exists in any case, and (ii) for small distance of injector, the injecting jet is bent sharply into downward direction caused by strong interaction between main and injecting flows. Another observation is that with the increase in distance of injector position, the expansion of injecting jet plume increases. This is caused by the loss of strength of main flow and early separation of boundary layer.

3.3.2 Penetration and Mixing of Hydrogen

Figures 3.3(a~e) show the penetration and mass concentration of hydrogen in the flow field. There are various definitions of “penetration” in literature. In this paper the term

“penetration” is referred to the edge of mixing region in the vertical direction where the mole fraction of hydrogen is 5%. Accordingly the Fig. 3.3 shows that there is little difference in penetration at both upstream and downstream of the configurations. Two competing phenomena are activated in this regard; (i) due to strong interaction in small distance of injector, high gradient of hydrogen mass concentration exists causing high penetration of hydrogen, and (ii) in longer distance of injector, large and elongated upstream recirculation causes high penetration dominated by convection of recirculation. The mass concentration of hydrogen in upstream and that in downstream can be explained separately. For small distance of injector, most of the upstream region contains high concentration of hydrogen. It can be pointed out that the flame holding requires longer residence time of flame in the burning range and this residence time strongly depends on the geometric expansion of the recirculation zone [44]. Also the equivalence ratio of fuel and oxidizer in mixture is an important factor for burning because among the mixture, the stoichiometric strength is good for combustion. Therefore, longer recirculation zone containing stoichiometric mixture strength results in a longer residence time and leads to a more stable flame. Accordingly, Case 1 does not have a good flame holding capability. The Cases having injector distance $d = 20$ and 30 mm can produce larger and elongated upstream recirculation where most of the region contains good proportion of hydrogen and oxygen (mole fraction is about $0.4\sim 0.7$) exists. Again in cases having $d = 40$ and 50 mm, far upstream ($d = 0\sim 17.5$ mm) contains lower mass concentration of hydrogen which is not good for flame holding. In far downstream the hydrogen distribution is seemed to be better (more uniform) in Cases 3 ~ 5 than that in Cases 1 ~ 2. This uniform distribution of hydrogen is caused by higher expansion of side jet.

Again in cases having $d = 40$ and 50 mm, far upstream ($d = 0\sim 17.5$ mm) contains lower mass concentration of hydrogen which is not good for flame holding. In far downstream the hydrogen distribution is seemed to be better (more uniform) in Cases 3 ~ 5 than that in Cases 1 ~ 2. This uniform distribution of hydrogen is caused by higher expansion of side jet. However, the uniform distribution does not mean higher mixing efficiency, which will be discussed later. The performance of different cases is evaluated by calculating mixing

efficiency. Figure 3.4 shows mixing efficiency along the length of physical model for different Cases.

Mathematically, the mixing efficiency is defined by

$$\eta_m = \frac{\int_A (f_H \rho \bar{u} d\bar{A}) / \phi'}{\dot{m}_H / \Phi}$$

Where,

A = arbitrary section plane

f_H = local mass fraction of hydrogen

ρ = total density

\bar{u} = velocity vector

$d\bar{A}$ = small area normal to velocity vector

\dot{m}_H = total mass flux of hydrogen

$$\phi' = \text{local equivalence ratio} = \begin{cases} 0.25 & \phi' < 0.25 \\ \phi' & \phi' \geq 0.25 \end{cases}$$

$$\Phi = \text{global equivalence ratio} = \begin{cases} 0.25 & \Phi < 0.25 \\ \Phi & \Phi \geq 0.25 \end{cases}$$

In the flow field where large amount of hydrogen is present with negligible amount of oxygen, the calculation of mixing efficiency is avoided by dividing the large value of ϕ' . On the other hand, where a very small amount of hydrogen is present, an error in calculation of mixing efficiency can be occurred by the small value of ϕ' . This error has been eliminated by setting the minimum value of $\phi' = 0.25$ which corresponds to the lower flammability limit. It can be pointed out that similar expression for mixing efficiency was used by Yokota et al. [19~20]. In this investigation, the global equivalence ratio for all cases is $\Phi = 2$. Figure 3.4 shows that mixing efficiency increases very sharply at injector position of respective cases. Generally, in upstream region, the increasing of mixing is moderate and in downstream it is very slow. Individually, Case 1 has the highest increment of mixing efficiency (31%) at injector position due to strong interaction of main and injecting flows as discussed earlier. Besides, Case 1 shows that in upstream the overall mixing efficiency is

lower (about 15%) than the other cases, and in downstream the mixing rate along the length of physical model is slower than Case 2 and considerably equal with the other cases. In upstream the same increment of mixing efficiency can be found in Cases 2 ~ 5. This tendency indicates that the longer distance of injector position other than Case 2 might increase the cost for construction of combustor provided the other parameters are identical. The mixing efficiency of Case 2 is higher than that of Cases 3 ~ 5 on the top of injector. In downstream, the increasing rate of mixing is slower for all cases caused by the supersonic nature of flow. However, among the cases investigated, Case 2 has the maximum increasing rate of mixing in downstream. This increasing rate of mixing can be understood by Fig.3.5, which shows the diffusion of hydrogen along the vertical axis at a distance 80 mm from left wall. From this figure we see that Case 2 has the maximum hydrogen diffusion($0.37 \text{ kg/m}^2\text{s}$) which indicates higher mixing rate in downstream. With the increase of injector distance from $d = 10 \sim 20 \text{ mm}$, diffusion increases and then decreases for further increase of d . This is quite expected, because for small value of d , the pressure in downstream increases due to earlier reattachment shock which eventually causes the decrease of diffusion. On the other hand, for higher value of d , the injecting jet plume expands more causing lower mass concentration of hydrogen and eventually diffusion decreases.

3.3.3 Characteristics of the Flow Field

The characteristics of the flow field are shown in Figs. 3.6 and 3.7(a~e) and 3.8(a~e). Figure 3.6 shows the pressure distribution along the axis at 80 mm from left wall. For small value of d , the high momentum of main flow causes the side jet to bend downward, resulting in the formation of compression shock and higher pressure in far downstream. With the increase of d , the compression shock becomes weaker and the pressure decreases. Opposite trend of pressure distribution can be found in upper part of the flow field as shown in Fig. 3.6. Other characteristic phenomena such as separation shock bow shock, Mach disk, reattachment shock can be seen in Figs. 3.7(a~e) and 3.8(a~e). Figure 3.7 shows the pressure contours by which the pressure distribution and different shocks of other cases can be understood. Flow separation is initiated by the backward-facing step at left boundary. The main flow is deflected upward by the existence of wall at the upper part of the left boundary. The

deflection angle decreases with the increase of injector distance caused by weak interaction. The under expanded side jet rapidly expands and forms a Mach disk and a bow shock due to the interaction with main flow. The size of Mach disk increases with the increase of injector distance 'd' caused by higher expansion of side jet. The Maximum pressure in the flow field rises about 2.3×10^6 Pa immediately behind the intersection of separation shock and bow shock, where as the temperature rises about 2280 K at the same position. In the downstream region the reattachment shock is more visible in the pressure contour of Fig. 7. The pressure is higher in the upstream recirculation region while it is much lower immediately behind the injector caused by the suction of injection.

3.4 Effect of Injecting angle

3.4.1 The Physics of Fluid Dynamics

Figures 3.9 (a~e) show the velocity vector in both upstream and downstream of injector. In upstream there is a pair of large and small recirculation. For case-6 the recirculations are not dominant. With the increase of injector angle the recirculations are observed clearly (case-7~8) and again for further increase of injector angle (case-9~10) they are not significant. The large primary clockwise recirculation is caused by the backward facing step and the secondary small counter clockwise recirculation close to injector is caused by the primary recirculation and the suction of injection. The primary recirculation increases the boundary layer thickness and therefore the injection into a thick boundary layer creates greater penetration, resulting in higher mixing. Due to the interaction between main flow and side jet, the velocity of the main flow is slowed down and air enters the upstream recirculation. On the other hand by diffusion and convection due to injection, the injected hydrogen enters the recirculation and mixes well with air. So upstream recirculations play a vital role on mixing and consequently case-8 and 9 show better mixing. In down stream there is no strong recirculation in any case. Case 8 shows a very small recirculation in the downstream of injector caused by the suction of the injection and bending of the side jet. This recirculation and convection due to injection immediately downstream of the injector cause better mixing in case 8.



3.4.2 Penetration and Mixing of Hydrogen

Figures 3.10 (a~e) show the penetration and mass concentration of hydrogen in the flow field. The definition of “penetration” is given earlier. Penetration and mixing of hydrogen in a numerical simulation can occur by means of (i) turbulence and convection due to recirculation and velocity of the flow (ii) molecular diffusion. For all cases (case 6 ~ 10) the mole fraction contours of hydrogen are concentrated in a narrow region on the top of the injector, as shown in figure 3.10 (a~e), which might become a high heat release zone in the reacting flowfield. The backward facing step associated with upstream recirculation brings the injected hydrogen up to the left boundary in all cases. The hydrogen penetration height at different downstream locations can also be compared from Fig 3.10 (a~e). As for example at 10 cm from left boundary the penetration height is upto 2 cm in case 6 where as it is 2.5 cm for case 7 and above 3 cm for case 8 and 9. The penetration height of the hydrogen is more for case-8 and 9 (above 0.03m) indicating more uniform distribution of hydrogen and consequently higher mixing efficiency. Recalling the Fig. 3.9 it can be pointed out that the flame holding requires longer residence time of flame in the burning range and this residence time strongly depends on the geometric expansion of the recirculation zone [44] as stated earlier. Also the equivalence ratio of fuel and oxidizer in mixture is an important factor for burning because among the mixture, the stoichiometric strength is good for combustion. Therefore, longer recirculation zone containing stoichiometric mixture strength results in a longer residence time and leads to a more stable flame. Accordingly case-8 ($\theta=90^\circ$) and 9 ($\theta=120^\circ$) have good flame holding capability, because they can produce larger and elongated upstream recirculation where most of the region contains good proportion of hydrogen and oxygen exists.

Again in cases having $\theta = 30^\circ$ and 150° upstream region contains lower mass concentration of hydrogen which is not good for flame holding. In downstream hydrogen distribution is seemed to be better in case 8~9 as mentioned earlier because of higher expansion of side jet. Figure 3.11 shows the mixing efficiency along the length of physical model for different cases (case 6~10). Mathematically, the mixing efficiency is defined earlier. Physically mixing efficiency indicates the ratio of hydrogen mass flow rate capable of burning to its

total mass flow rate at the exit of side jet. Figure 3.11 shows that mixing efficiency increases sharply at injector position of respective cases. Generally, in upstream region, the increasing of mixing is moderate and in downstream it is very slow. Individually, case 8 ($\theta=90^\circ$) and 9 ($\theta=120^\circ$) have the highest increment of mixing efficiency (28%) at injector position due to strong upstream recirculation. In downstream the increasing rate of mixing along the length of physical model for case 8 ($\theta=90^\circ$) is higher than case 9 ($\theta=120^\circ$) whereas for case 10 ($\theta=150^\circ$) it remains almost constant which indicates that for case 10, the larger combustor might increase the cost of construction of combustor provided the other parameters are identical. So case 8 ($\theta=90^\circ$) has the maximum increasing rate of mixing in downstream. This increasing rate of mixing can be understood by figure 3.12 which shows the diffusion of hydrogen along the vertical axis at a distance 80 mm from left wall. From this figure we can see that case 8 ($\theta=90^\circ$) has the maximum hydrogen diffusion ($0.27 \text{ kg/m}^2\text{s}$) which indicates higher mixing rate in downstream that we have seen in figure 3.11.

3.4.3 Characteristics of the Flow Field

The characteristics of the flow field are shown in figs. 3.13, 3.14 (a~e) and 3.15 (a~e). Figure 3.13 shows the pressure distribution along the axis at 80 mm from left wall. For case-8 ($\theta=90^\circ$) the pressure in the downstream is relatively lower at upper part of the flow field. As diffusion of hydrogen is inversely proportional with pressure distribution so lower value of pressure indicates higher diffusion at downstream and higher diffusion means greater mixing rate in the downstream. Other characteristic phenomena such as separation shock, bow shock, Mach disk, reattachment shock can be seen in figure 3.14 (a~e) and 3.15 (a~e). Figure 3.14 (a~e) shows the pressure contours by which the pressure distribution and different shocks can be understood. Flow separation is initiated by the backward facing step at left boundary. The main flow is deflected upward by the existence of wall at the upper part of the left boundary. The deflection angle first increases with the increase of injecting angle and then decreases for further increase of injecting angle. The deflection angle is maximum for case-8 ($\theta=90^\circ$) caused by strong interaction. The under expanded side jet rapidly expands and forms a Mach disk and a bow shock due to the interaction with main flow. The size of the Mach disk increases with the increase of injecting angle first and then

decrease for higher injecting angle (case-9 and 10). This increasing Mach disk is caused by higher expansion of side jet. For the injecting angle $\theta=90^\circ$ the slope of the bow shock is steeper indicating high interaction between the main and side jet. Due to strong interaction high gradient of mass concentration exist and this indicates more uniform mixing. The maximum pressure and temperature in the flow field rises immediately behind the intersection of separation shock and bow shock. In the downstream region the reattachment shock is more visible in the pressure contour of figure 3.14 (a~e). The reattachment shock starts more or less at the same point for all cases (case 6~10). The pressure is higher in the upstream recirculation region while it is much lower immediately behind the injector caused by the suction of injection. Figure 3.15 (a~e) shows the temperature contours of cases (6~10). Among the all cases the maximum temperature rises in case 8 (about 2430 K) immediately behind the intersection of separation shock and bow shock. It is also clear from the Fig. 3.15 that the interaction between the main and the side flow is maximum in case 8. Other characteristics such as separation shock and Mach disk can also be understood from the Fig. 3.15.

3.5 Effect of Airstream Angle

3.5.1 The Physics of Fluid Dynamics

Figures 3.16 (a~c) show the velocity vector in both upstream and downstream of injector. For case-11 ($\psi=60^\circ$) the free air stream strike the wall near injector with a high momentum. At the region of striking there is a very strong interaction between the main flow and the side jet and the flow is deflected at an angle more than 60° in the upward direction. Due to the high momentum of the main flow at mixing region there is no upstream recirculation of main jet. For case 12 ($\psi=90^\circ$) two upstream recirculation exists. One is primary clockwise recirculation caused by the backward facing step and the other is secondary anticlockwise recirculation caused by primary recirculation and suction of injection. For case 13 ($\psi=120^\circ$) the airstream angle is 120° so the interaction between the main flow and injecting hydrogen is very weak. There is no upstream recirculation for this case as the main flow deflected upward after weak interaction with the side jet flow. In downstream there is no recirculation

in any case. Another observation is that for case 12 ($\psi=90^\circ$) the injecting jet plume expand caused by the early separation of boundary layer which increase the thickness of the boundary layer.

3.5.2 Penetration and Mixing of Hydrogen

Figures 3.17 (a~c) show the penetration and mass concentration of hydrogen in the flow field. Figure 3.17 (a~c) shows that there is a difference in penetration at both upstream and downstream of the configurations. It is pointed out earlier that recirculation plays a key role for penetration of Hydroden in upstream of the injector. For case-11 ($\psi=60^\circ$) we see that there is no hydrogen in upstream of the injector because a high momentum main flow strikes the wall near the injector results in high interaction at that region. It is then deflected away at an angle more than 60° ; so at 30mm from the left boundary the mixing of main flow and side jet is maximum. But in upstream region of the injector there is no hydrogen. We know that recirculation is an important factor for mixing of hydrogen with air in upstream region and as there is no recirculation so no mixing of hydrogen and air in upstream of the injector which is clear from figure 3.17(a). Due to primary and secondary upstream recirculations figure 3.17(b) indicates that there is good mixing between air and hydrogen upstream of the injector. Again we know that the flame holding requires longer residence time of flame in the burning range and this residence time strongly depends on the geometric expansion of the recirculation zone [44]. Also the equivalence ratio of fuel and oxidizer in mixture is an important factor for burning because among the mixture, the stoichiometric strength is good for combustion. Therefore longer recirculation zone containing stoichiometric mixture strength results in a longer residence time and leads for a more stable flame. Accordingly case 12 ($\psi=90^\circ$) has a good flame holding capability because it can produce larger and elongated upstream recirculation where most of the region contains good proportion of hydrogen and oxygen.

Figure 3.18 shows mixing efficiency along the length of physical model for different cases (case 11~13). The mass flow rate of hydrogen remains constant so the global equivalence ratio for all cases (case 11~13) is taken as $\phi=2$. Figure 3.18 shows that mixing efficiency

increases sharply at injector position of respective cases. Generally in upstream region the increasing rate of mixing is moderate and in downstream it is very slow. Individually case 11 ($\psi=60^\circ$) has the highest increment of mixing efficiency at injector position due to large gradient of mass concentration. But the mixing efficiency up to 0.03 m [from left boundary] is zero for case 11 ($\psi=60^\circ$). Because of high momentum of flow of air stream there is no hydrogen upstream of the injector which makes the mixing efficiency zero. For case 13 ($\psi=120^\circ$) the mixing efficiency in downstream of injector is not increasing (about 36%) indicating longer length of combustor might increase the cost for construction of combustor. In downstream, the increasing rate of mixing is slower for all cases caused by the supersonic nature of flow. However, among the cases investigated, case 11 ($\psi=60^\circ$) has the maximum increasing rate of mixing in downstream but as in upstream mixing efficiency is zero, so the overall mixing efficiency is lower than case 12 ($\psi=90^\circ$) and the mixing is also not uniform.

The increasing rate of mixing can be understood by figure 3.19 which shows the diffusion of hydrogen along the vertical axis at a distance 80 mm from left wall. From this figure we see that case 12 ($\psi=90^\circ$) has the maximum hydrogen diffusion ($0.27 \text{ kg/m}^2\text{s}$) which indicates higher mixing rate in downstream.

3.5.3 Characteristics of the Flow Field

The characteristics of the flow field are shown in figures 3.20, 3.21 (a~c) and 3.22 (a~c) figure 3.20 shows the pressure distribution along the axis at 80 mm from left wall which indicates that in downstream at 80 mm from left wall and 20 mm from bottom wall the pressure for case 12 ($\psi=90^\circ$) is moderately low indicating higher diffusion in downstream. Characteristic phenomenon such as separation shock, bow shock, Mach disk, reattachment shock can be seen in figure 3.21 (a~c) and 3.22 (a~c). Figure 3.21 (a~c) shows the pressure contours by which the pressure distribution and different shocks can be understood. For case 12 flow separation is initiated by the backward facing step at left boundary and the main flow is deflected upward by the existence of wall at the upper part of the left boundary. But for case 11 ($\psi=60^\circ$) due to high momentum of flow, after striking the wall the flow is deflected in the upward direction. Mach disk is also prominent in case 12 because of the

rapid expansion of the side jet. The maximum pressure and temperature are obtained immediately behind the intersection of separation shock and bow shock. All the characteristics phenomenon such as separation shock and bow shock are also clear from Fig.3.22 (a~c). From the Fig.3.22(a~c) we see that the maximum temperature rises in cases 11, 12 and 13 are 2375 K, 2430 K and 2525 K, respectively.

3.6 Effect of Mach No. of the Injecting Hydrogen

3.6.1 The Physics of Fluid Dynamics

The physics of flow is very important to understand the penetration and mixing of hydrogen with air stream. Figure 3.23 (a~c) shows the velocity vector in both upstream and downstream of injector for varying Mach number (0.7, 1, 1.3) of the injector. Strong interaction is occurring between the main and injecting flow in case 16 (Mach No. 1.3) shown in figure 3.23 (c). By seeing the slope of vectors just at the top of injector the strength of interaction can be understood. For all cases (case-14~16) in upstream there are two recirculations. One is primary caused by the backward facing step and the other is secondary due to primary recirculation and suction of injection. As it mentioned earlier that upstream recirculation plays an important role in mixing of hydrogen with air so better mixing is obtained in upstream for Mach No. 1.3. With the increase in Mach number of the injecting hydrogen the recirculations are increasing in areas and the primary one expands towards left and for case 16 (Mach No. 1.3) it touches the left boundary. In downstream two features are to be mentioned; (i) no strong recirculation exists in any case, and (ii) for large Mach No. (case-16) the injecting jet is bent sharply into upward direction caused by strong interaction between main and injecting flows.

3.6.2 Penetration and Mixing of Hydrogen

Figures 3.24 (a~c) show the penetration and mass concentration of hydrogen in the flow field. Accordingly the figure 3.24 shows that there is difference in penetration at both upstream and downstream. For high Mach No. (case~16) large and elongated upstream

recirculation causes high penetration dominated by convection of recirculation. At the same time due to strong interaction high gradient of hydrogen mass concentration exists causing high penetration of hydrogen. The mass concentration of hydrogen in upstream and downstream can be explained separately. Due to primary and secondary recirculations most of the upstream region contains high concentration of hydrogen for all cases (case 14~16). In downstream due to strong interaction for case 16 (Mach No. 1.3) the injecting jet bent more in upward direction results in more penetration height of hydrogen (above 0.04m) in downstream indicating more uniform distribution of hydrogen. Again the flame holding requires longer residence time of flame in the burning range and this residence time strongly depends on the geometric expansion of the recirculation zone [44]. Also the equivalence ratio of fuel and oxidizer in mixture is an important factor for burning. Therefore longer recirculation zone containing stoichiometric mixture strength results in a longer residence time and leads to a more stable flame. Accordingly case 16 (Mach No. 1.3) has the good flame holding capability because it can produce larger and elongated upstream recirculation where most of the region contains good proportion of hydrogen and oxygen. In far downstream the hydrogen distribution is seemed to be better (more uniform) in case 16 (Mach No. 1.3). This uniform distribution of hydrogen is caused by higher expansion of side jet.

Figure 3.25 shows the mixing efficiency along the length of physical model for different cases (case 14~16). Figure 3.25 shows that mixing efficiency increases very sharply at injector position of respective cases. Generally in upstream region, the increasing rate of mixing is moderate and in downstream it is slow. Individually, case 16 (Mach No. 1.3) has the highest increment (about 31%) of mixing efficiency at injector position due to strong upstream recirculation and high interaction between free stream air and side jet. Again case 16 shows that in downstream the mixing rate along the length of physical model is almost constant (38%) whereas the slope of the increasing mixing rate is slower for case 15 than case 14 (Mach No. 0.7) indicating that the longer length of combustor for case 16 might increase the cost for construction of combustor provided the other parameters are identical. The mixing efficiency of case 16 is higher than that of cases 14 and 15 on the top of injector. In downstream the increasing rate of mixing is slower for all cases caused by the supersonic

nature of flow. However, among the cases investigated, case 14 has the maximum increasing rate of mixing in downstream. This increasing rate of mixing can be understood by figure 3.26 which shows the diffusion of hydrogen along the vertical axis at a distance 80 mm from left wall. From the figure we see that case 14 has the maximum hydrogen diffusion ($0.33 \text{ kg/m}^2\text{s}$) which indicates higher mixing rate in downstream. The diffusion of hydrogen for case 16 is minimum ($0.01 \text{ kg/m}^2\text{s}$) which is clear from figure 3.25 as the mixing efficiency curve for case 16 (Mach No. 1.3) is almost horizontal in the downstream.

3.6.3 Characteristics of the Flow Field

The characteristics of the flow field are shown in figures 3.27, 3.28 (a~c) and 3.29 (a~c). Figure 3.27 shows the pressure distribution along the axis at 80 mm from left wall. For higher value of Mach No. the pressure in the downstream is higher at upper part of the flow field. Again we know that diffusion of hydrogen is inversely proportional with the pressure so definitely in the downstream for Mach No. (1.3) diffusion of hydrogen will be minimum which we have seen from figure 3.26 earlier. Other characteristics phenomena such as separation shock, bow shock, Mach disk, reattachment shock can be seen in figure 3.28 (a~c) and 3.29 (a~c). Figure 3.28 (a~c) shows the pressure contours by which the pressure distribution and different shocks can be understood. Flow separation is initiated by the backward facing step at left boundary. The main flow is deflected upward by the existence of wall at the upper part of the left boundary. The deflection angle decreases with the decrease of Mach number caused by weak interaction. The under expanded side jet rapidly expands and forms a Mach disk and a bow shock due to the interaction with main flow. The size of Mach disk increases with the increase of Mach number caused by higher expansion of side jet. For high Mach number the slope of the bow shock is steeper indicating high interaction between the main and side jet resulting in the high gradient of mass concentration and consequently higher mixing efficiency. The maximum pressure and temperature in the flow field rises immediately behind the intersection of separation shock and bow shock. In the downstream region the reattachment shock is more visible in the pressure contour of figure 3.28 (a~c). The pressure is higher in the upstream recirculation region while it is much lower immediately behind the injector caused by the suction of

injection. Fig. 3.29 (a~c) shows the temperature contours for the cases (Case 14~16). The maximum temperature rises for cases 14, 15 and 16 are 2343 K, 2430 K and 2594 K respectively. The separation shock, bow shock and Mach disk can also be understood from the Fig. 3.29 (a~c). From Fig. 3.29 (a~c) we can also see the position of the maximum temperature for each case (case 14~16) which is behind the intersection of the separation shock and the bow shock.

CHAPTER-IV

CONCLUSION

4.1 Summary of the Study

A numerical study on the mixing of hydrogen in supersonic airstream has been studied by solving two-dimensional full Navier-Stroke equations. The ultimate goal of this study is to increase mixing efficiency and flame holding capability. It was found that in supersonic combustion, high penetration and mixing of fuel with oxidizer is difficult due to their short residence time in combustor. Therefore it is necessary to analyze and find out the means of increasing mixing efficiency.

This study is completed with several investigations. Here I have reported (i) the effect of change of injector position (ii) the effect of change of injecting angle (iii) the effect of change of air stream angle and (iv) the effect of change of Mach number of the injector on mixing of hydrogen with air. As an injectant, gaseous hydrogen is used because it is the most suitable fuel and has high potential of heat release. This is why a considerable number of researches [4, 15, 16, 18 ~ 21, 24] has been performed their investigations using hydrogen as an injectant. For the present investigation first I changed the position of the injector taking as 10, 20, 30, 40 and 50 mm respectively from left boundary. Then I changed the injecting angle as (30° , 60° , 90° , 120° , 150°) anticlockwise by taking the injector 30 mm from the left boundary. Thirdly I changed the air stream angle taking as (60° , 90° , 120°) anticlockwise by considering the same height of the backward facing step (5mm). Finally I changed the Mach number of the injecting flow taking as (0.7, 1, 1.3) without changing the position (30mm) of the injector from the left boundary. The purpose of this analysis is to search the configuration of a supersonic combustor, which can increase the penetration, and mixing of gaseous hydrogen into an air stream.

It can be pointed out that most of the previous researchers used infinite parallel flow configuration for investigations about penetration and mixing of side jet. But the finite

parallel flow configuration shows higher penetration, more uniform distribution and rapid mixing of hydrogen and that's why I have used finite flow configuration in all of my investigations.

It has been found that in case of varying injector distance, strong interaction is occurring between the main and injecting flows for small distance of injector position. For long distance of injector position both main and injecting flows lose their strength due to viscous action and upstream recirculation. Small distance of injector position does not have strong recirculation but long distances have strong recirculations due to wide space in upstream. The small distance of injector position increases the mixing efficiency but decreases the flame holding capability. The pressure loss increases with the increase of injector distance. In conclusion, the range of setting the injector is from 20~30mm, preferably near 20mm, by which the configuration might act as a good flame holder and become efficient in mixing. For very long distance of injector position (40mm or more), the configuration reduces both the mixing efficiency and flame holding capability.

Investigation showed that for varying injector angle (taking as anticlockwise), small ($\theta=30^\circ$) and large ($\theta=120^\circ$ and 150°) injecting angle have no significant upstream recirculation. Upstream recirculation is dominant for injecting angle 60° and 90° . Perpendicular injection i.e. injecting angle ($\theta=90^\circ$) increases the both mixing efficiency and flame holding capability. Small injecting angle ($\theta=30^\circ$) and very large injecting angle ($\theta=150^\circ$) have good flame holding capability but mixing efficiency is poor. So finally it has been found out that for injecting angle ($\theta=90^\circ$) the combustor might act as a good flame holder and become efficient in mixing.

The third investigation was carried out by changing the value of airstream angle taking as $\psi=60^\circ$, 90° and 120° . Investigation showed that small airstream angle ($\psi=60^\circ$) increases the mixing efficiency from injector position to downstream but in upstream mixing efficiency is zero. Airstream angle ($\psi=120^\circ$) has better mixing efficiency than ($\psi=90^\circ$) but does not have good flame holding capability. So in conclusion we can say that

airstream angle ($\psi=90^0$) has better mixing efficiency and flame holding capability and might act as a good combustor.

Finally the Mach number of the injector was changed taking as 0.7, 1.0 and 1.3. It is found that strong interaction is occurring between the main and injecting flows for higher Mach number ($M=1.3$). With the increase of Mach number of the injecting hydrogen the recirculations are increasing in areas and the primary one expands towards the left and for Mach number 1.3 it touches the left boundary. Higher Mach number increases both the mixing efficiency and flame holding capability. Pressure loss decreases with the increase of Mach number. So injecting hydrogen having Mach number 1.3 might act as a good flame holder and become efficient in mixing.

4.2 Recommendations for Future Study

A good supersonic combustor requires efficient mixing. A number of researches have been carried out on mixing. More investigations are required to overcome these problems. In fact, in supersonic combustion, high penetration and mixing of injectant with main stream is difficult due to their short residence time in combustor. In present investigation although I have found out some significant results with increasing mixing efficiency, more mixing is desired.

In my thesis I have used zero equation turbulence model. But there are some limitations of this model. This model takes no account of convection and diffusion of turbulence and it is not suitable for flows containing recirculating flow regions. A two-equation turbulence model is suggested.

Schematic with Numerical Parameters

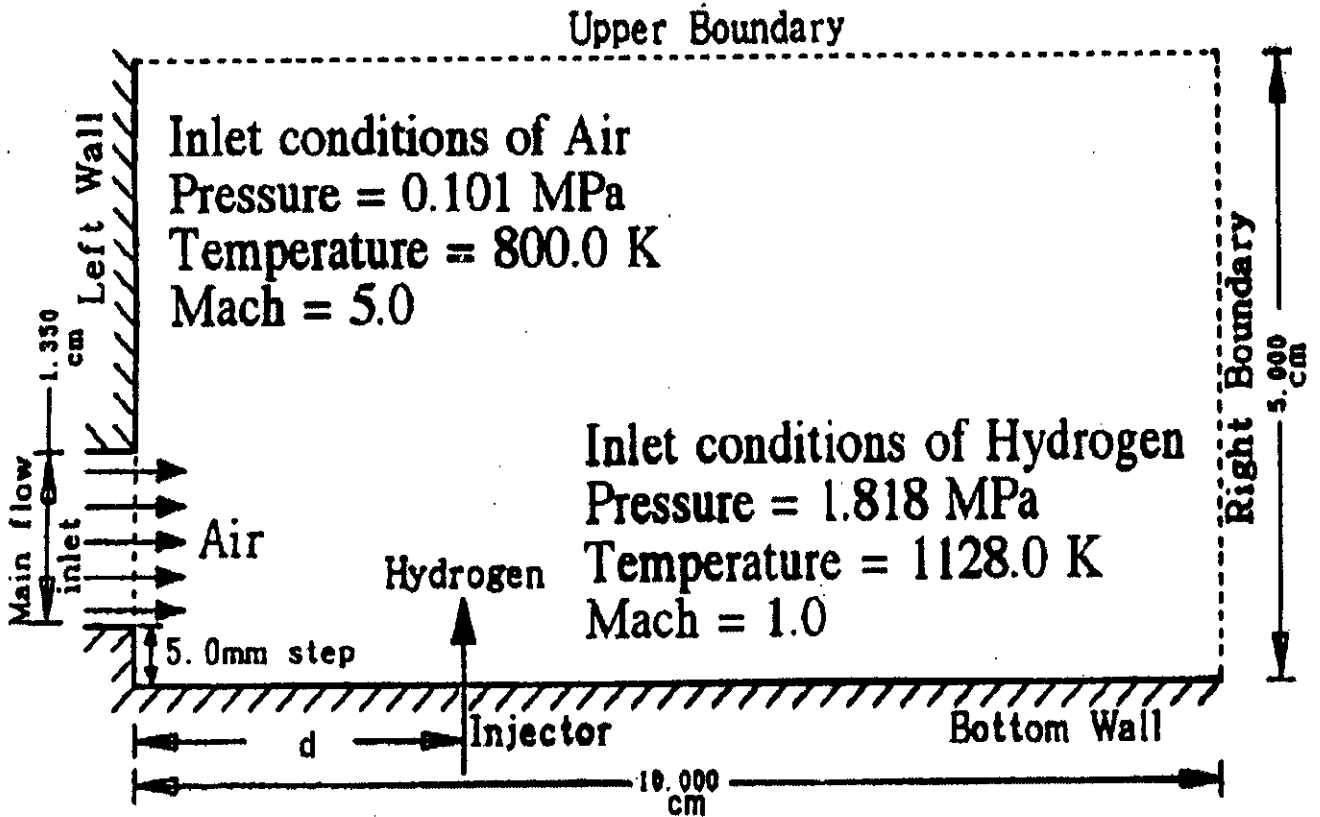


Fig. 3.1 (a) Schematic with numerical parameters for varying injector position, ($d = 10, 20, 30, 40, 50$ mm)

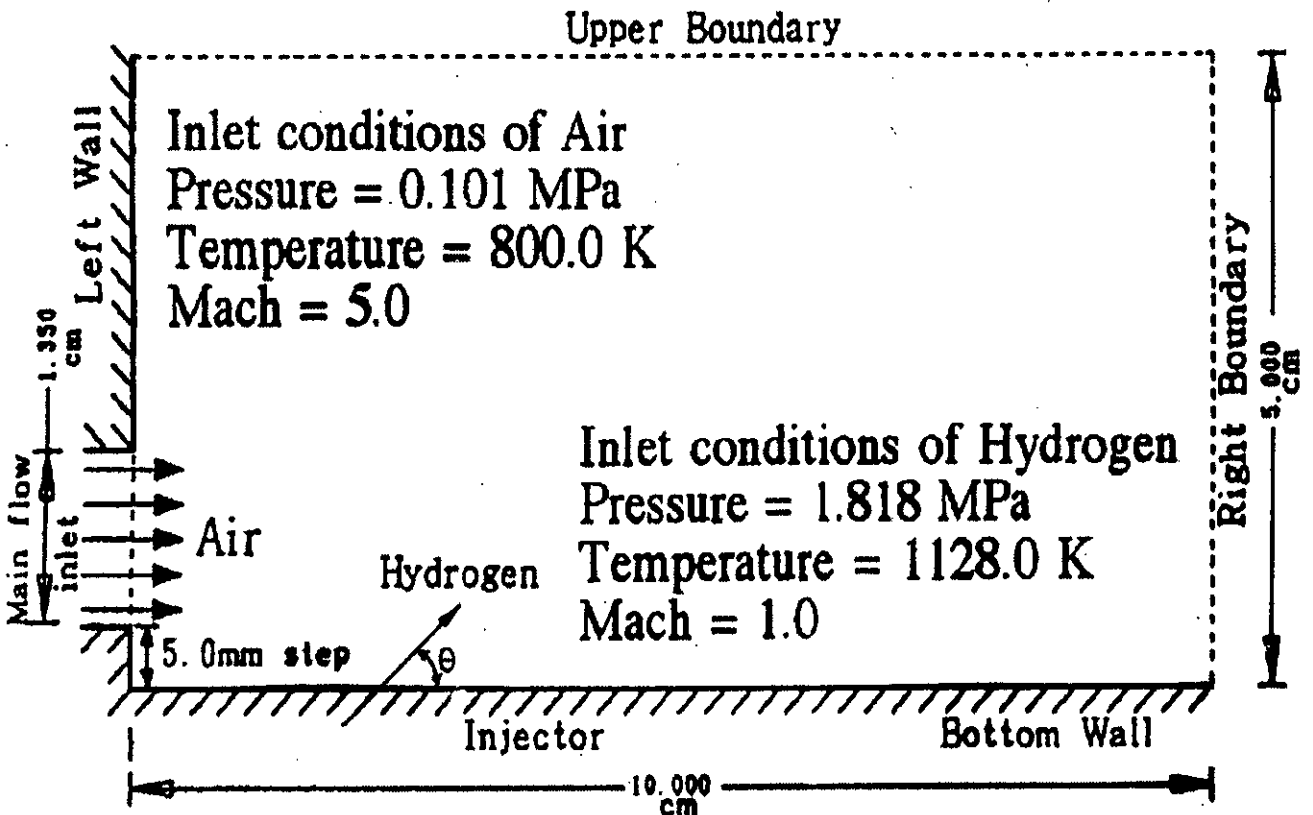


Fig. 3.1 (b) Schematic with numerical parameters for varying injector angle, (injector angles are 30, 60, 90, 120 and 150 degree)

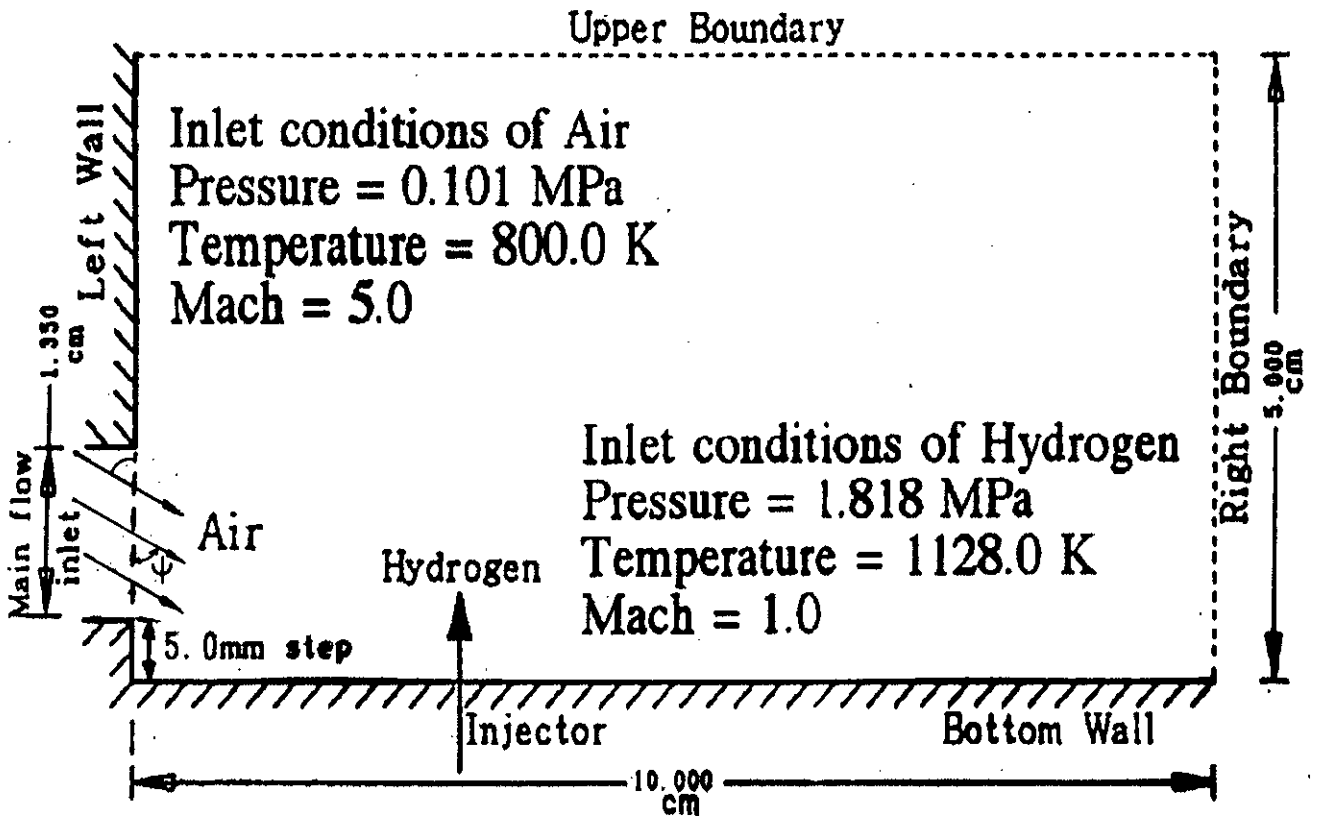


Fig. 3.1 (c) Schematic with numerical parameters for varying air stream angle, (air stream angles are 60, 90, 120 degree)

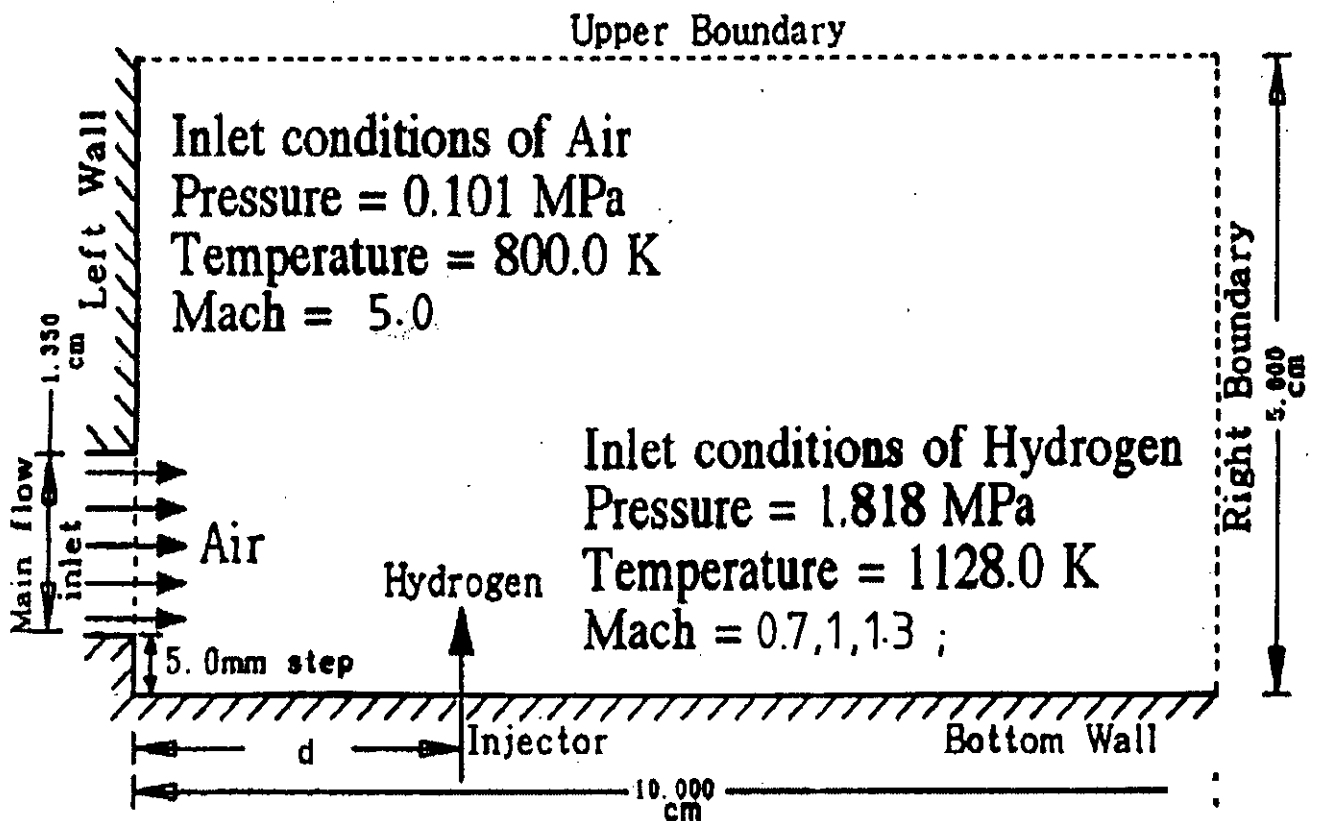
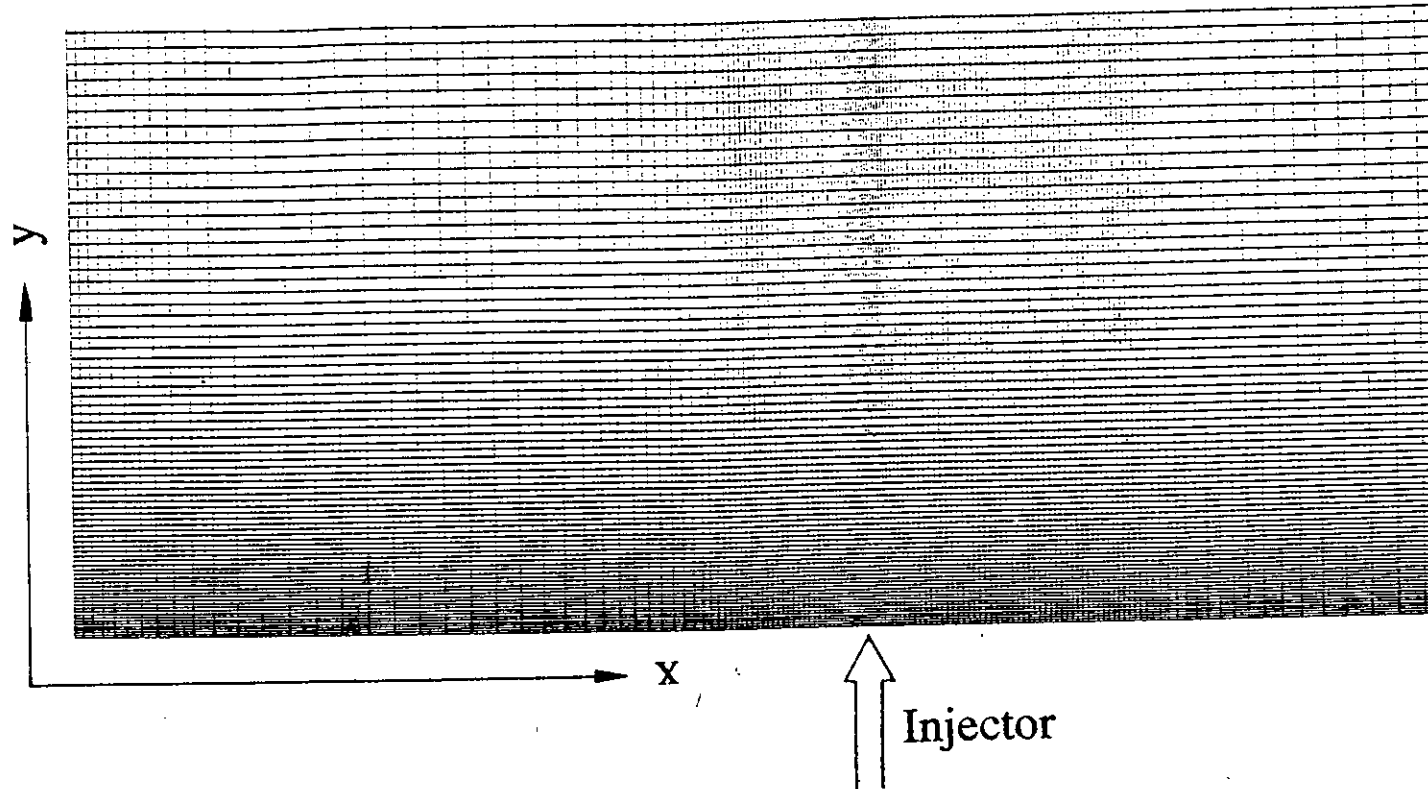


Fig. 3.1 (d) Schematic with numerical parameters for varying Mach No. of the injecting H_2 ($M = 0.7, 1.0, 1.3$)

Grid System of the Calculation Flowfield



35

- * Grid system consists of 194 nodes in the x-direction and 121 in the y-direction.
- * The grid points around the wall and injector are clustered.
- * 10 grid points are provided at the exit of injector.

Fig. 3.1 (e) Grid system of the calculation flowfield

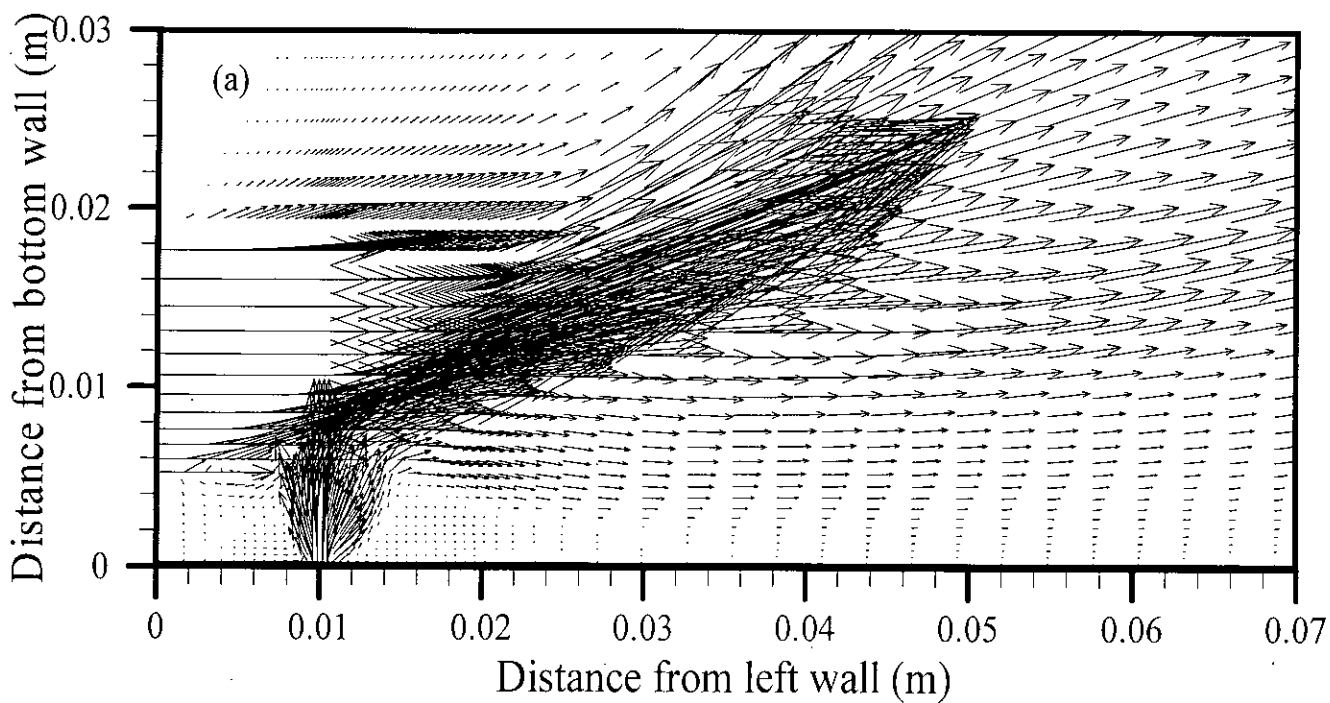


Fig. 3.2 (a) Velocity vector near injector; Case-1 ($d=10$ mm)

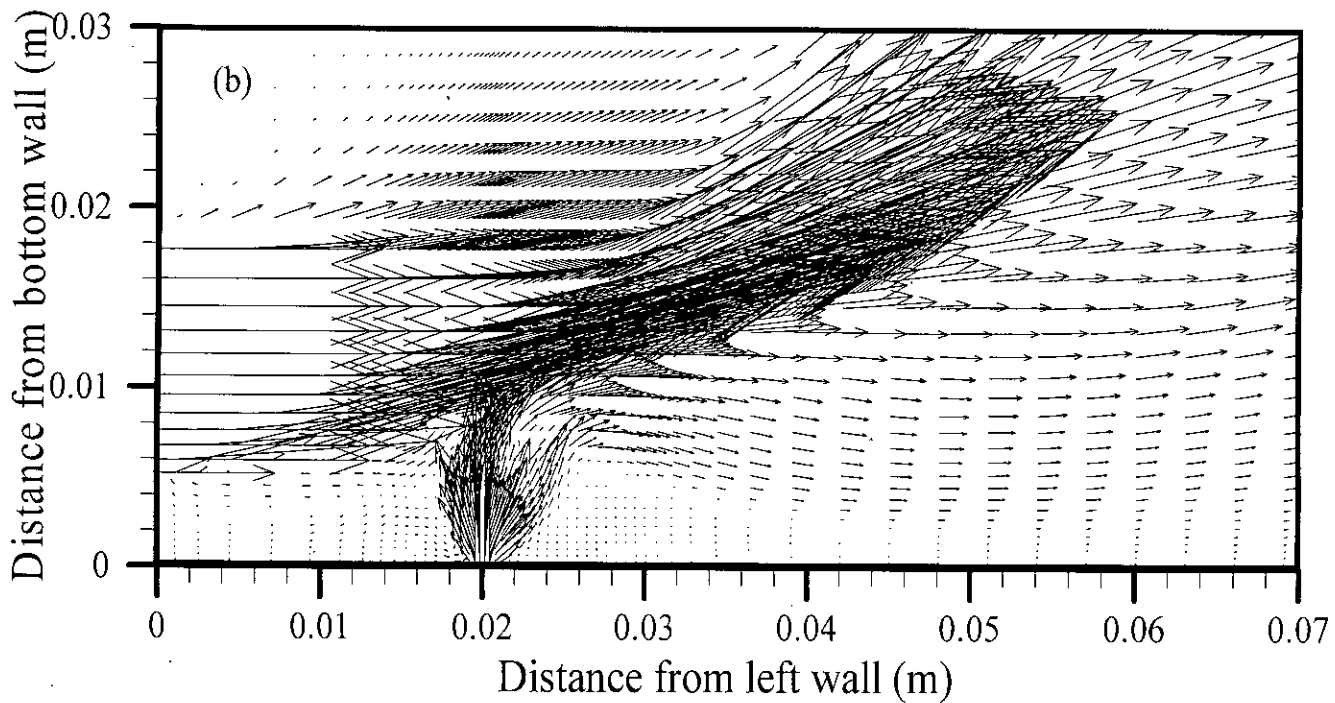


Fig. 3.2 (b) Velocity vector near injector; Case-2 ($d=20$ mm)

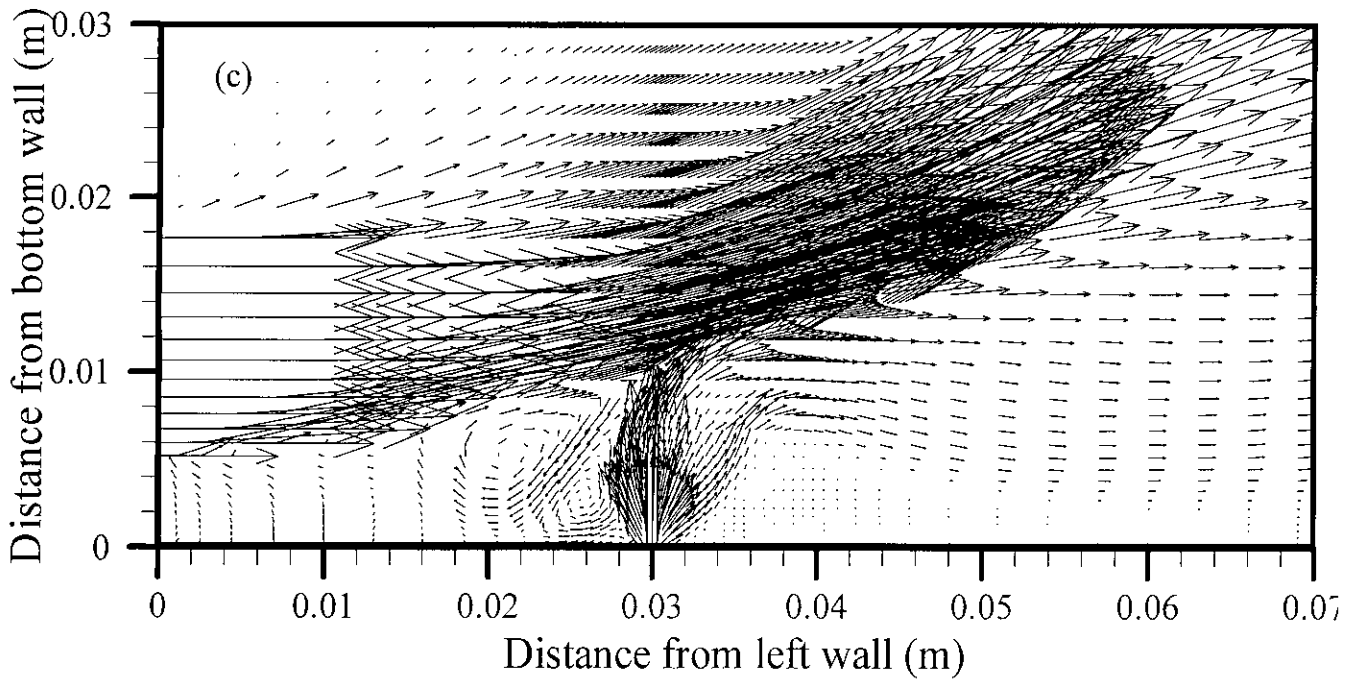


Fig. 3.2 (c) Velocity vector near injector; Case-3 ($d=30$ mm)

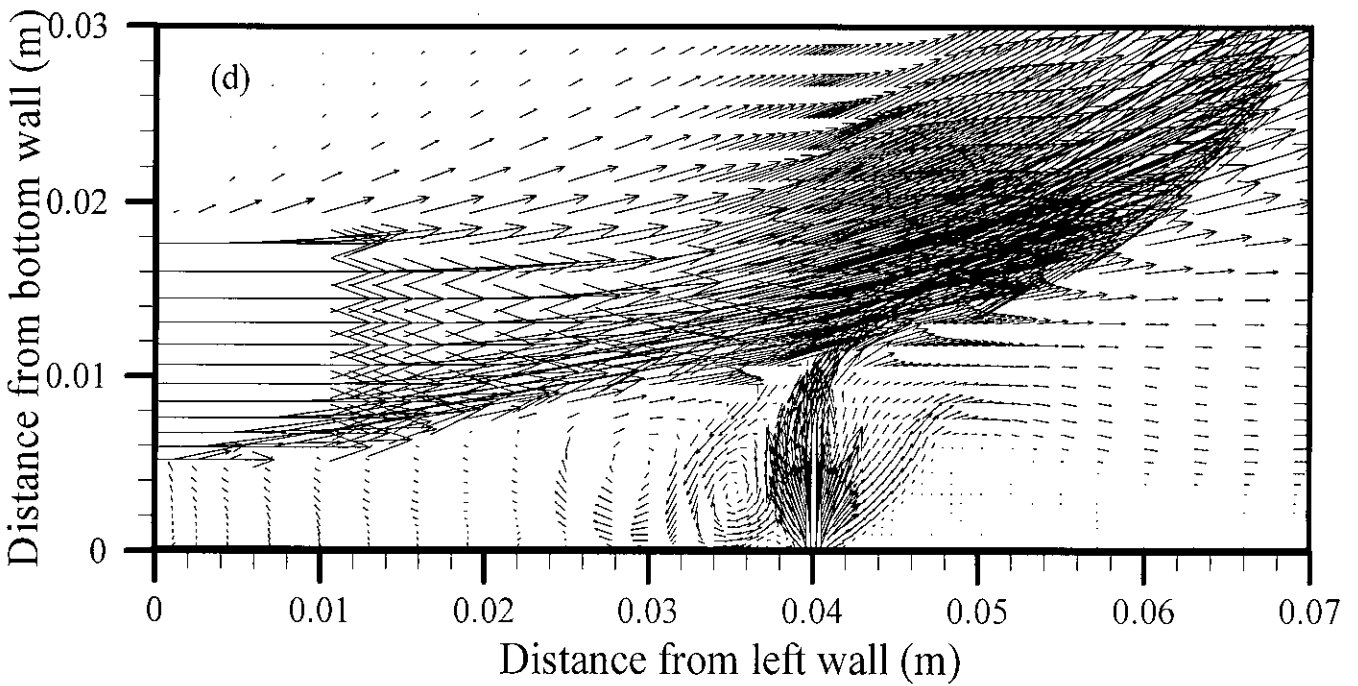


Fig. 3.2 (d) Velocity vector near injector; Case-4 ($d=40$ mm)

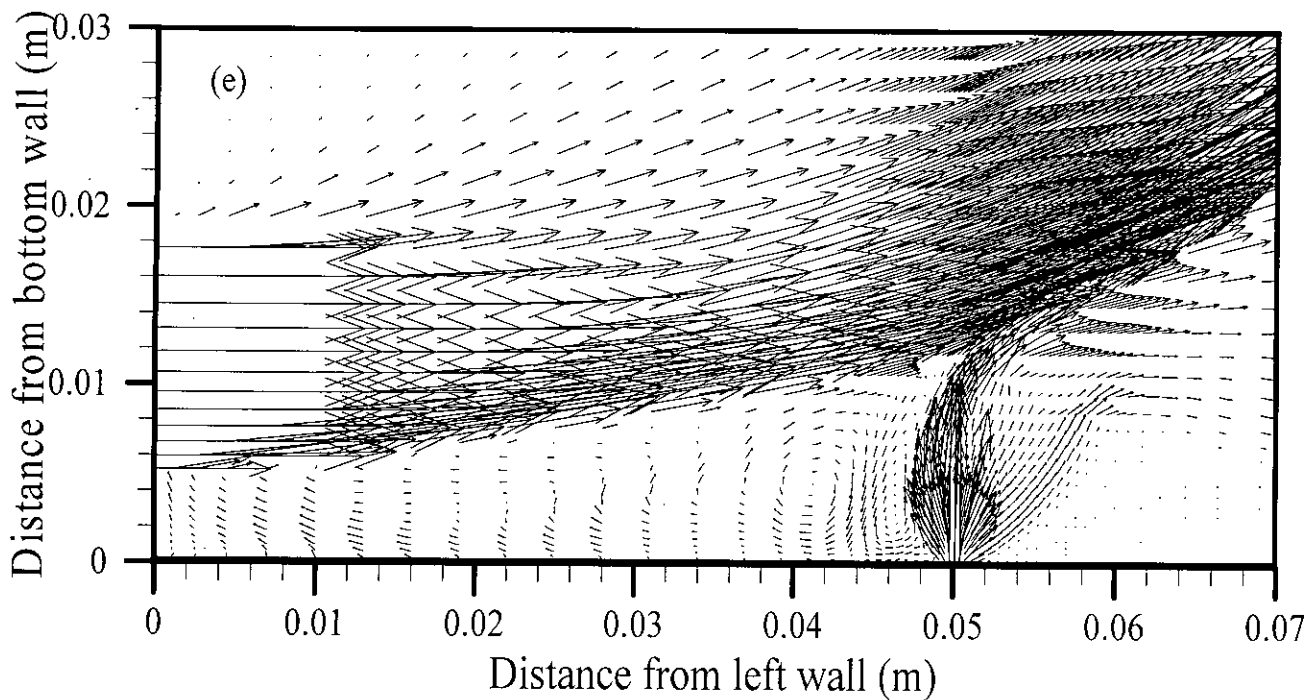


Fig. 3.2 (e) Velocity vector near injector; Case-5 ($d=50$ mm)

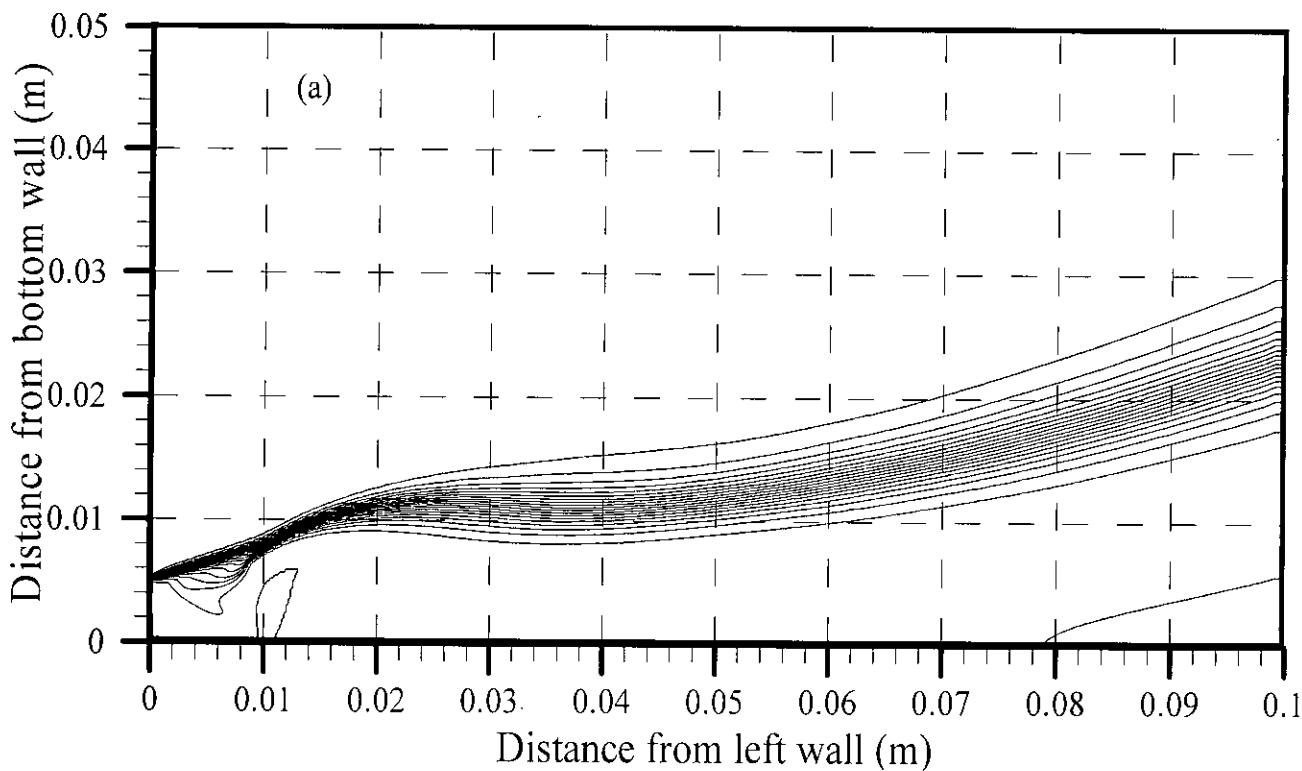


Fig. 3.3 (a) Mole fraction contour of Hydrogen, ϕ (0.05, 1.0, 0.05); Case-1 ($d=10$ mm)

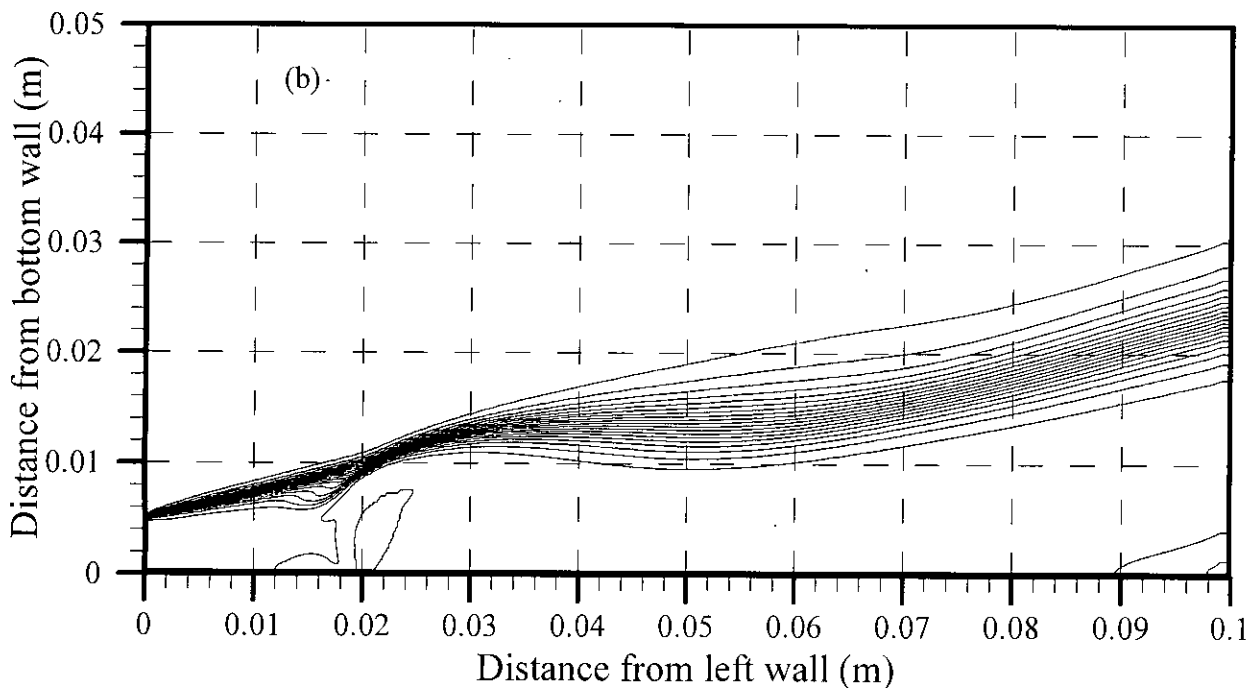


Fig. 3.3 (b) Mole fraction contour of Hydrogen, ϕ (0.05, 1.0, 0.05); Case-2 ($d=20$ mm)

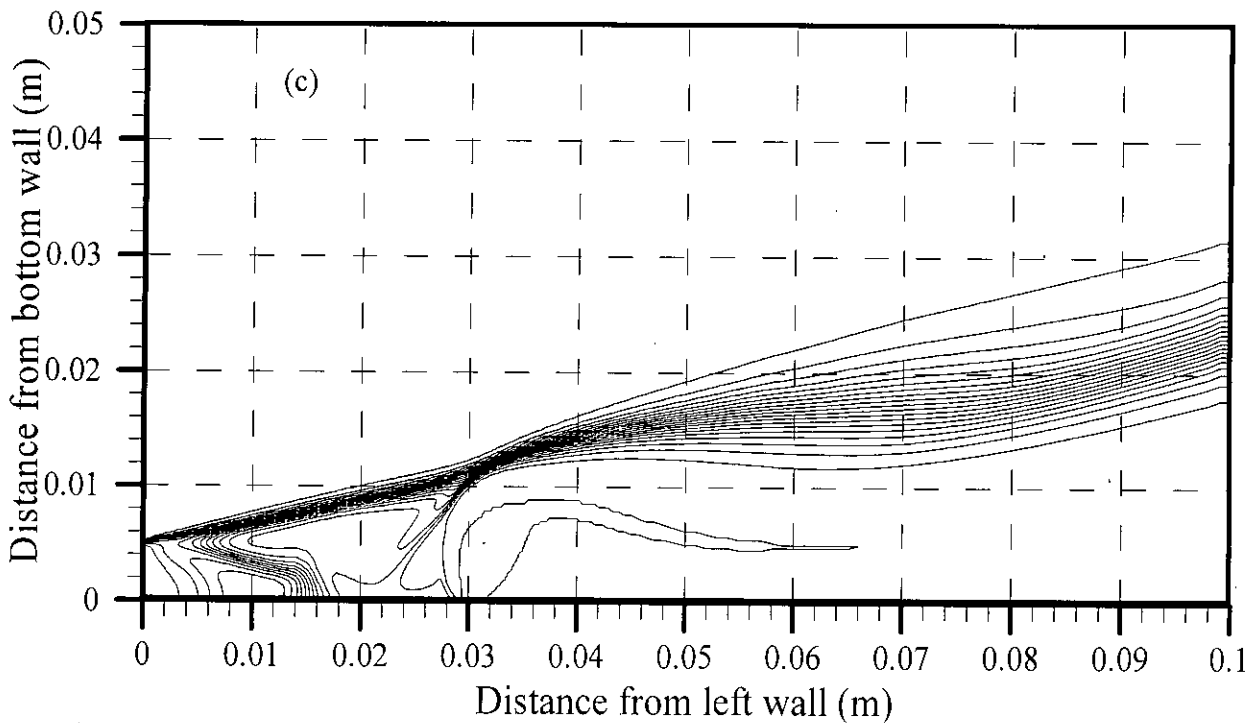


Fig. 3.3 (c) Mole fraction contour of Hydrogen, ϕ (0.05, 1.0, 0.05); Case-3 ($d=30$ mm)

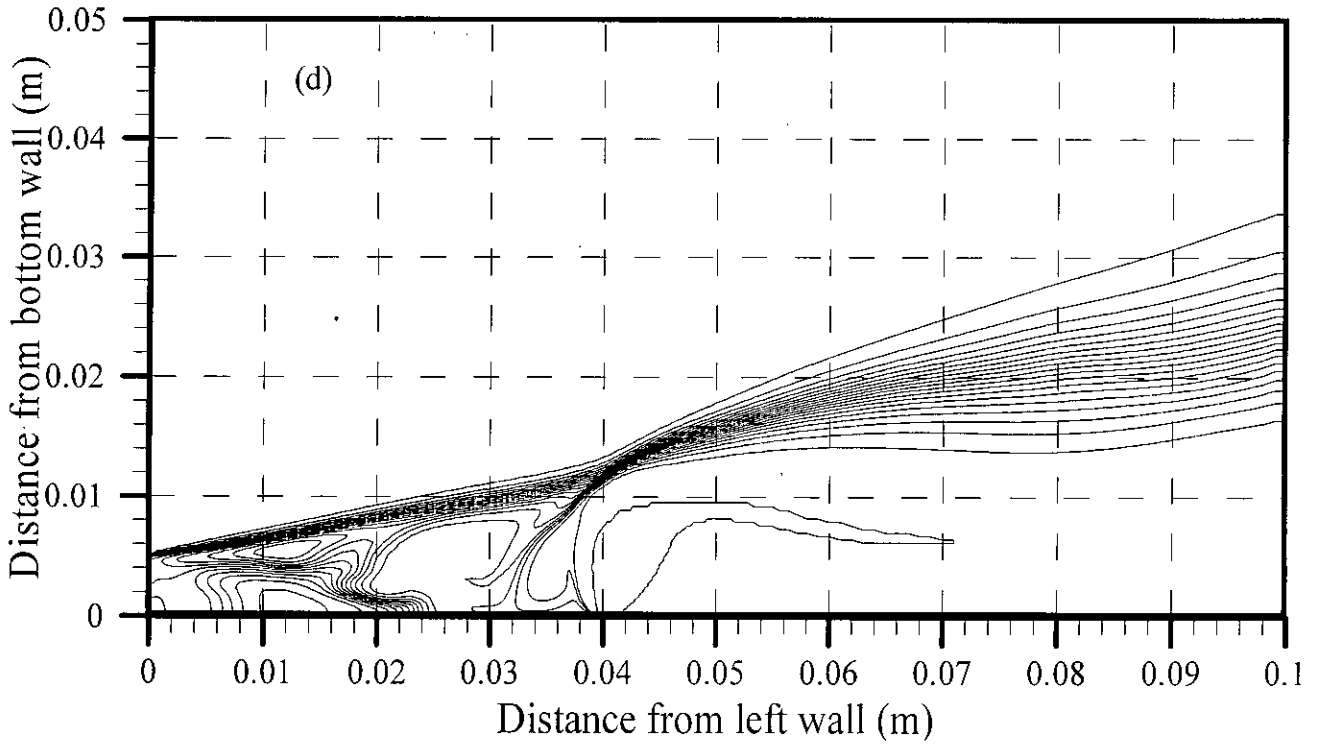


Fig. 3.3 (d) Mole fraction contour of Hydrogen, ϕ (0.05, 1.0, 0.05); Case-4 ($d=40$ mm)

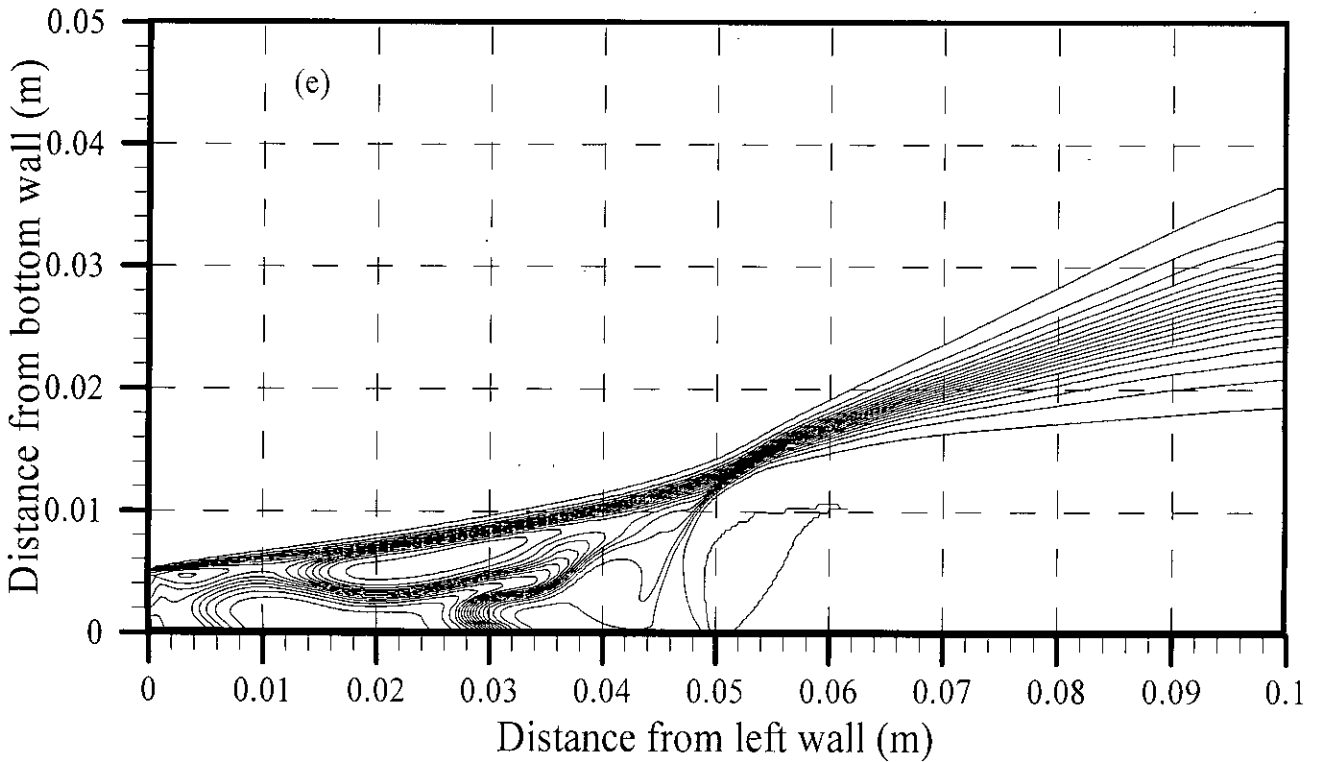


Fig. 3.3 (e) Mole fraction contour of Hydrogen, ϕ (0.05, 1.0, 0.05); Case-5 ($d=50$ mm)

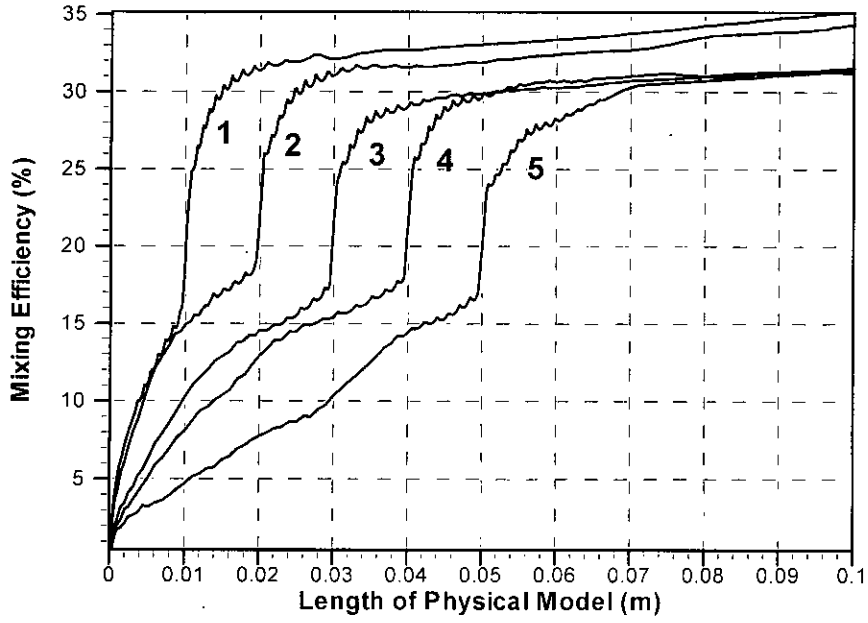


Fig. 3.4 Mixing efficiency along the length of physical model.

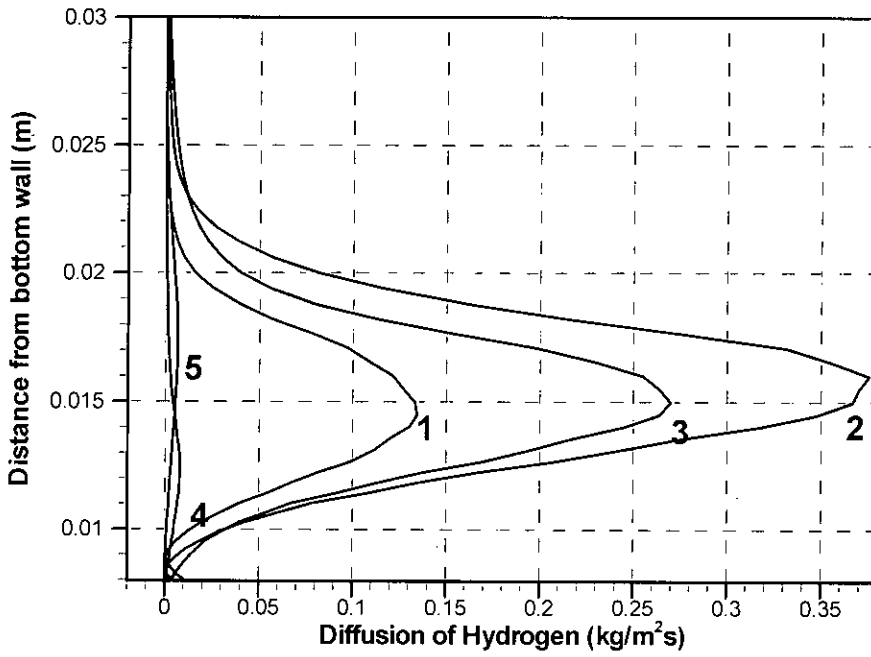


Fig. 3.5 Diffusion of Hydrogen at 0.08m from left wall

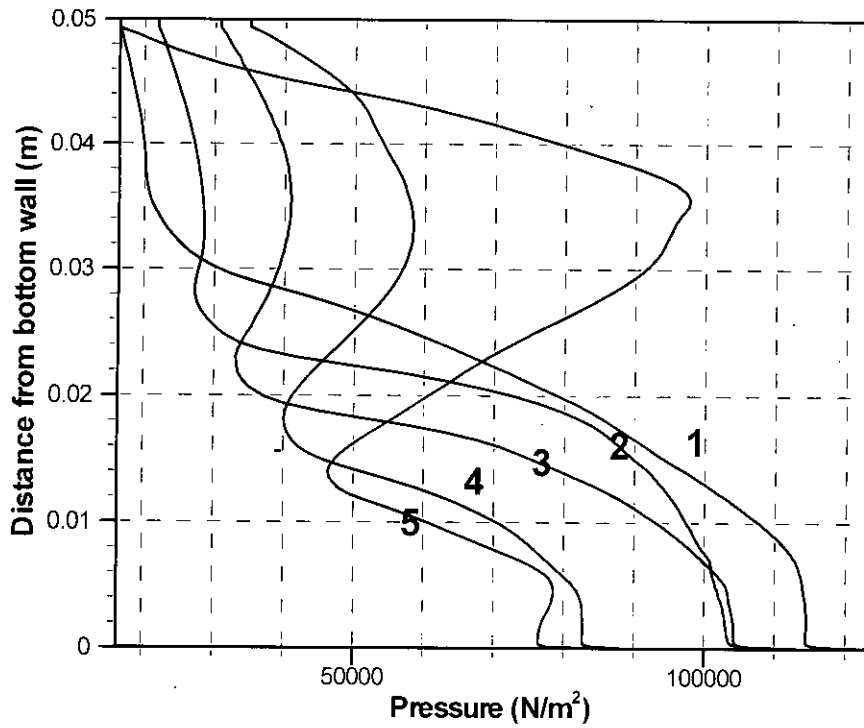


Fig. 3.6 pressure distribution at 0.08m from left wall

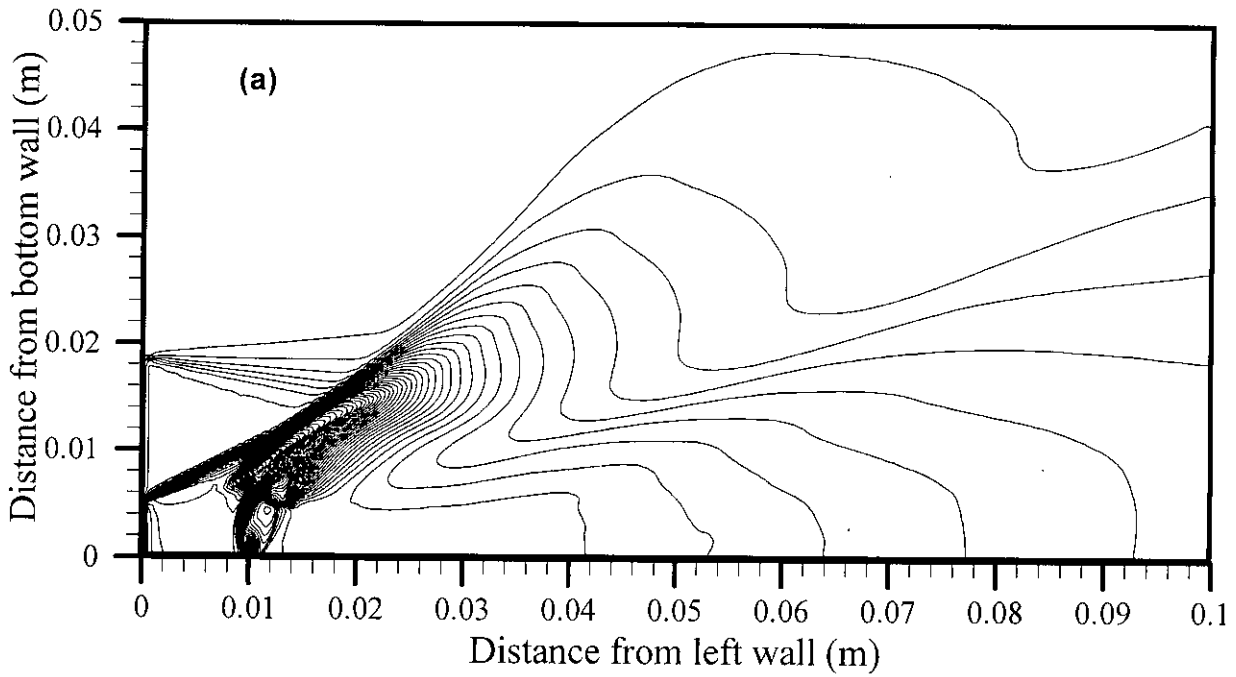


Fig. 3.7 (a) pressure (Pa) contour, ϕ ($2 \cdot 10^4$, $2 \cdot 10^6$, $2 \cdot 10^4$); Case-1 ($d=10$ mm)

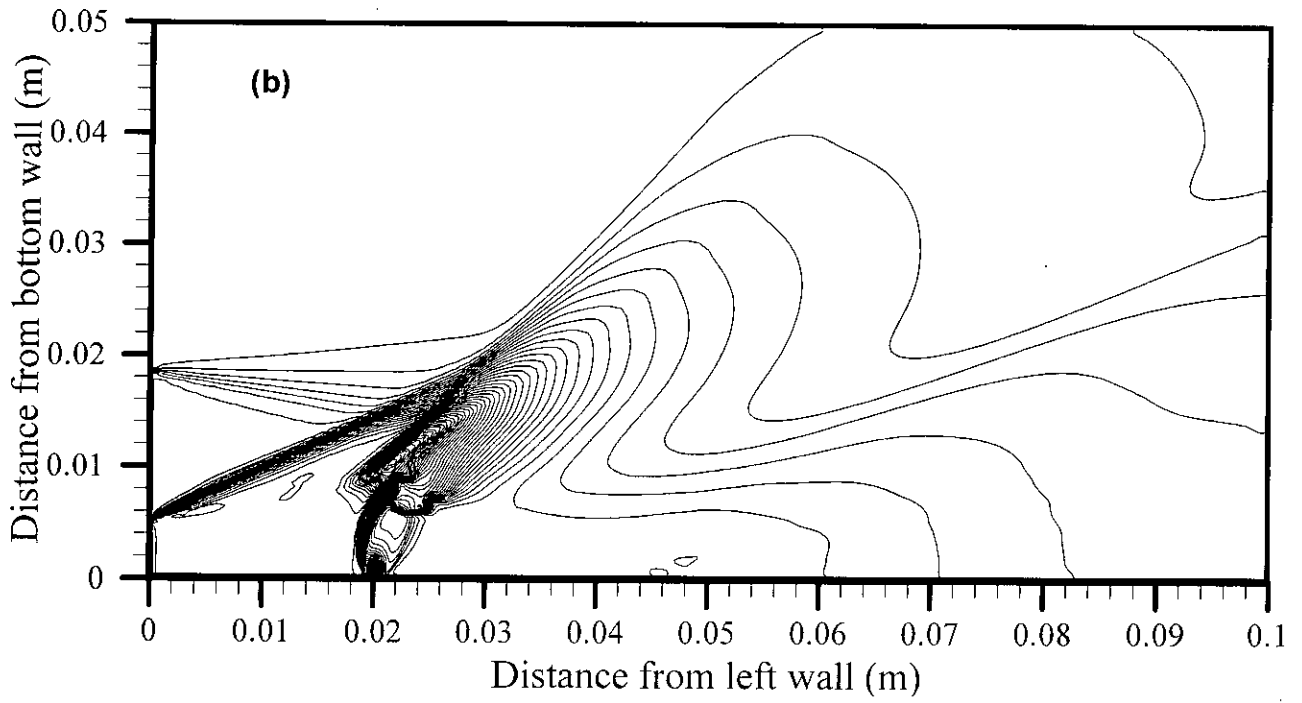


Fig. 3.7 (b) pressure (Pa) contour, $\phi (2 \cdot 10^4, 2 \cdot 10^6, 2 \cdot 10^4)$; Case-2 ($d=20$ mm)

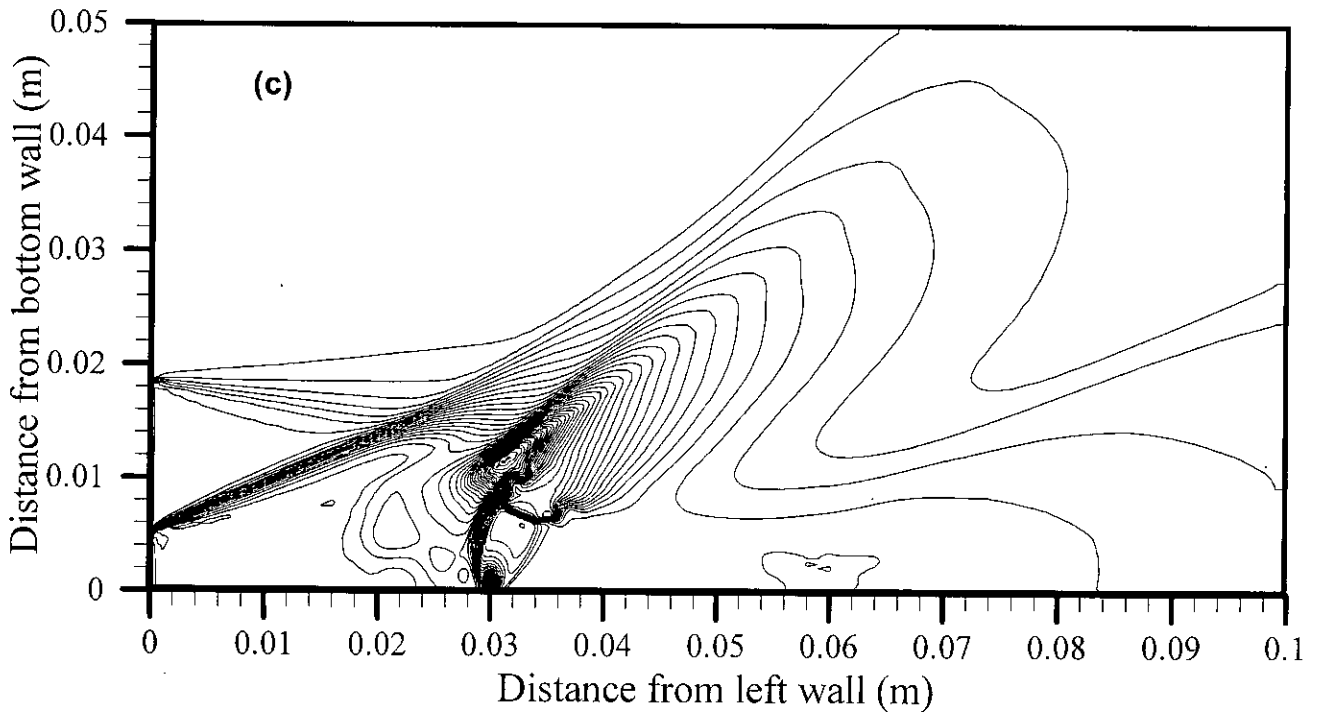


Fig. 3.7 (c) pressure (Pa) contour, $\phi (2 \cdot 10^4, 2 \cdot 10^6, 2 \cdot 10^4)$; Case-3 ($d=30$ mm)

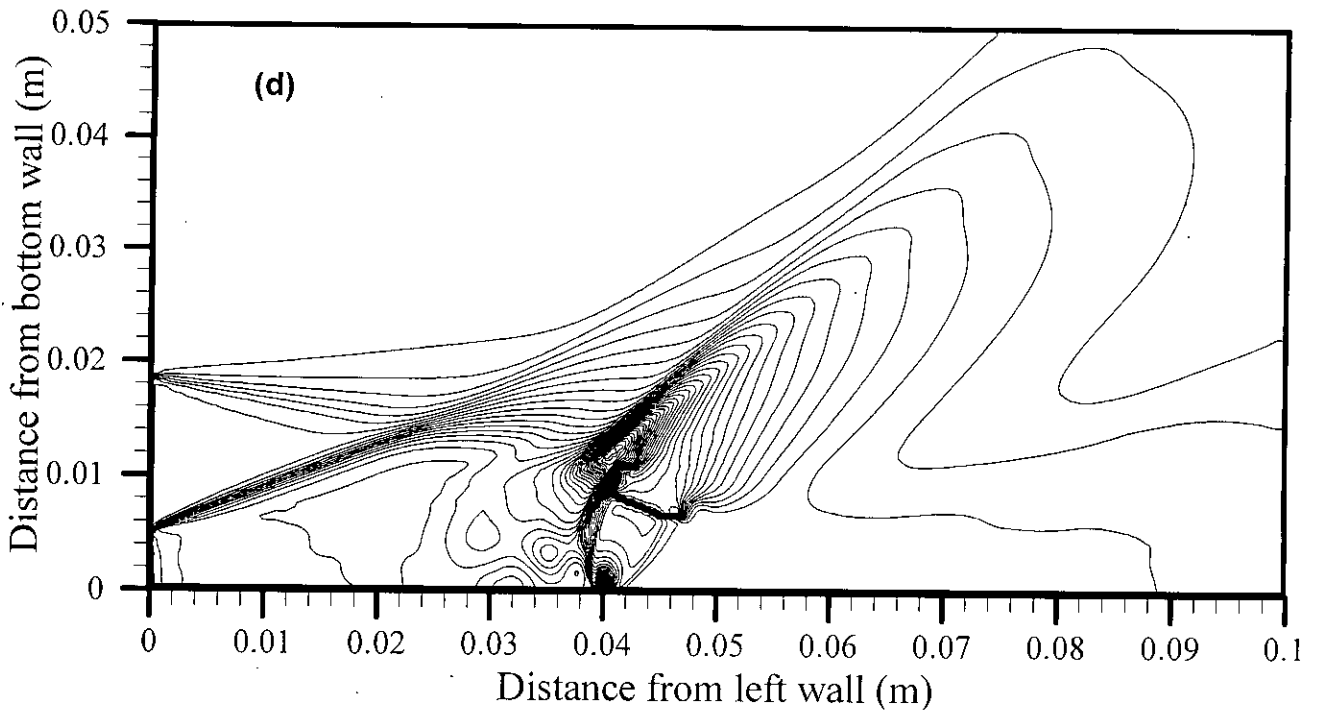


Fig. 3.7 (d) pressure (Pa) contour, $\phi (2 \cdot 10^4, 2 \cdot 10^6, 2 \cdot 10^4)$; Case-4 ($d=40$ mm)

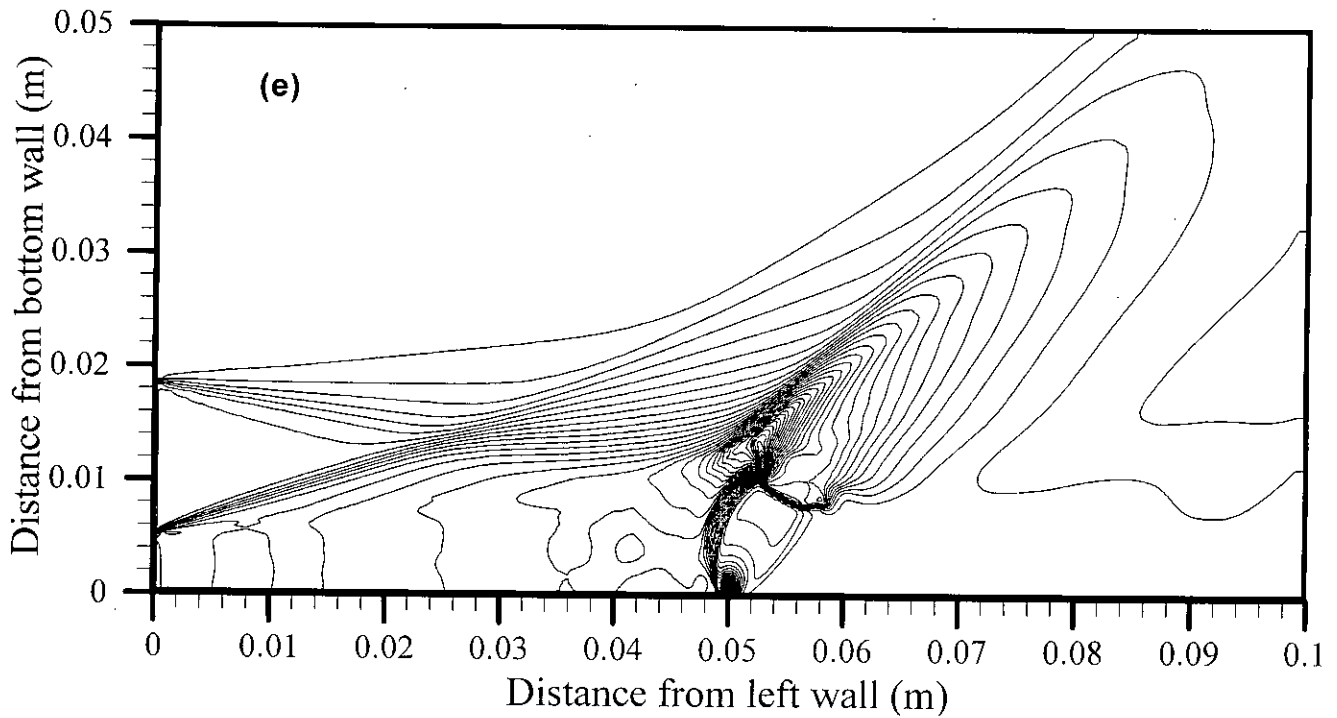


Fig. 3.7 (e) pressure (Pa) contour, $\phi (2 \cdot 10^4, 2 \cdot 10^6, 2 \cdot 10^4)$; Case-5 ($d=50$ mm)

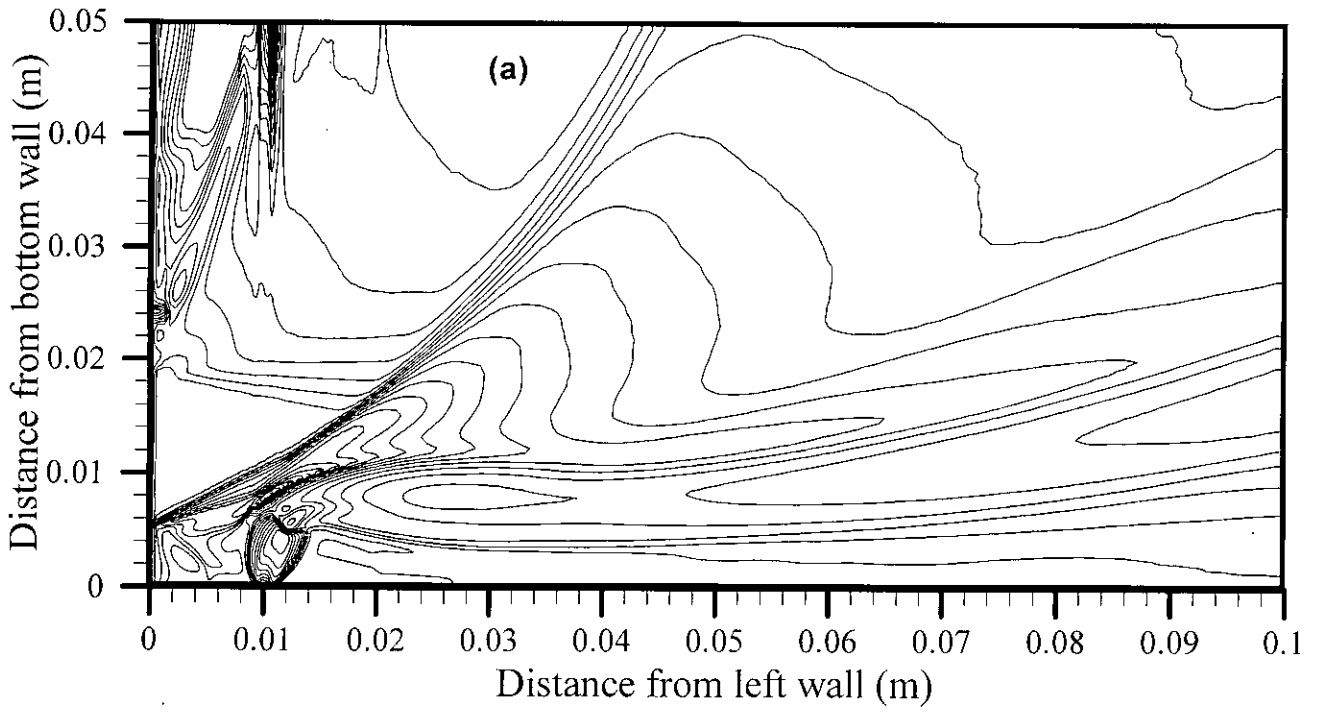


Fig. 3.8 (a) Temperature (K) contour, ϕ (250, 2550,100); Case-1 (d=10 mm)

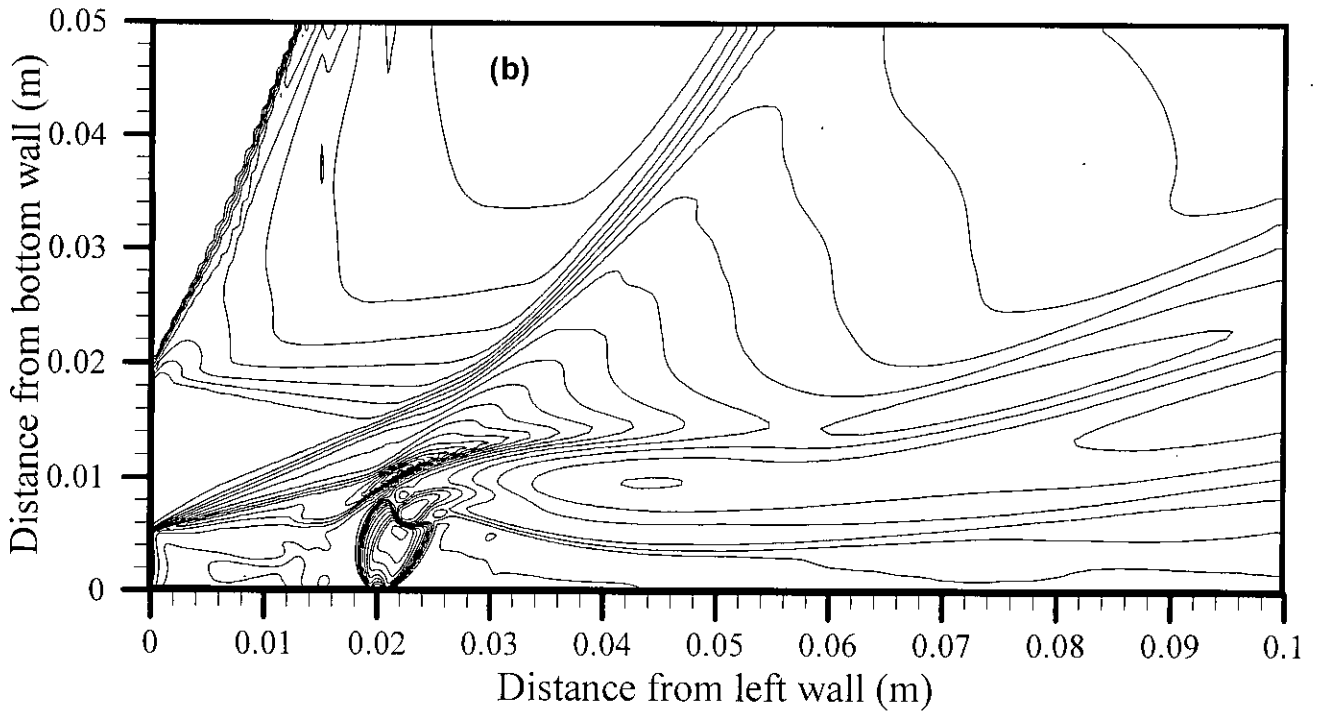


Fig. 3.8 (b) Temperature (K) contour, ϕ (250, 2550,100); Case-2 (d=20 mm)

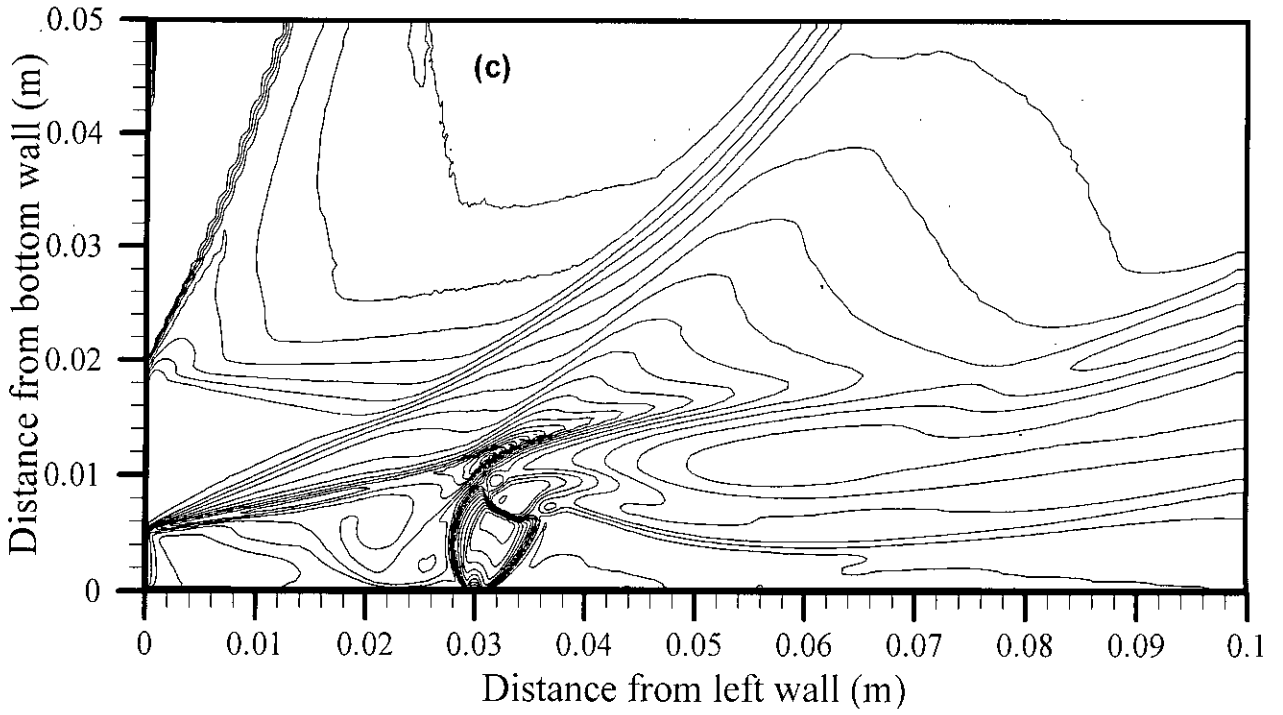


Fig. 3.8 (c) Temperature (K) contour, ϕ (250, 2550,100); Case-3 (d=30 mm)

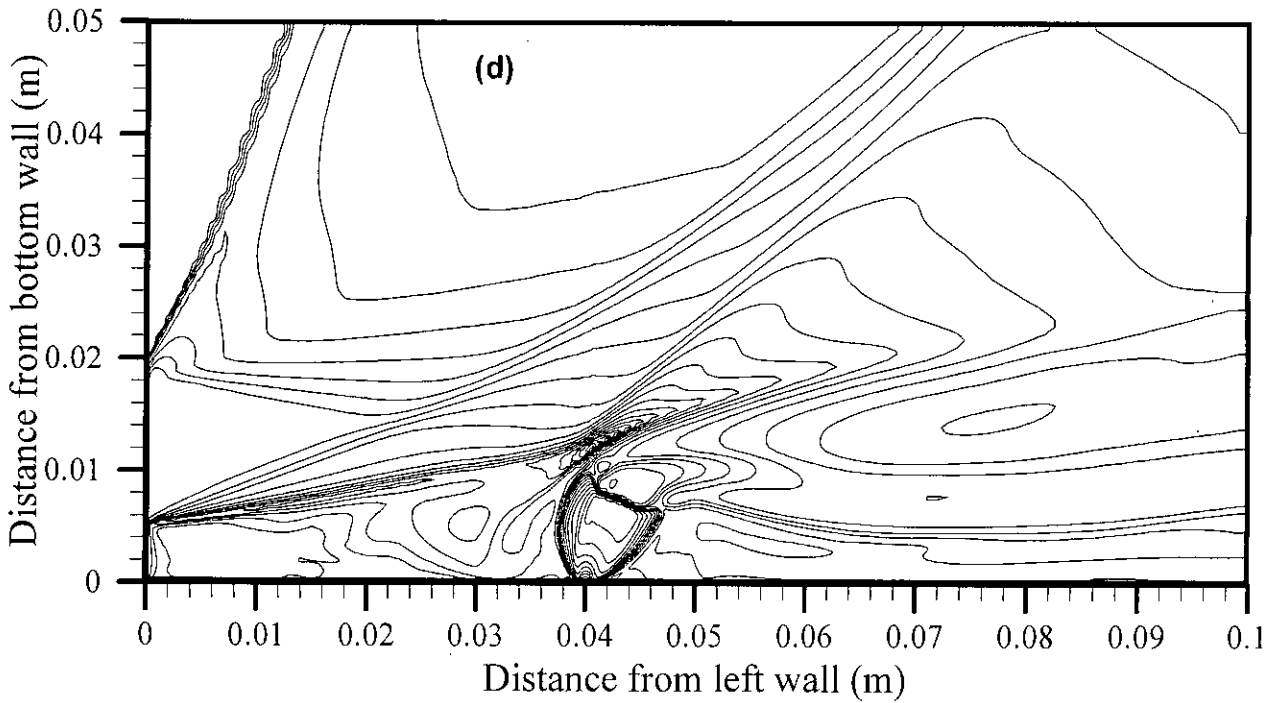


Fig. 3.8 (d) Temperature (K) contour, ϕ (250, 2550,100); Case-4 (d=40 mm)

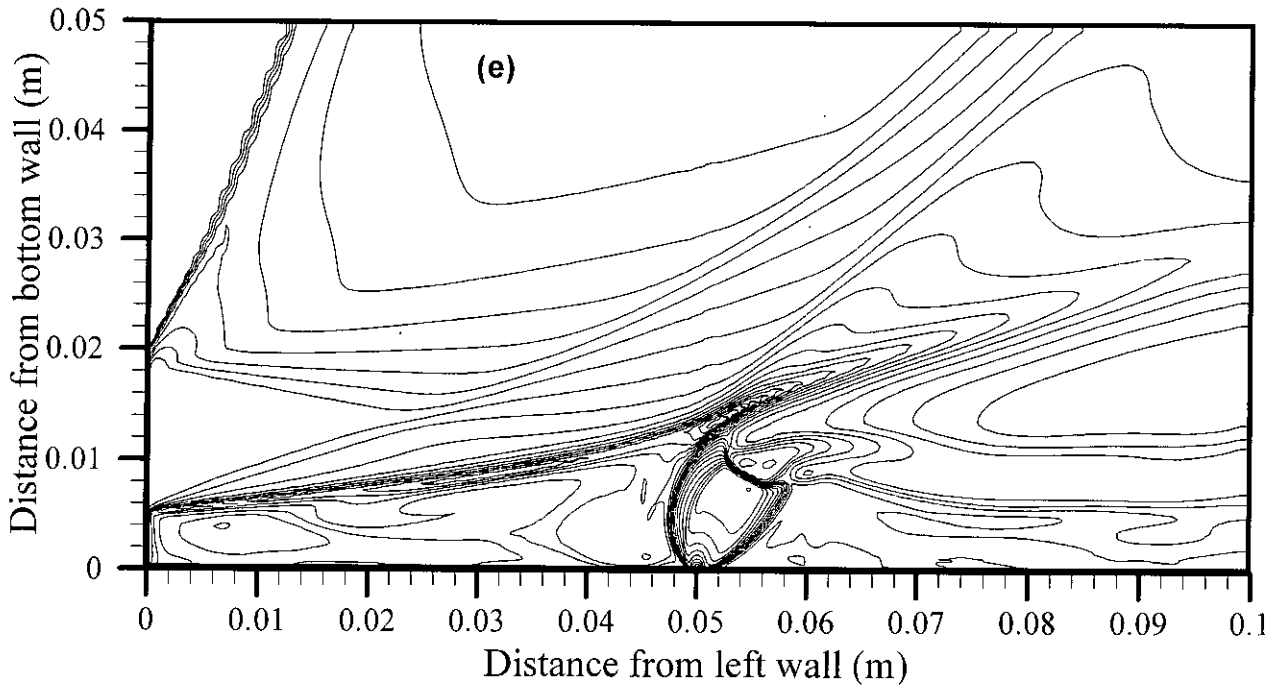


Fig. 3.8 (e) Temperature (K) contour, ϕ (250, 2550, 100); Case-5 ($d=50$ mm)

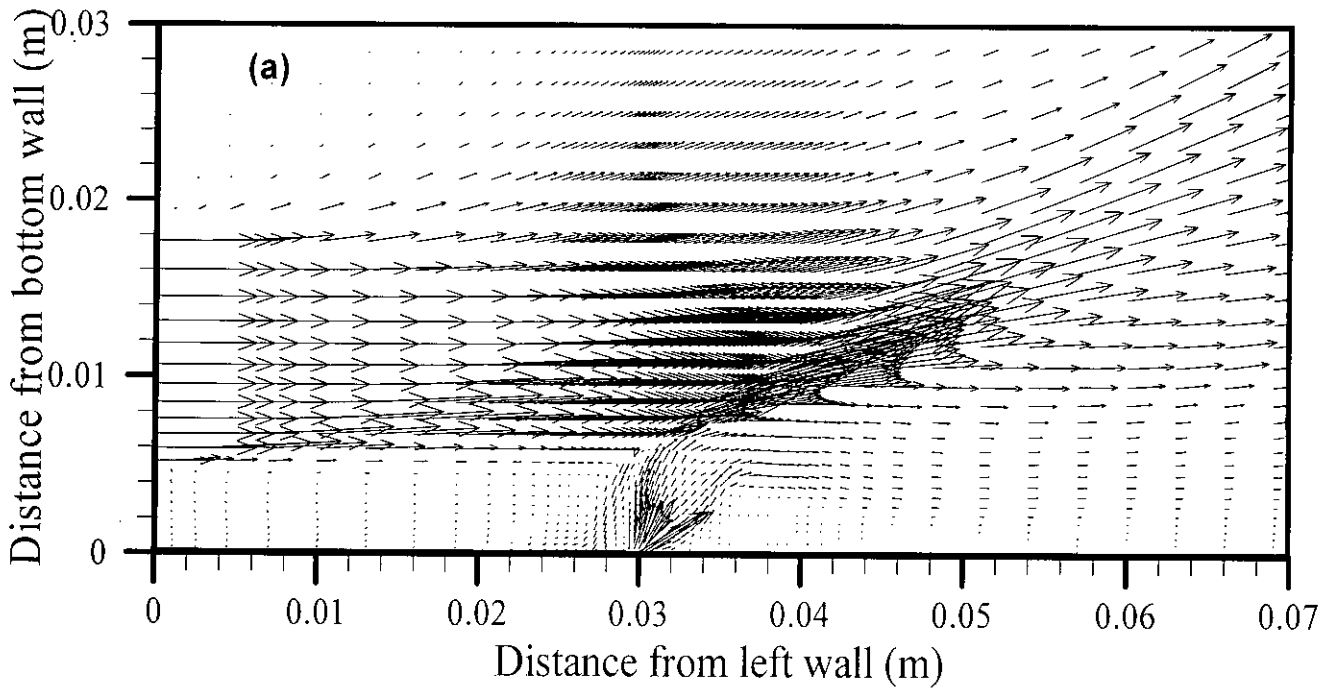


Fig. 3.9 (a) Velocity vector near injector; Case-6 ($\theta = 30^\circ$)

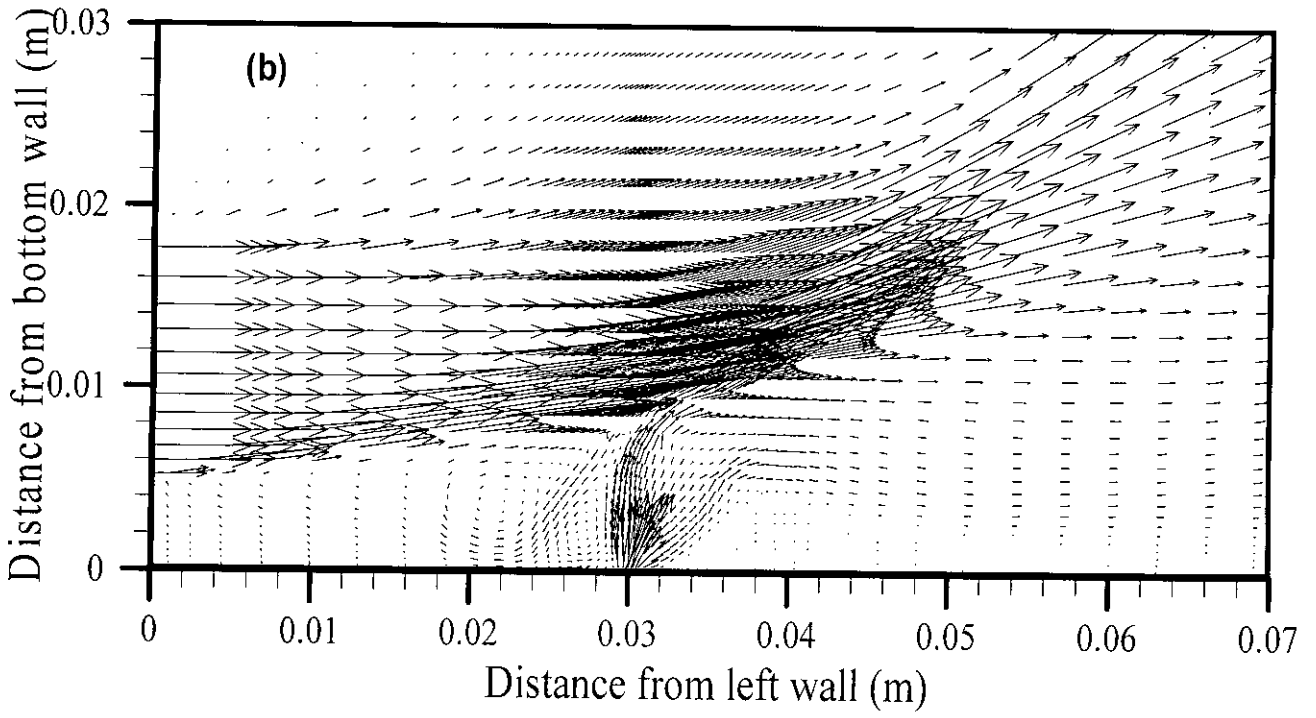


Fig. 3.9 (b) Velocity vector near injector; Case-7 ($\theta = 60^\circ$)

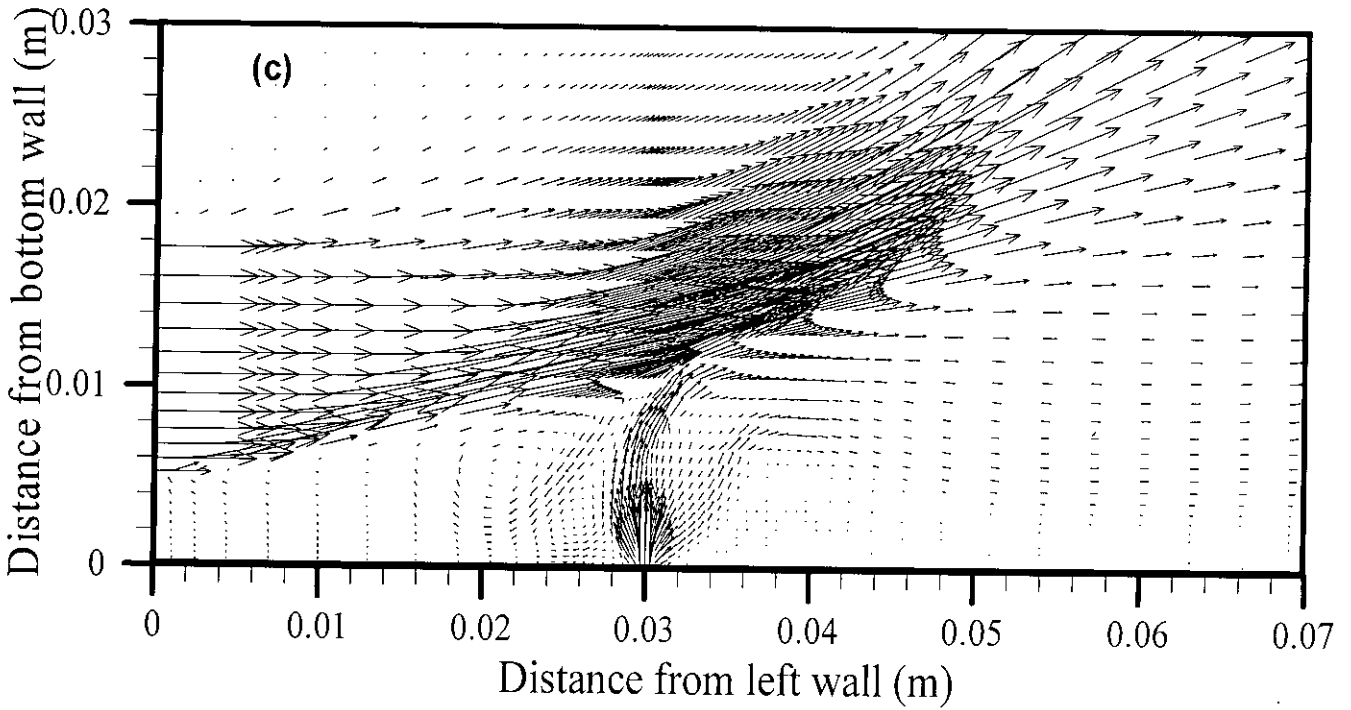


Fig. 3.9 (c) Velocity vector near injector; Case-8 ($\theta = 90^\circ$)

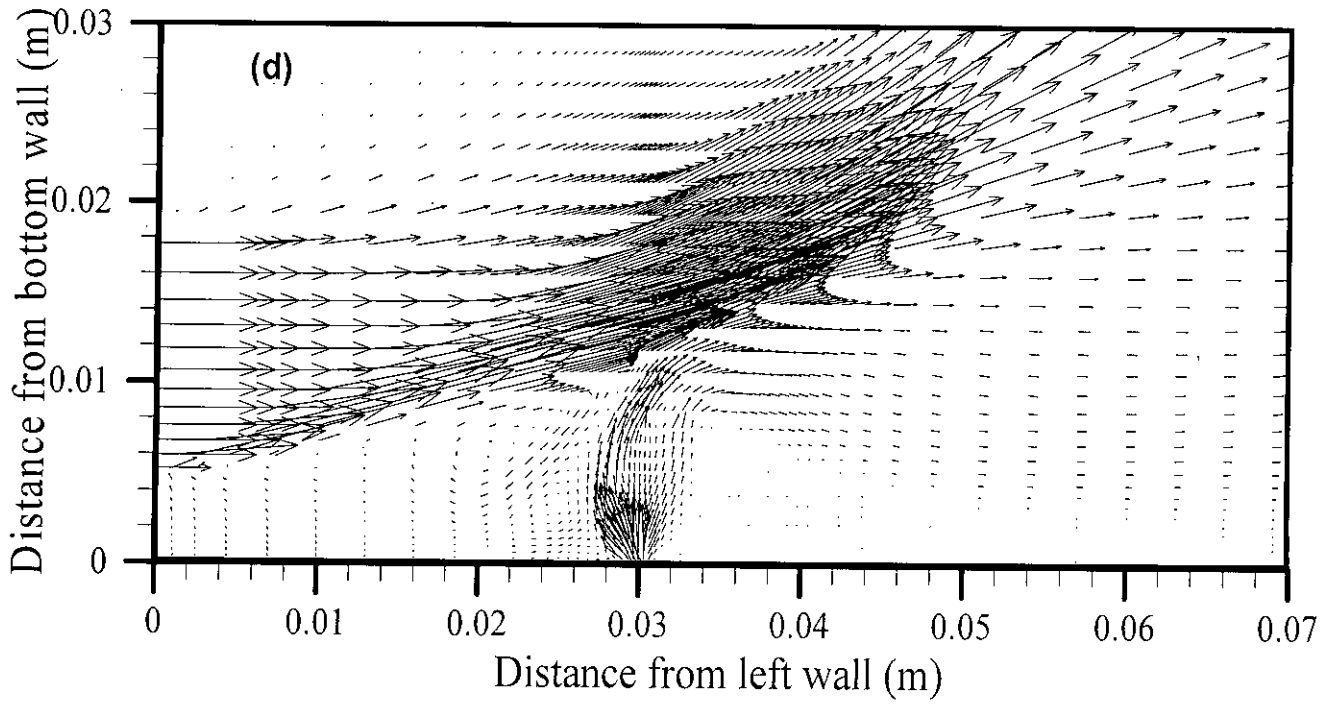


Fig. 3.9 (d) Velocity vector near injector; Case-9 ($\theta = 120^\circ$)

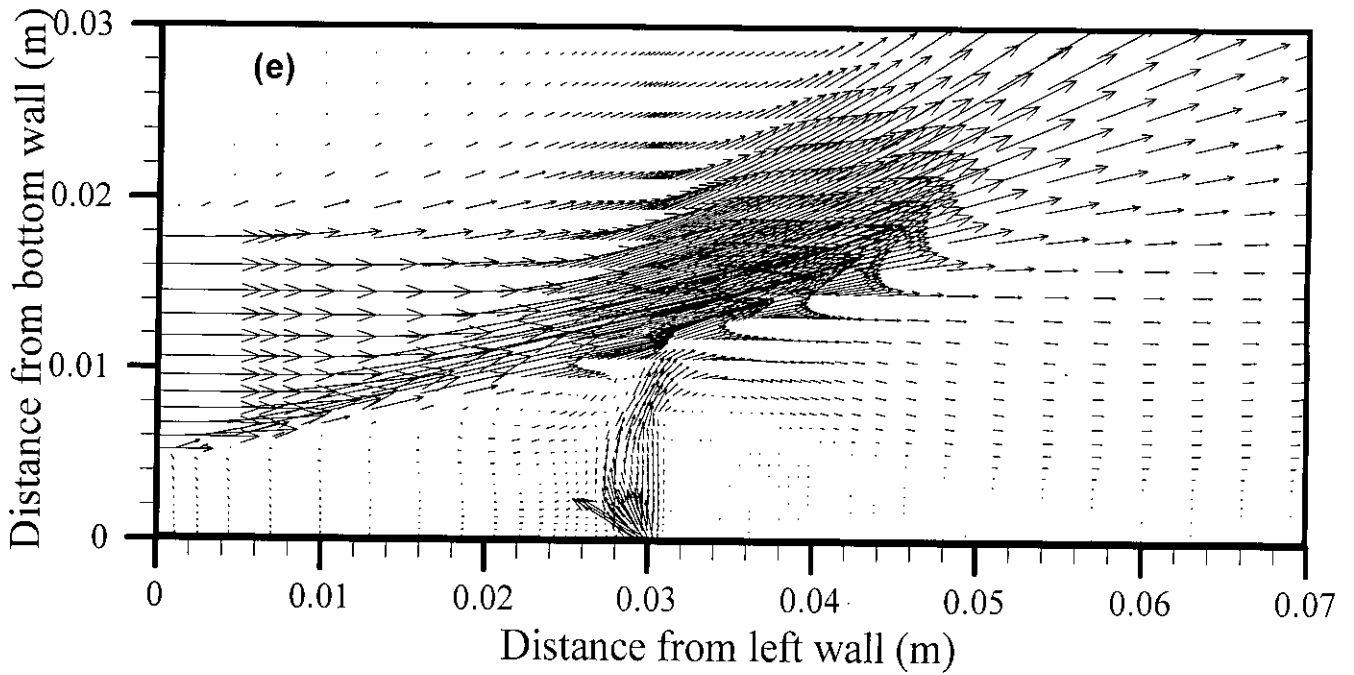


Fig. 3.9 (e) Velocity vector near injector; Case-10 ($\theta = 150^\circ$)

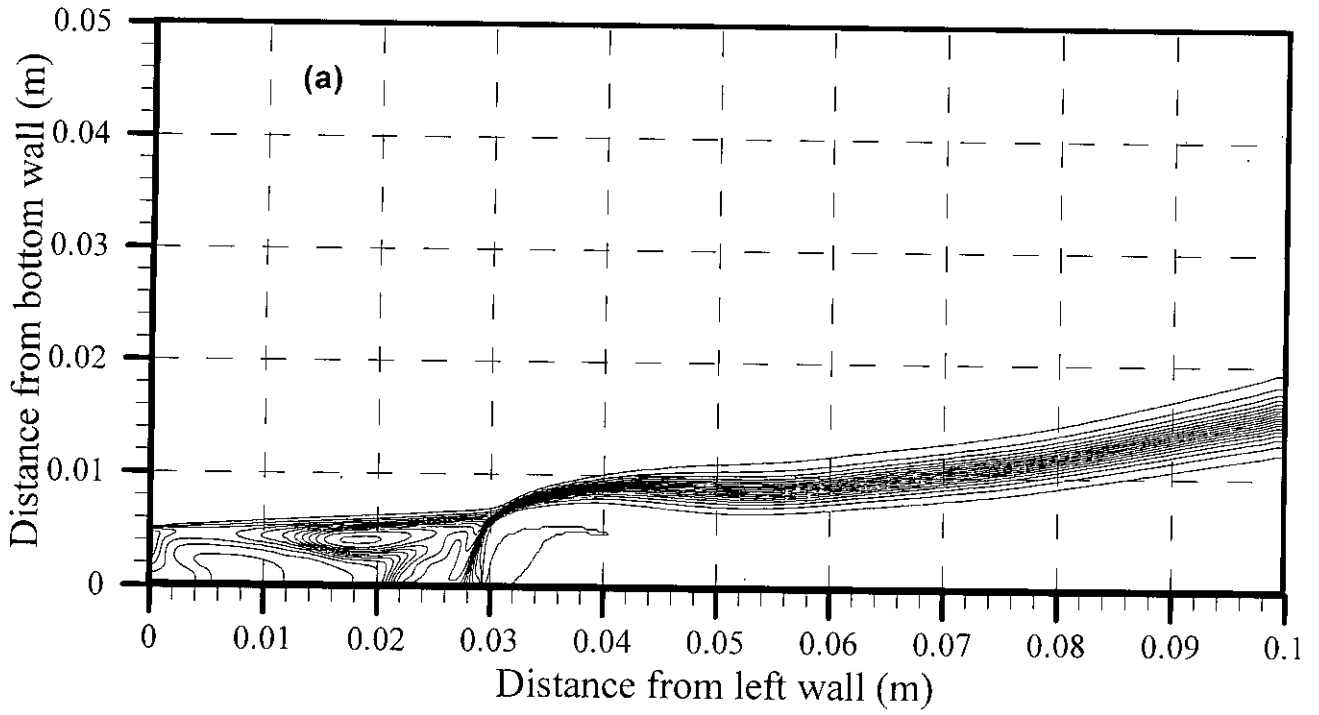


Fig. 3.10 (a) Mole fraction contour of Hydrogen, ϕ (0.05, 1.0, 0.05); Case-6 ($\theta = 30^\circ$)

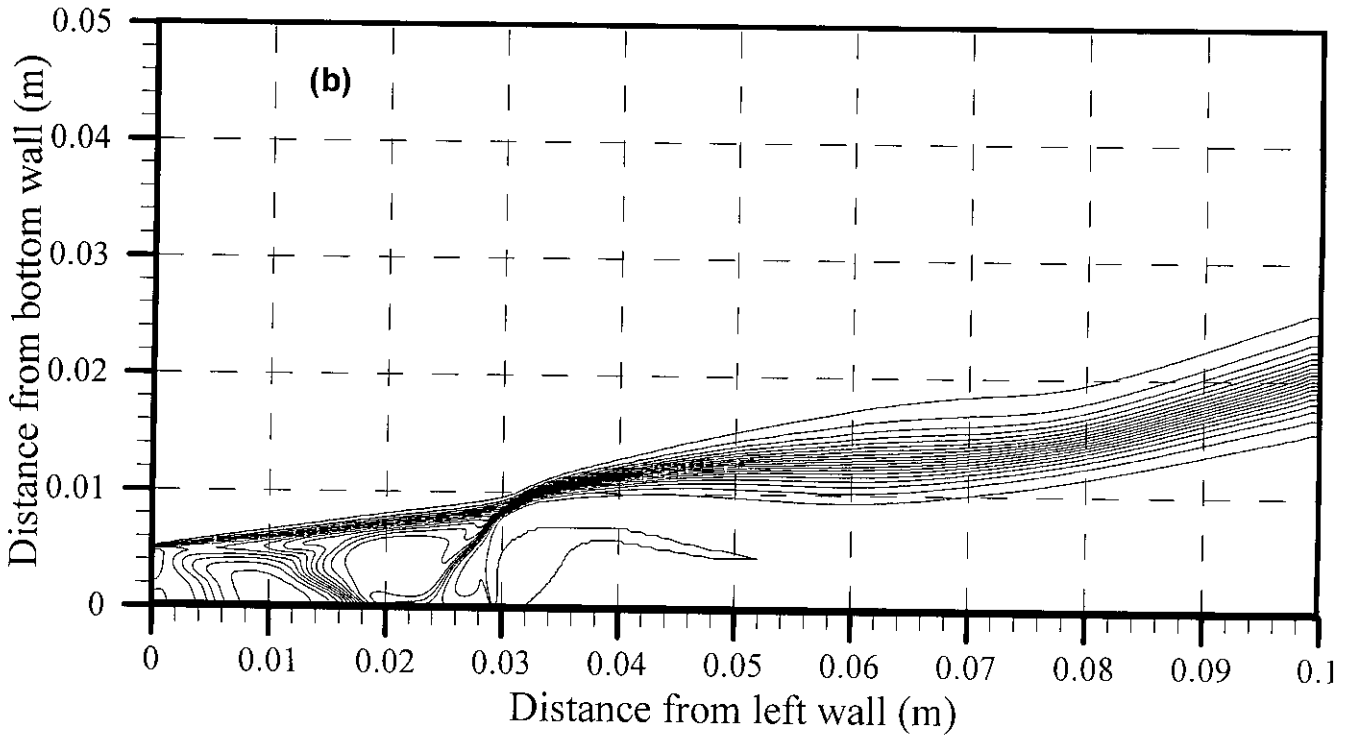


Fig. 3.10 (b) Mole fraction contour of Hydrogen, ϕ (0.05, 1.0, 0.05); Case-7 ($\theta = 60^\circ$)

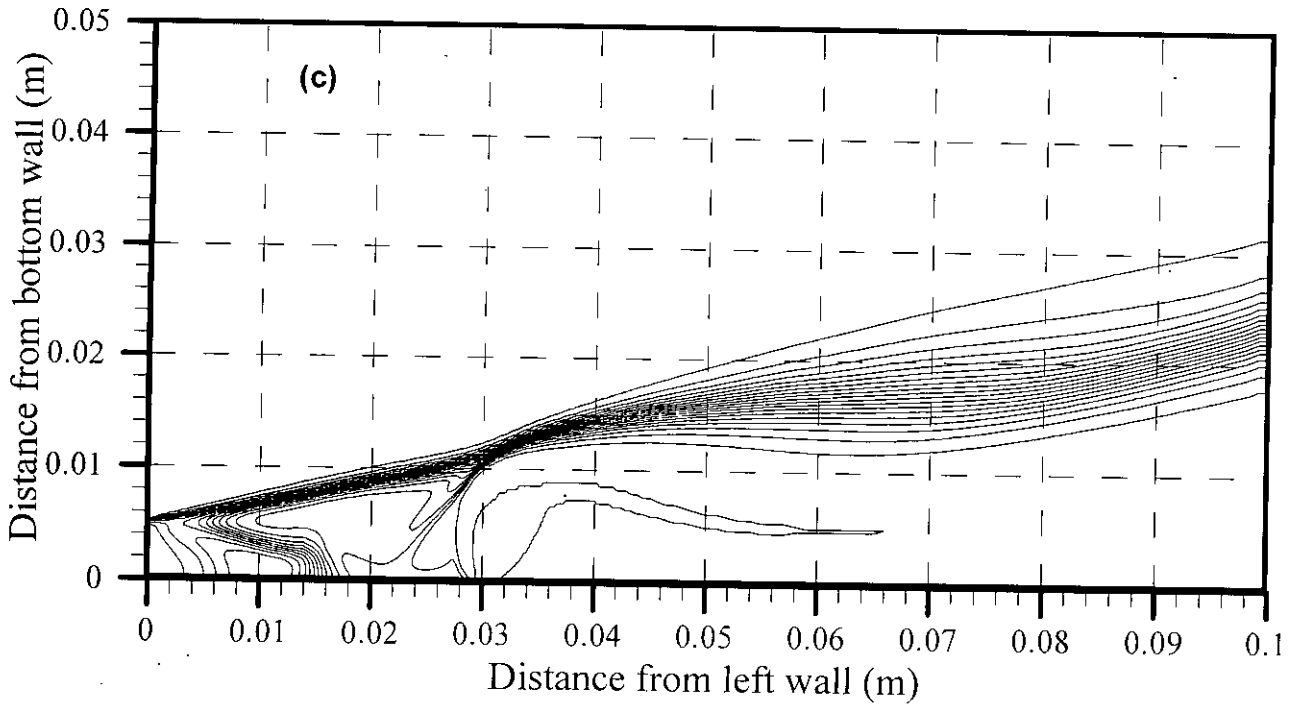


Fig. 3.10 (c) Mole fraction contour of Hydrogen, ϕ (0.05, 1.0, 0.05); Case-8 ($\theta = 90^\circ$)

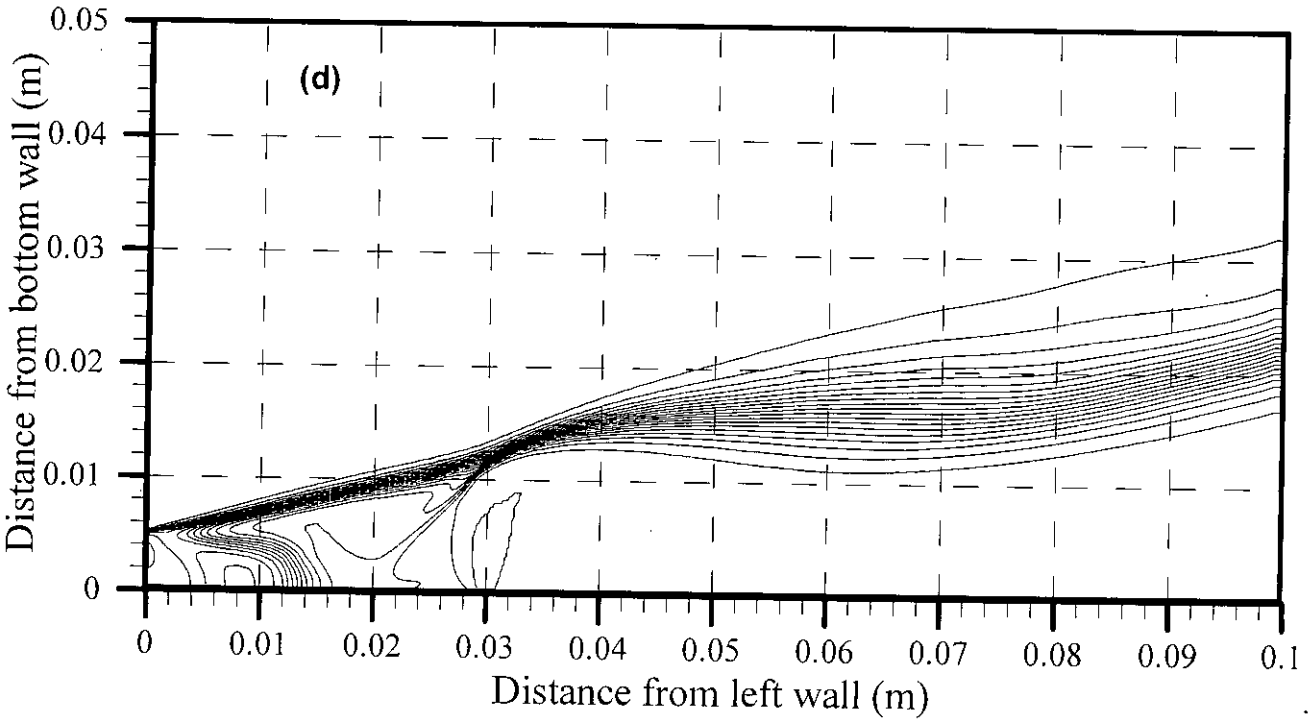


Fig. 3.10 (d) Mole fraction contour of Hydrogen, ϕ (0.05, 1.0, 0.05); Case-9 ($\theta = 120^\circ$)

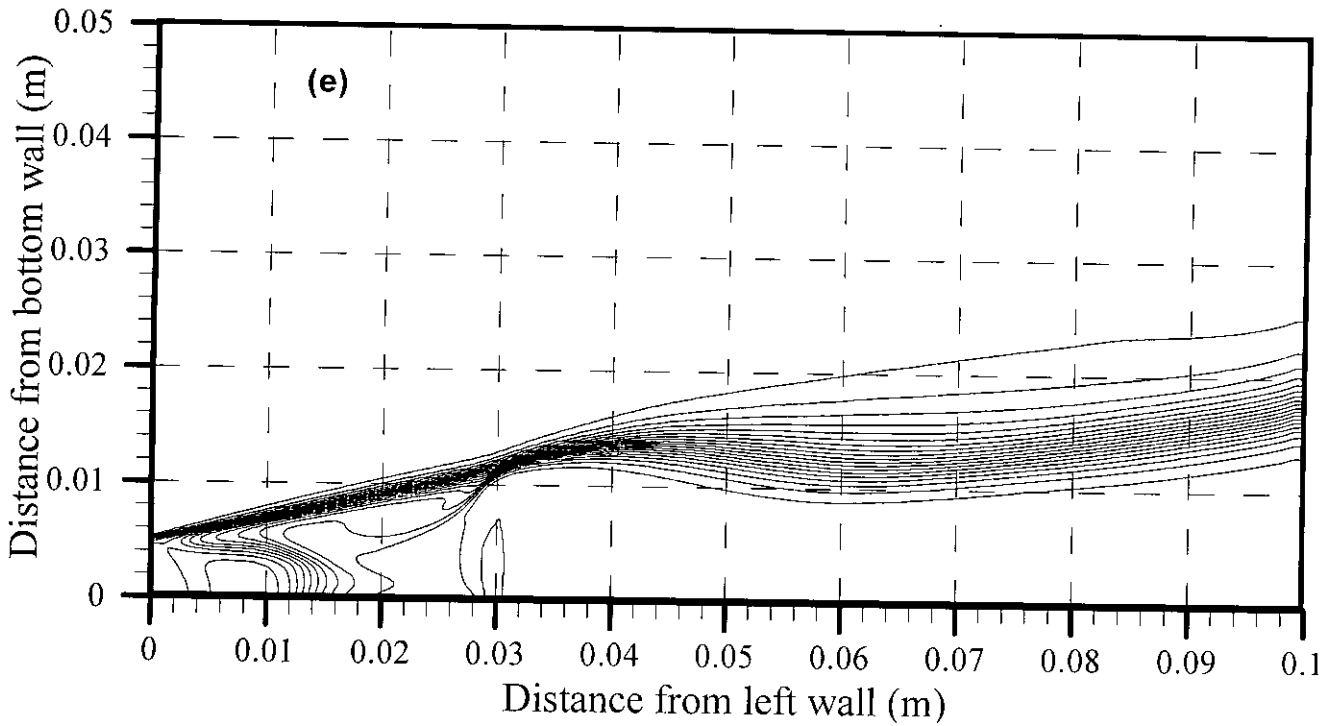


Fig. 3.10 (e) Mole fraction contour of Hydrogen, ϕ (0.05, 1.0, 0.05); Case-10 ($\theta = 150^\circ$)

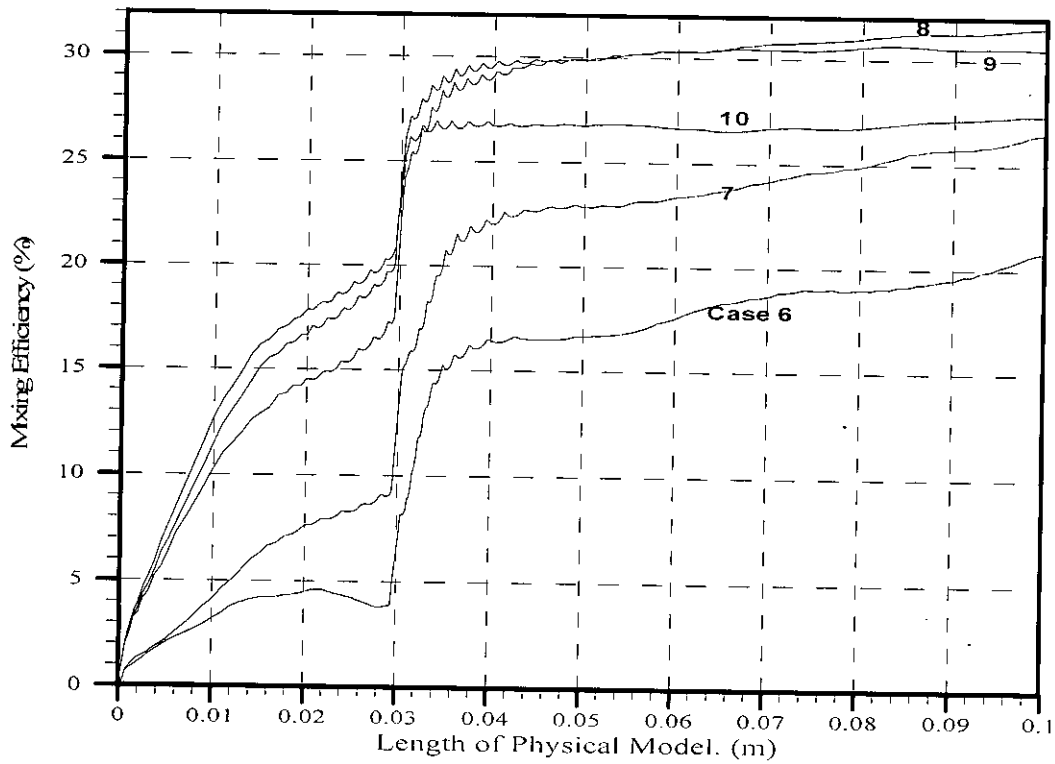


Fig. 3.11 Mixing efficiency along the length of physical model

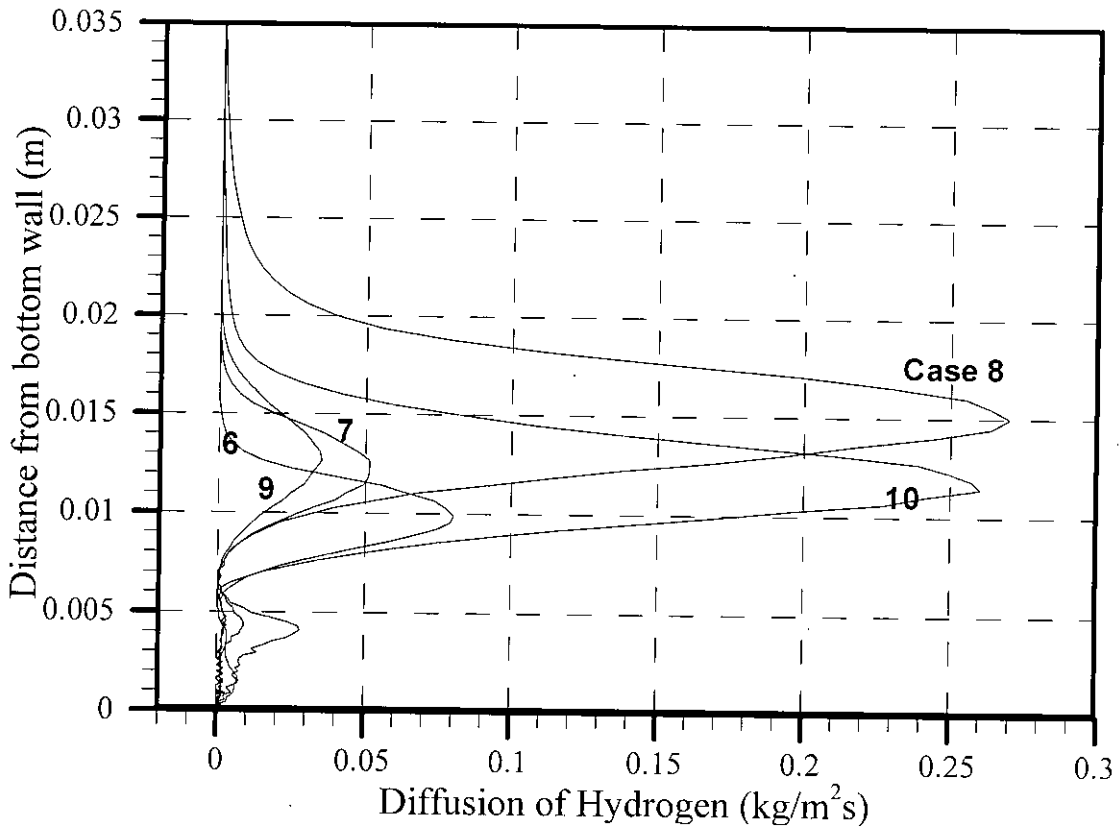


Fig. 3.12 Diffusion of Hydrogen at 0.08m from left wall

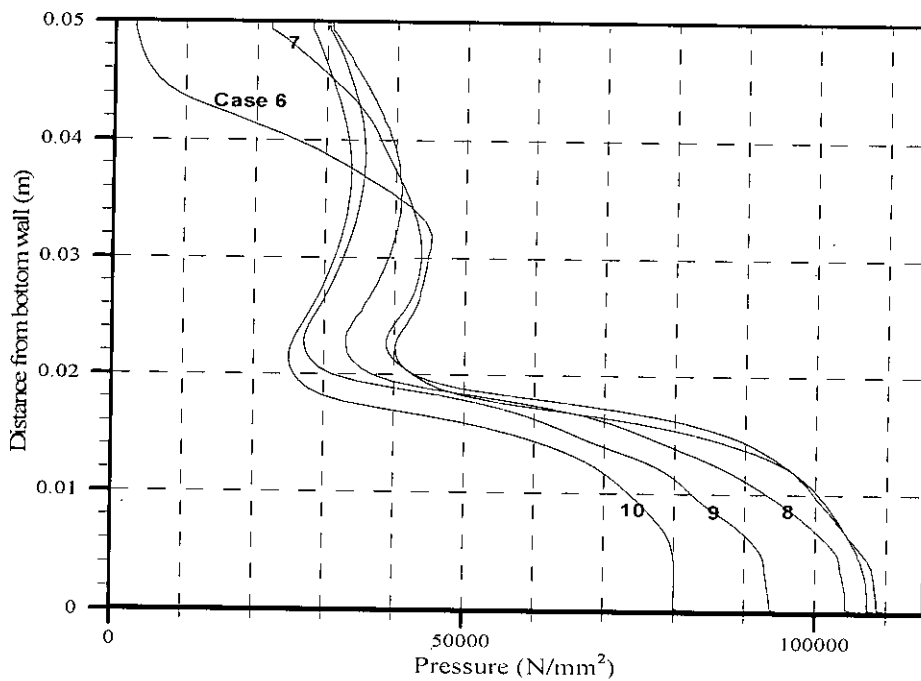


Fig. 3.13 Pressure distribution at 0.08m from left wall.

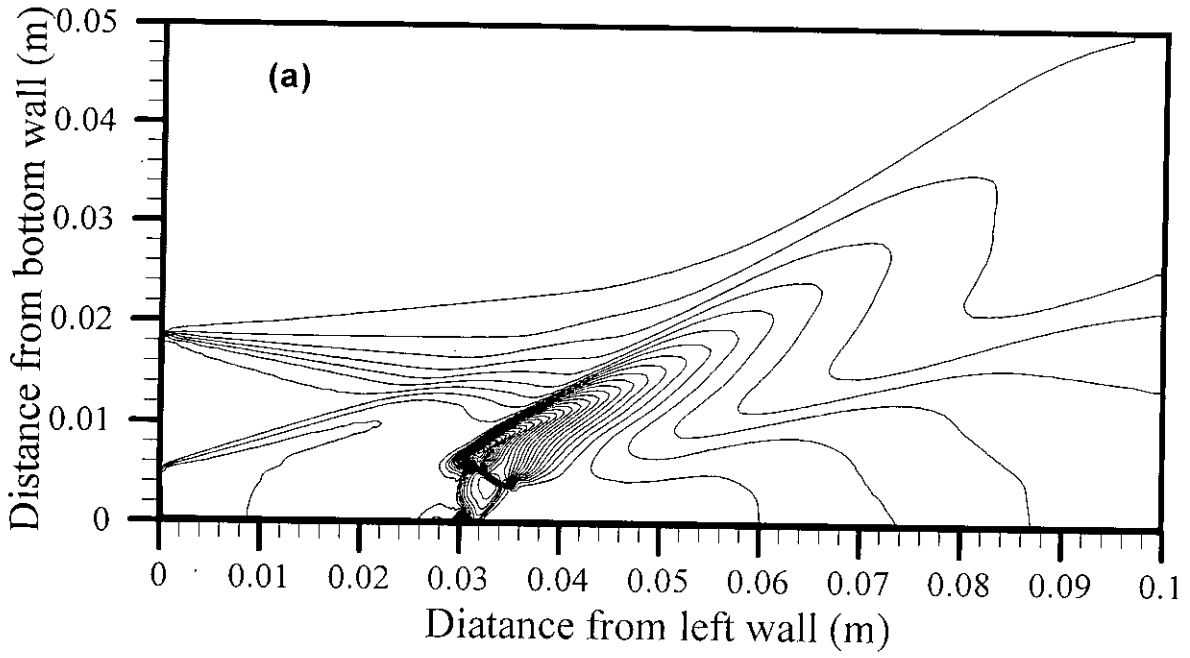


Fig. 3.14 (a) Pressure (Pa) contour, ϕ ($2 \cdot 10^4$, $2 \cdot 10^6$, $2 \cdot 10^4$); Case-6 ($\theta = 30^\circ$)

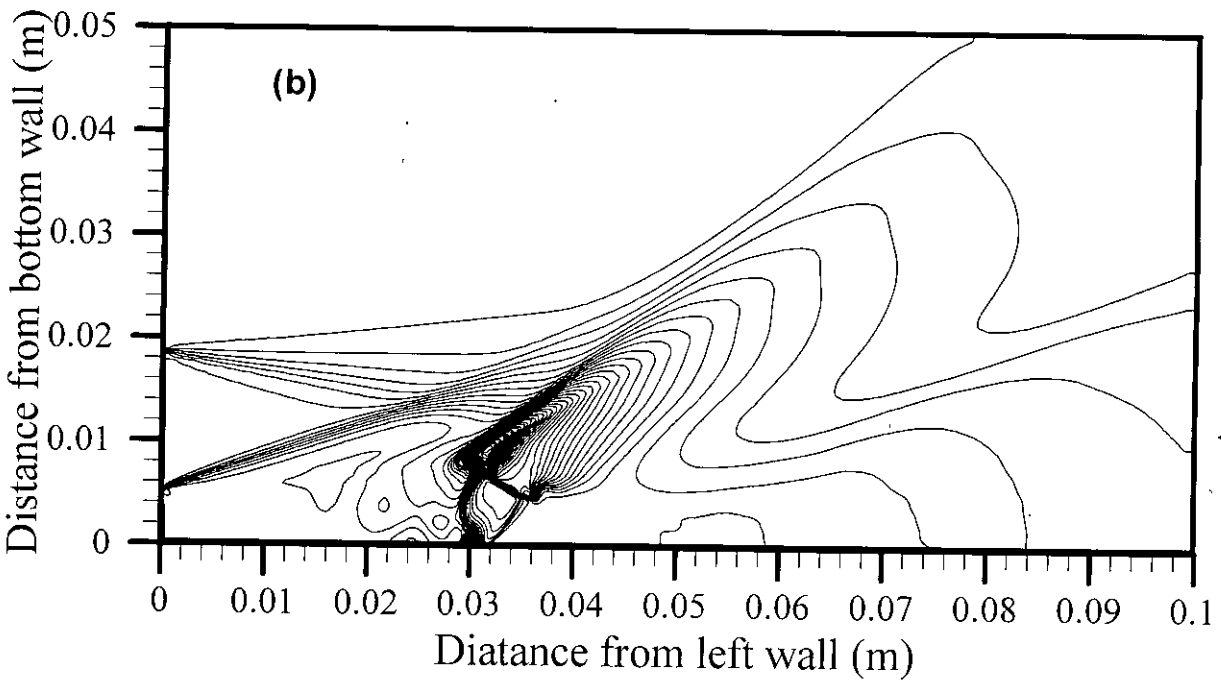


Fig. 3.14 (b) Pressure (Pa) contour, ϕ ($2 \cdot 10^4$, $2 \cdot 10^6$, $2 \cdot 10^4$); Case-7 ($\theta = 60^\circ$)

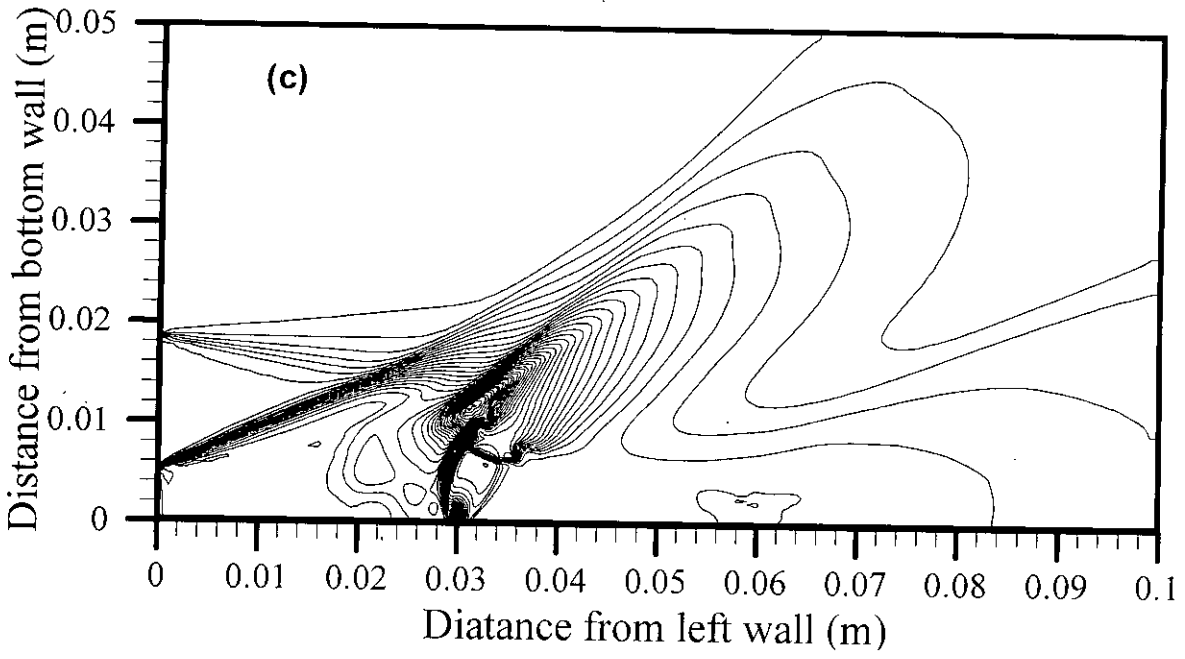


Fig. 3.14 (c) Pressure (Pa) contour, ϕ ($2 \cdot 10^4$, $2 \cdot 10^6$, $2 \cdot 10^4$); Case-8 ($\theta = 90^\circ$)

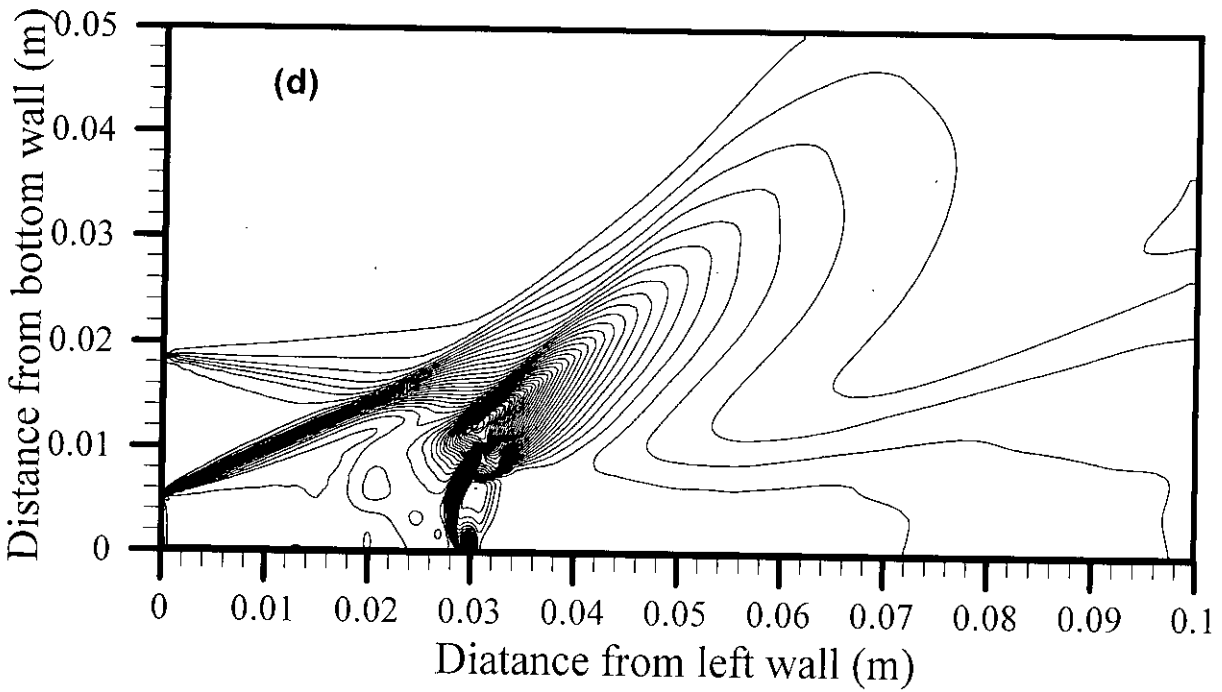


Fig. 3.14 (d) Pressure (Pa) contour, ϕ ($2 \cdot 10^4$, $2 \cdot 10^6$, $2 \cdot 10^4$); Case-9 ($\theta = 120^\circ$)

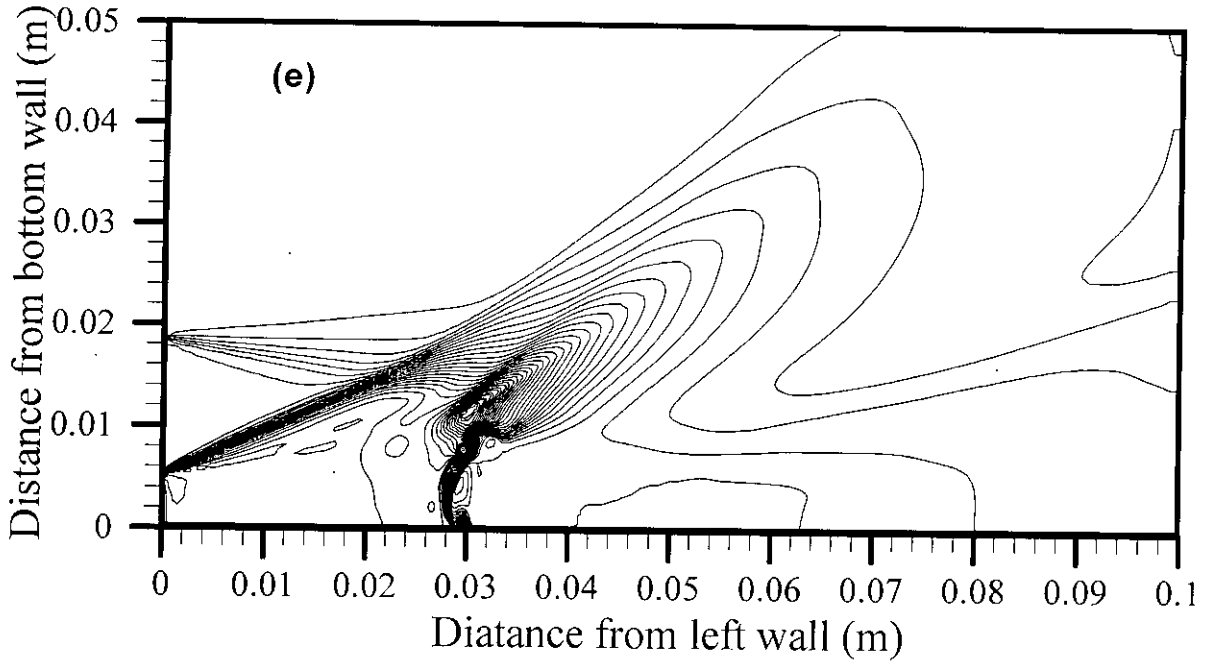


Fig. 3.14 (e) Pressure (Pa) contour, ϕ ($2 \cdot 10^4$, $2 \cdot 10^6$, $2 \cdot 10^4$); Case-10 ($\theta = 120^\circ$)

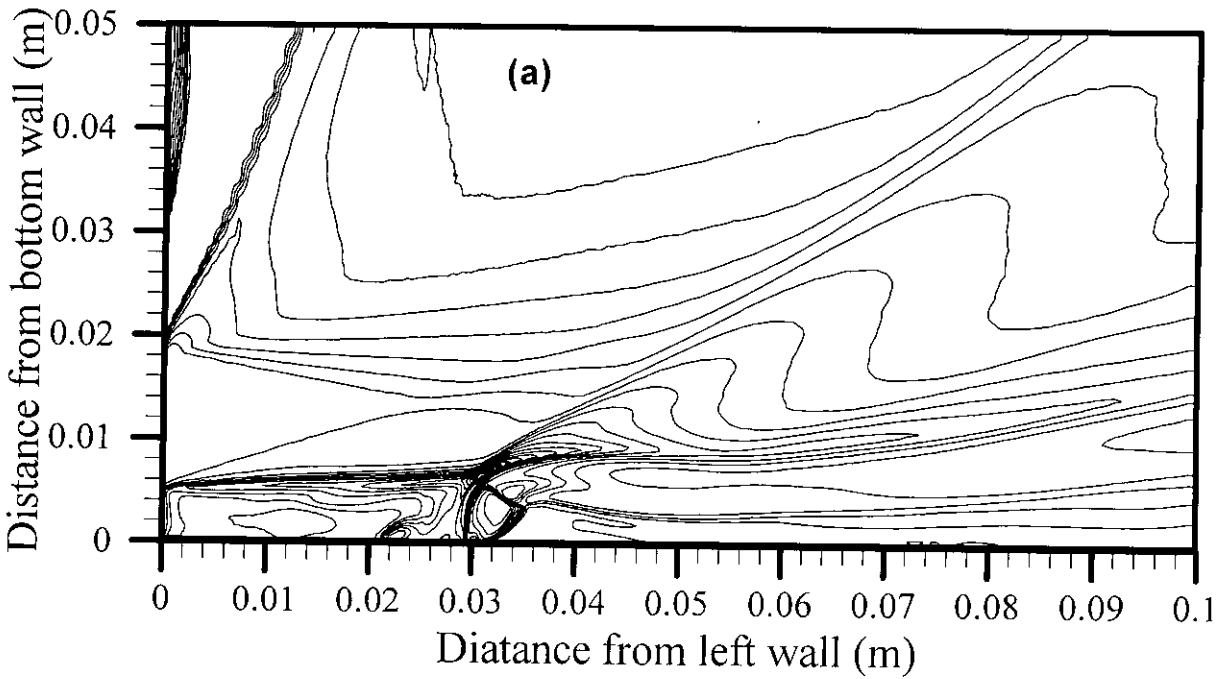


Fig. 3.15 (a) Temperature (K) contour, ϕ (250, 2550, 100); Case-6 ($\theta = 30^\circ$)

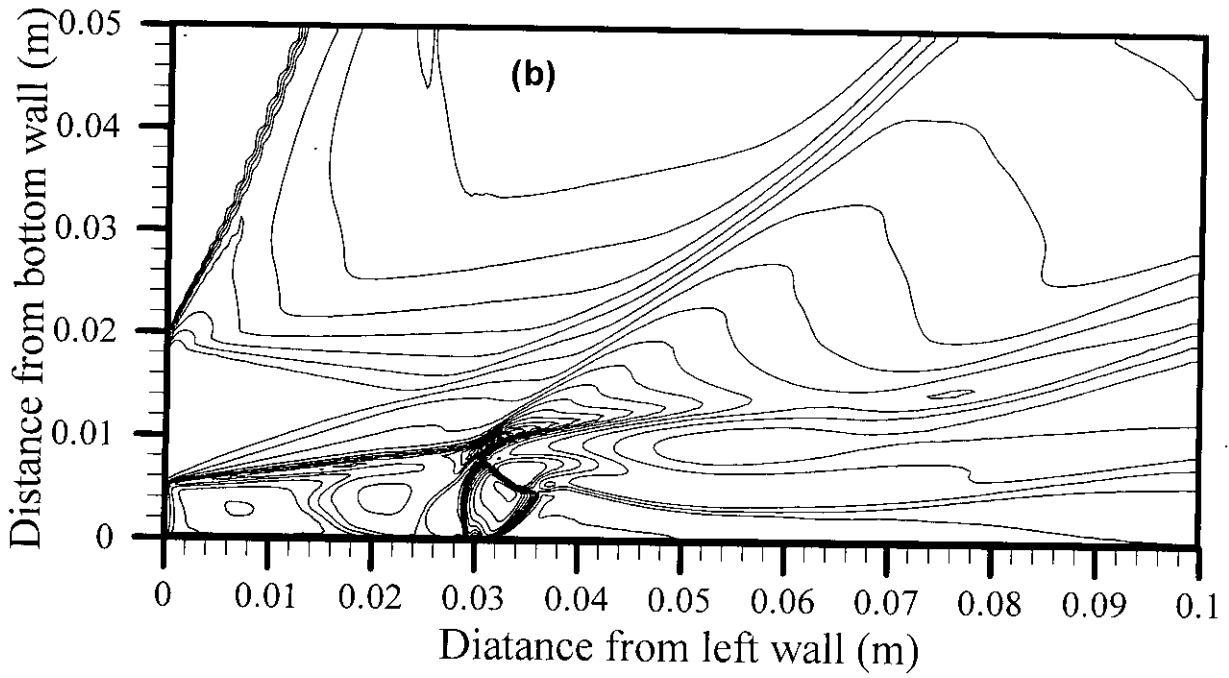


Fig. 3.15 (b) Temperature (K) contour, ϕ (250, 2550,100); Case-7 ($\theta = 60^\circ$)

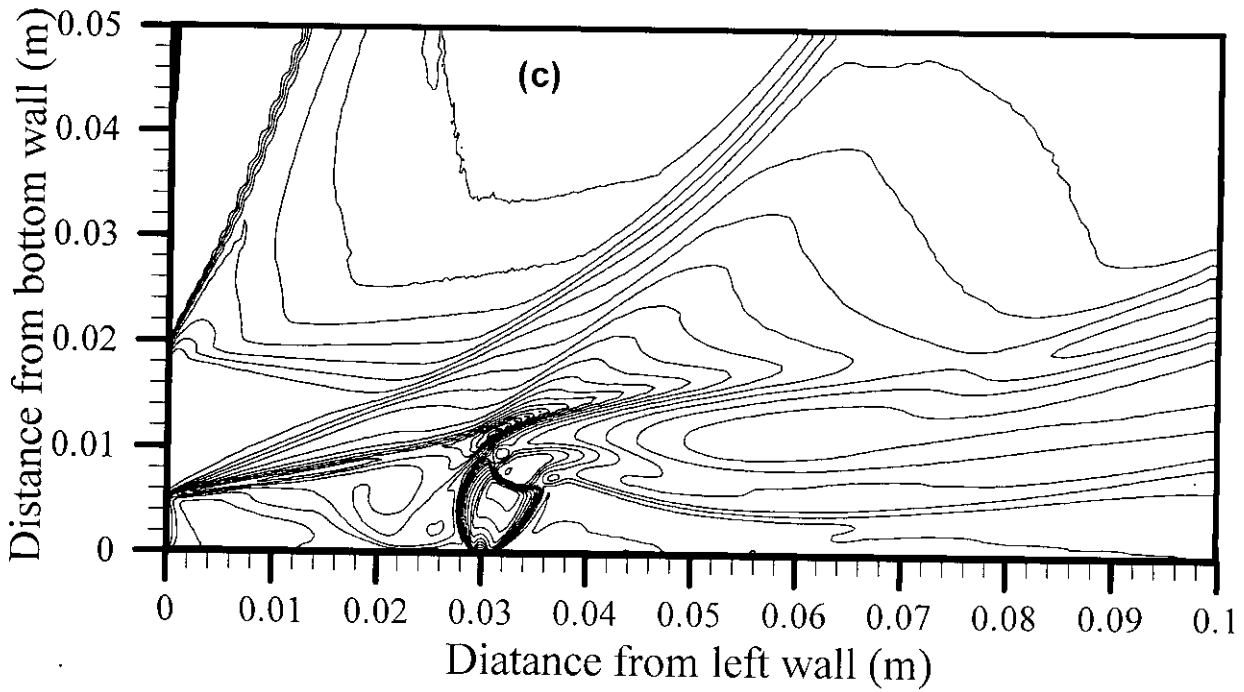


Fig. 3.15 (c) Temperature (K) contour, ϕ (250, 2550,100); Case-8 ($\theta = 90^\circ$)

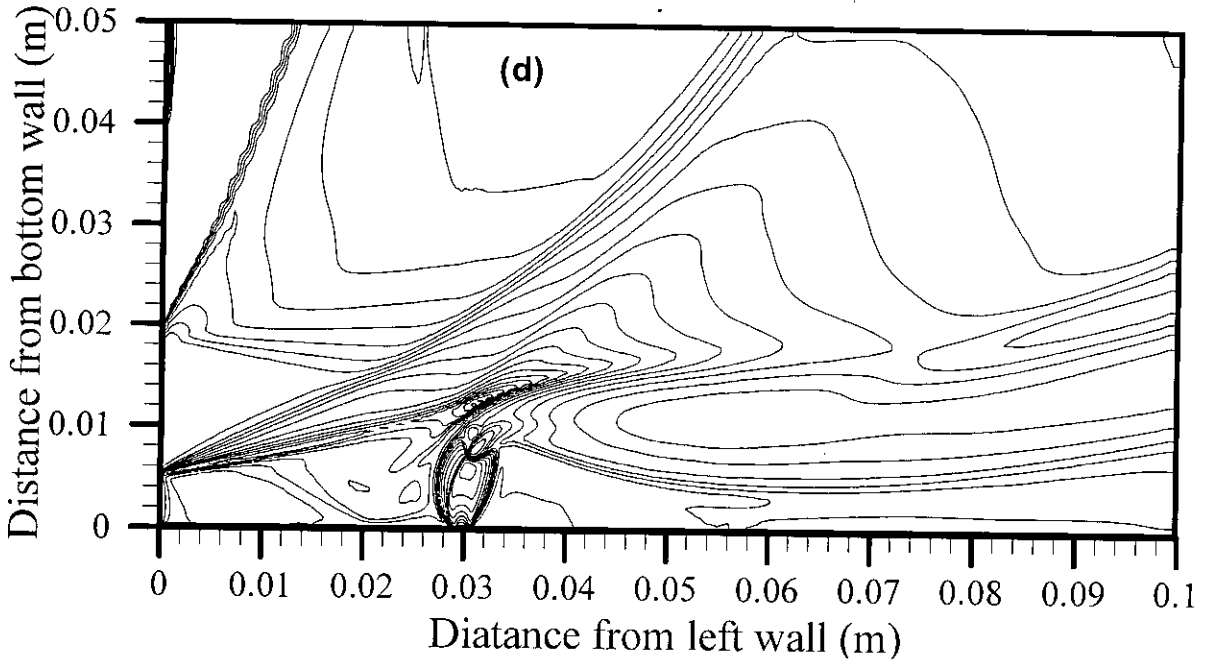


Fig. 3.15 (d) Temperature (K) contour, ϕ (250, 2550,100); Case-9 ($\theta = 120^\circ$)

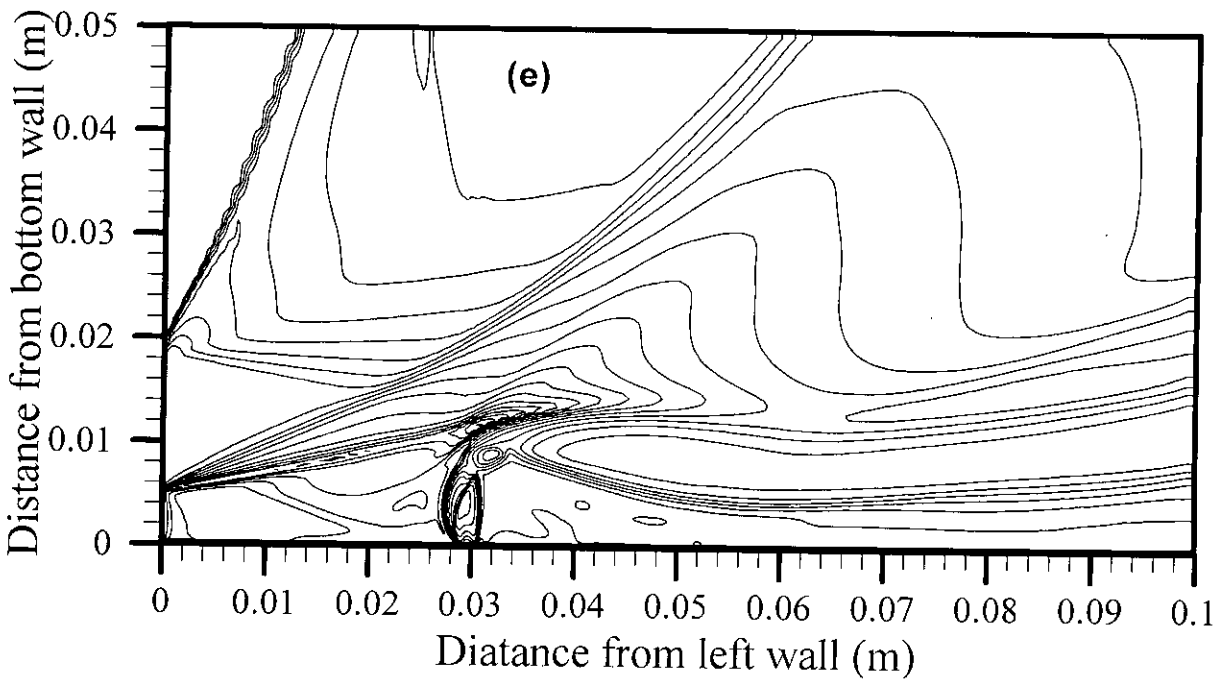


Fig. 3.15 (e) Temperature (K) contour, ϕ (250, 2550,100); Case-10 ($\theta = 150^\circ$)

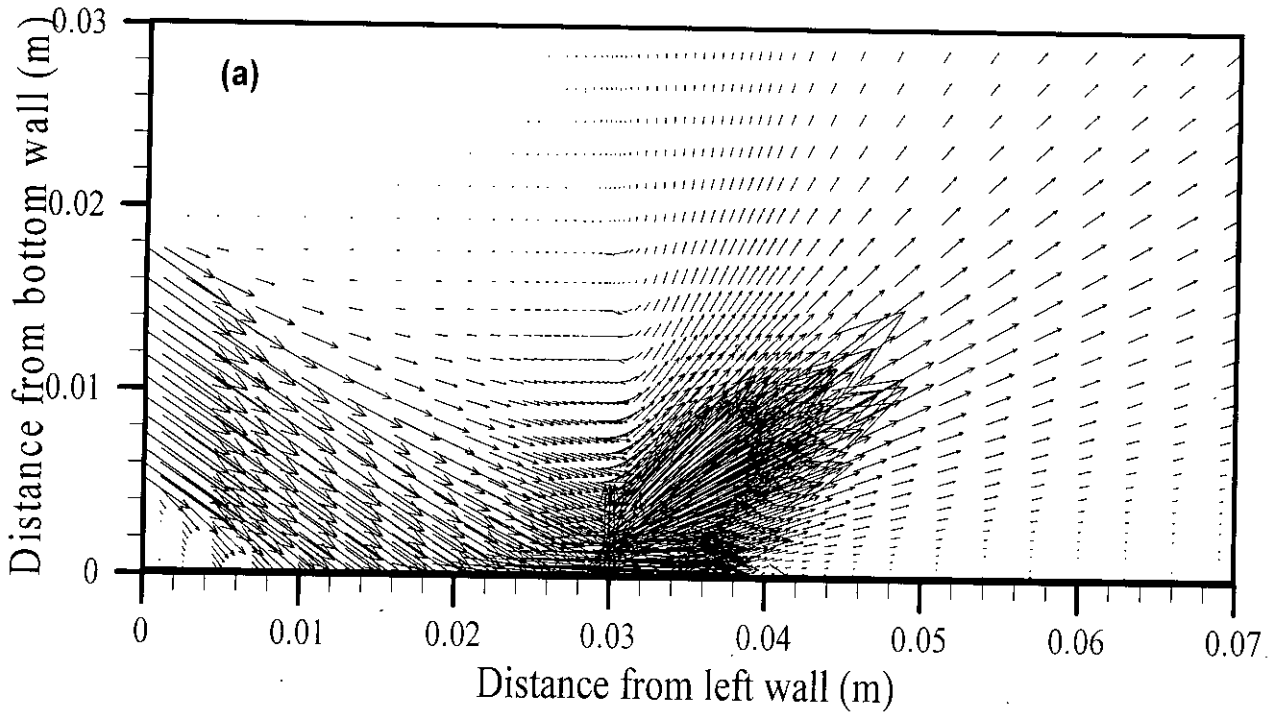


Fig. 3.16 (a) Velocity vector near injector; Case-11 ($\psi = 60^\circ$)

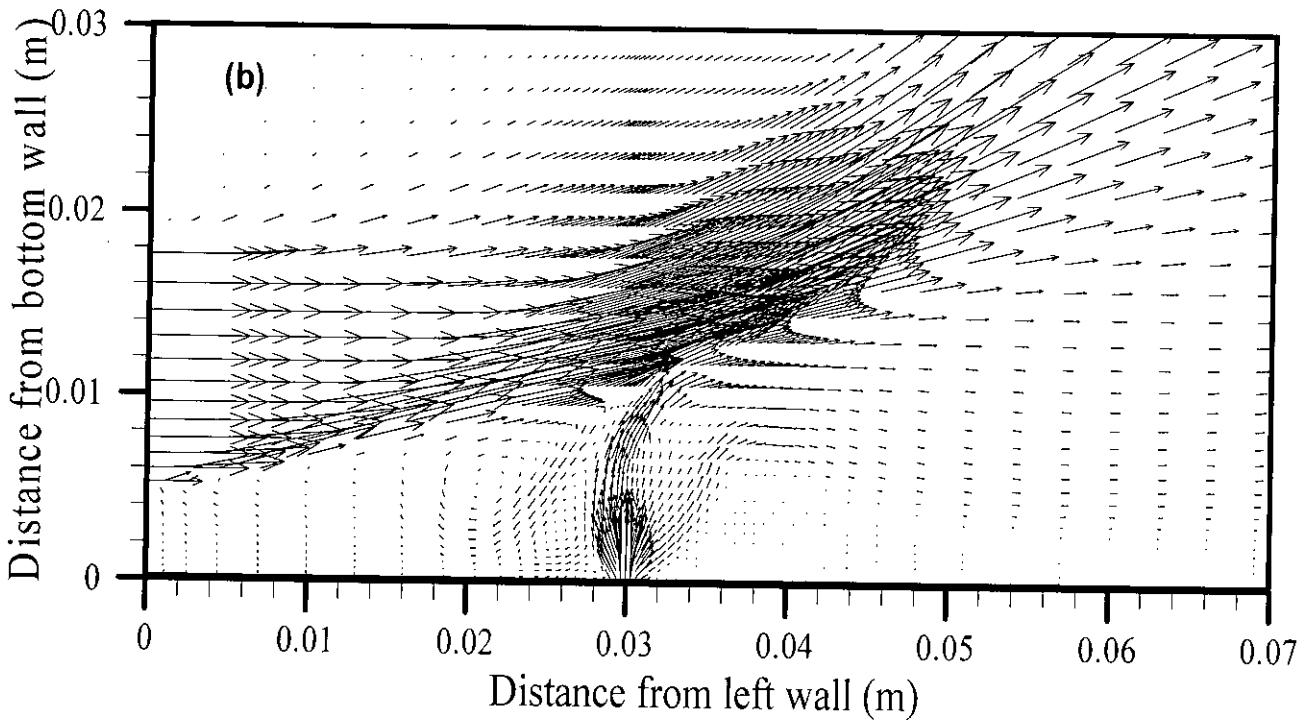


Fig. 3.16 (b) Velocity vector near injector; Case-12 ($\psi = 90^\circ$)

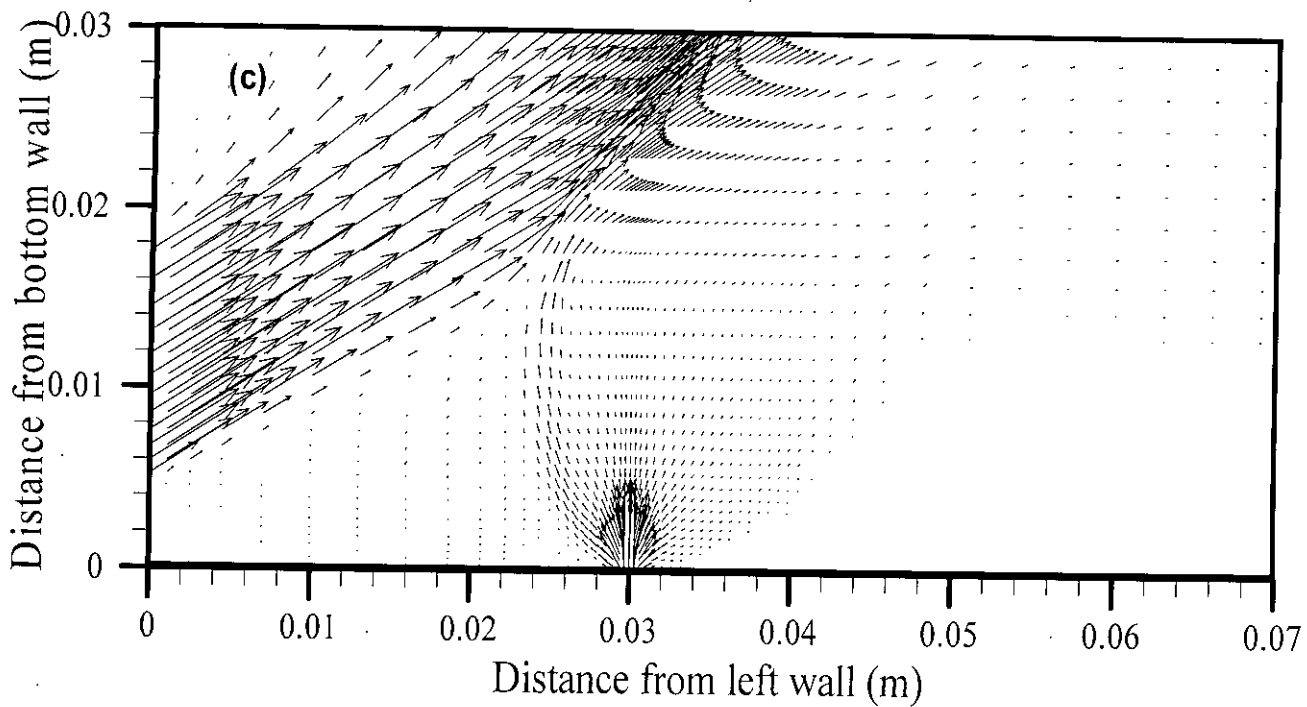


Fig. 3.16 (c) Velocity vector near injector; Case-13 ($\psi = 120^\circ$)

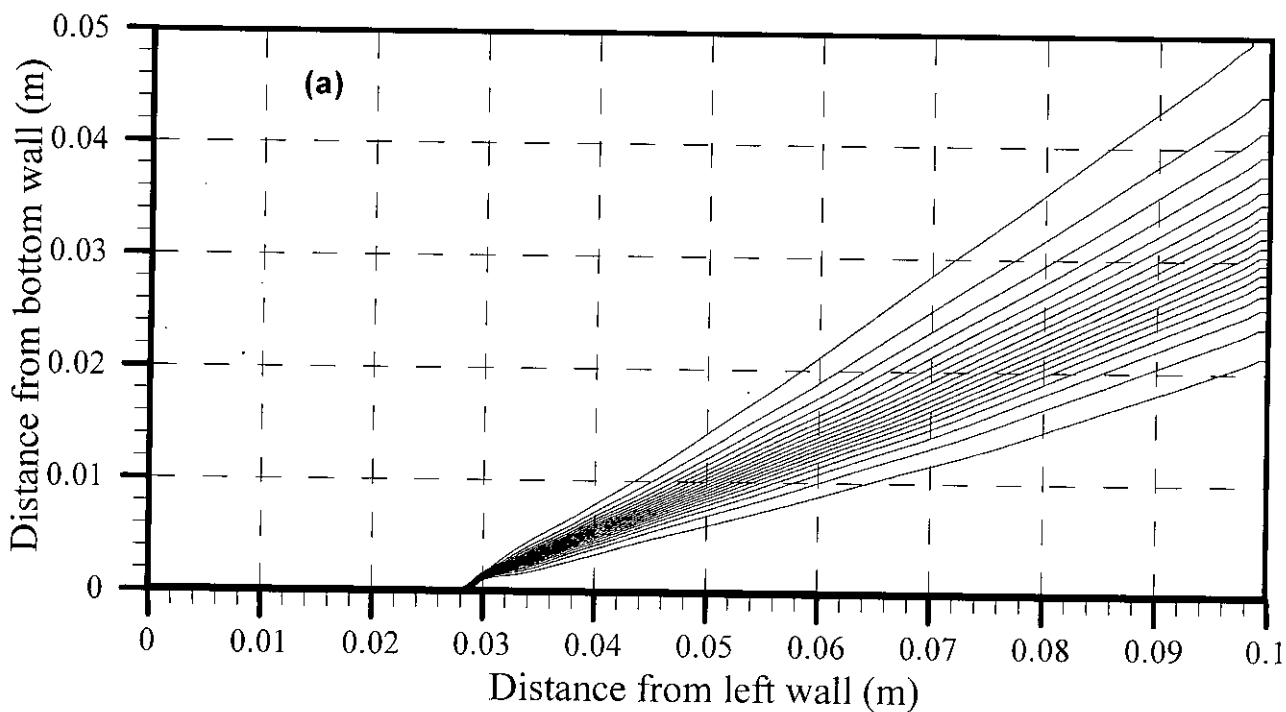


Fig. 3.17 (a) Mole fraction contour of Hydrogen, ϕ (0.05, 1.0, 0.05); Case-11 ($\psi = 60^\circ$)

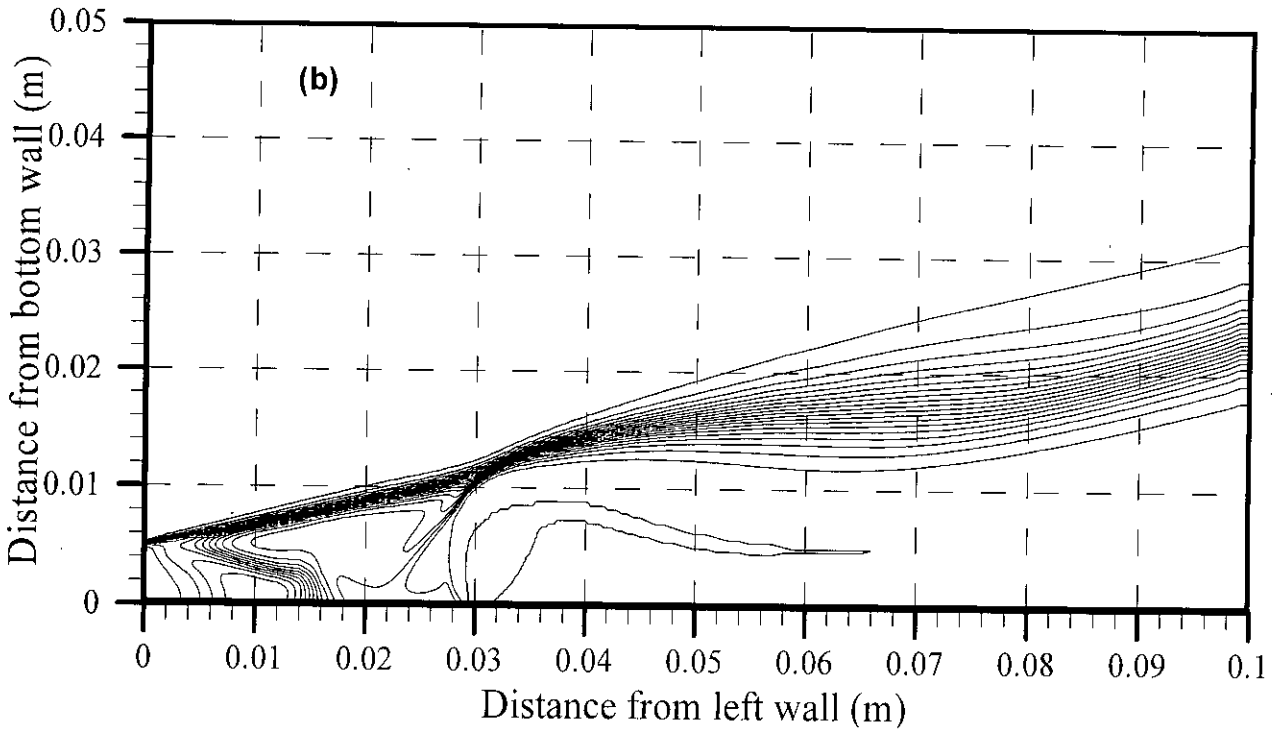


Fig. 3.17 (b) Mole fraction contour of Hydrogen, ϕ (0.05, 1.0, 0.05); Case-12 ($\psi = 90^\circ$)

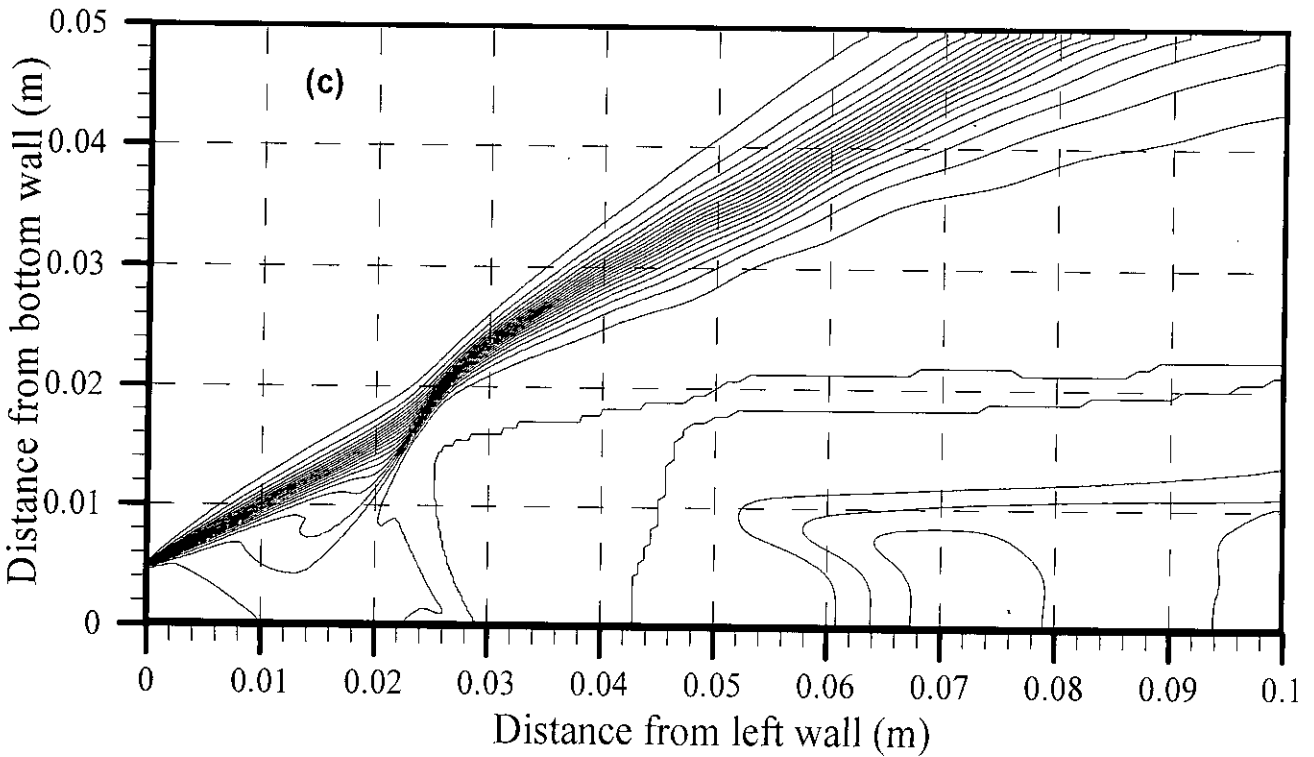


Fig. 3.17 (c) Mole fraction contour of Hydrogen, ϕ (0.05, 1.0, 0.05); Case-13 ($\psi = 120^\circ$)

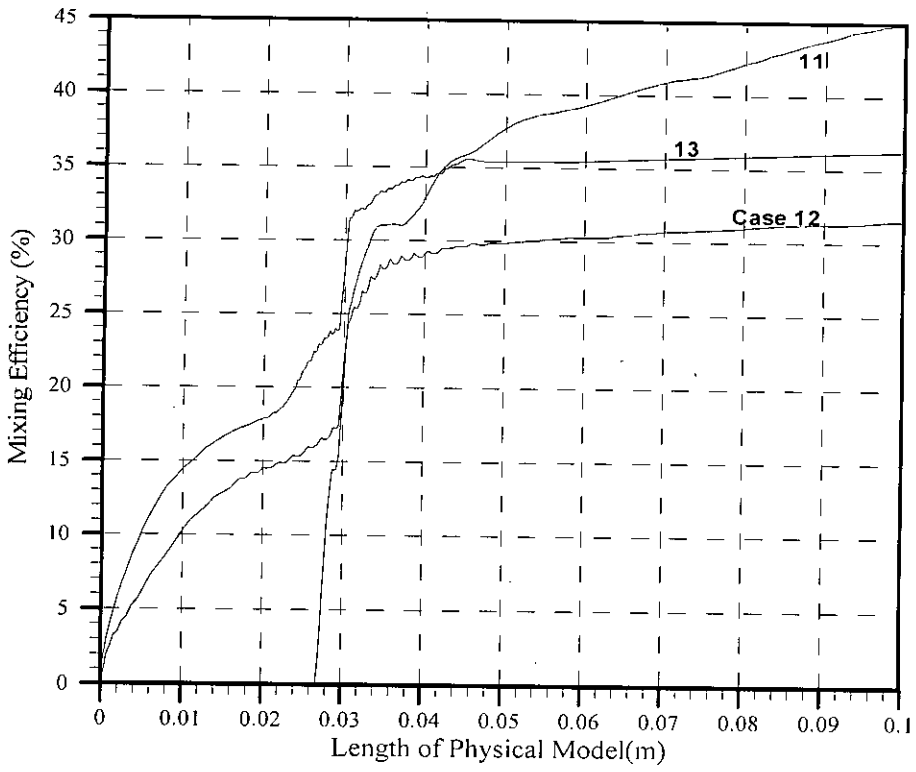


Fig. 3.18 Mixing efficiency along the length of physical model

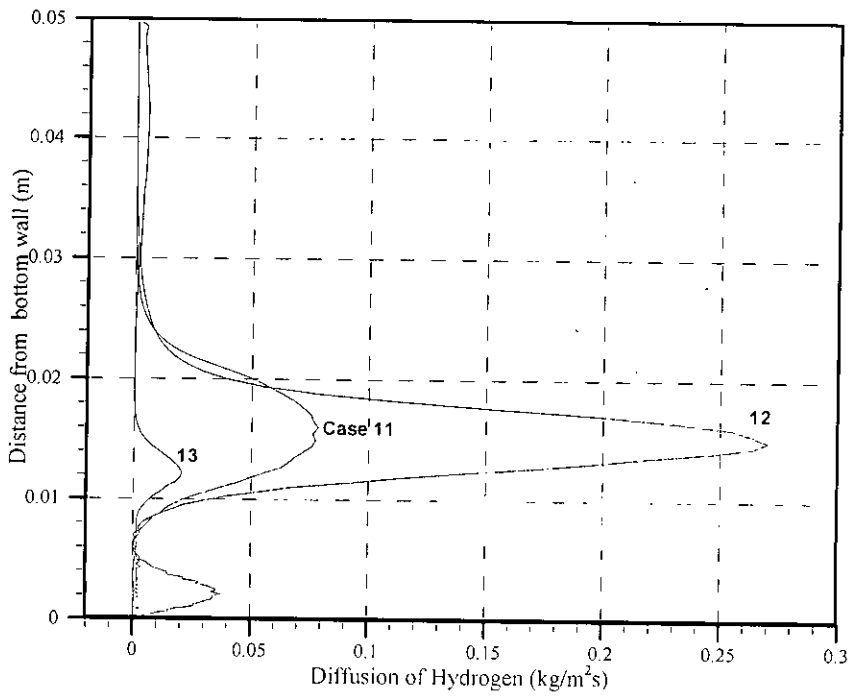


Fig. 3.19 Diffusion of Hydrogen at 0.08m from left wall

94972

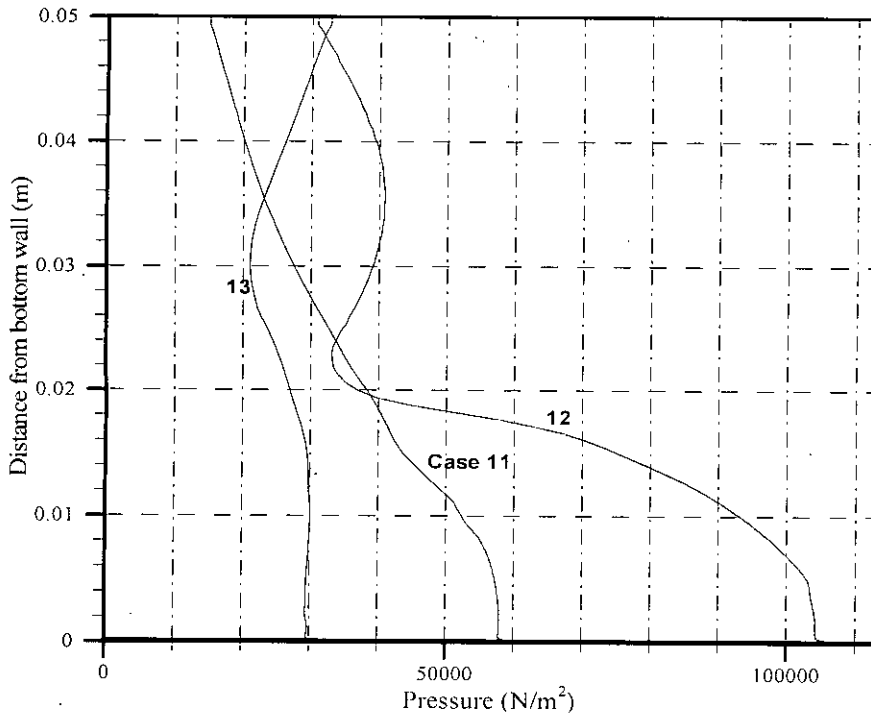


Fig. 3.20 Pressure distribution at 0.08m from left wall

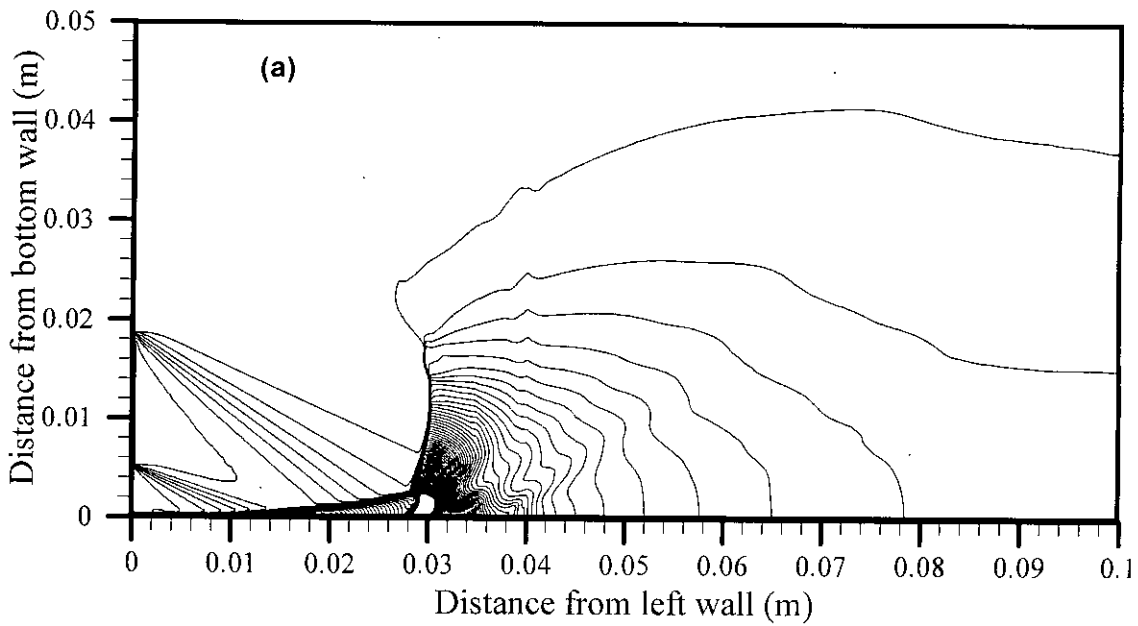


Fig. 3.21 (a) Pressure (Pa) contour, ϕ ($2 \cdot 10^4, 2 \cdot 10^6, 2 \cdot 10^4$); Case-11 ($\psi = 60^\circ$)

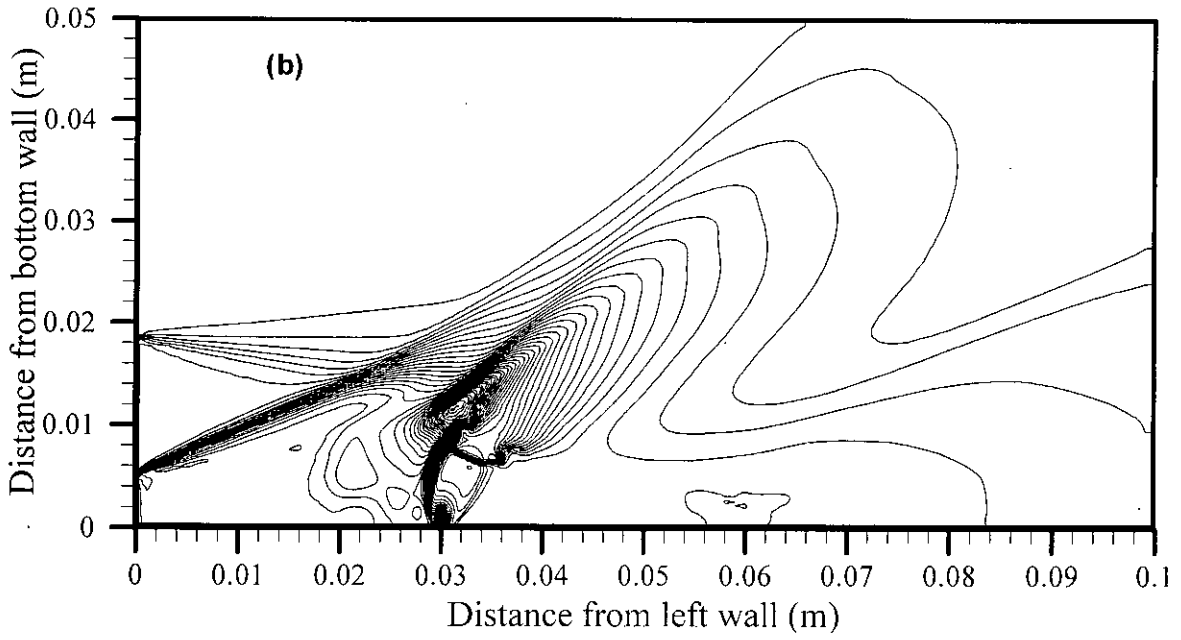


Fig. 3.21 (b) Pressure (Pa) contour, $\phi (2 \cdot 10^4, 2 \cdot 10^6, 2 \cdot 10^4)$; Case-12 ($\psi = 90^\circ$)

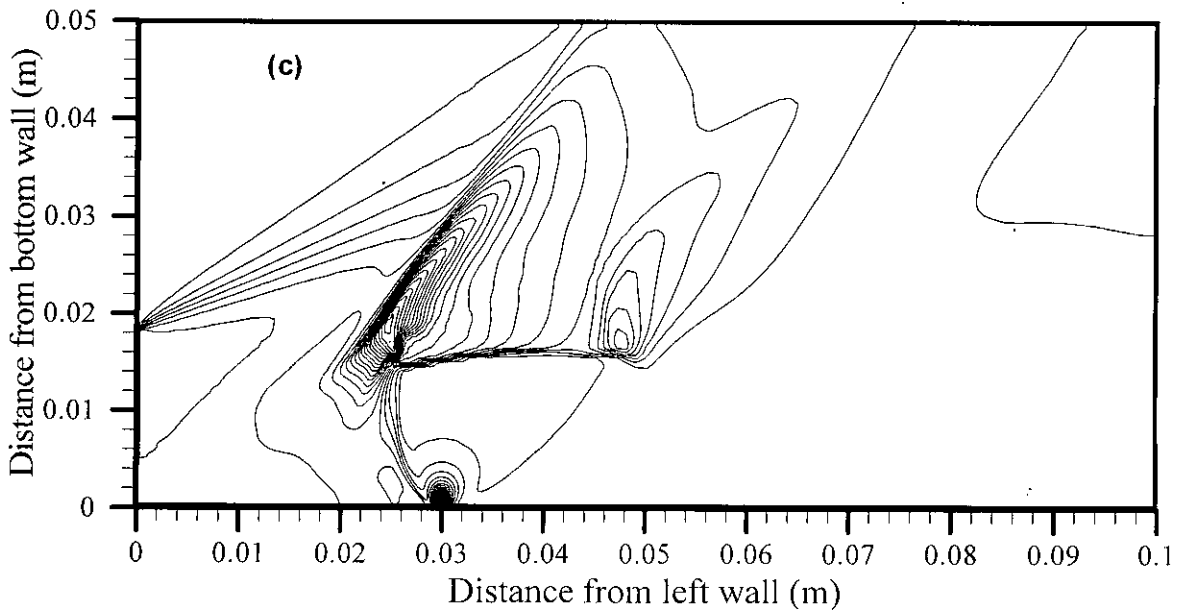


Fig. 3.21 (c) Pressure (Pa) contour, $\phi (2 \cdot 10^4, 2 \cdot 10^6, 2 \cdot 10^4)$; Case-13 ($\psi = 120^\circ$)

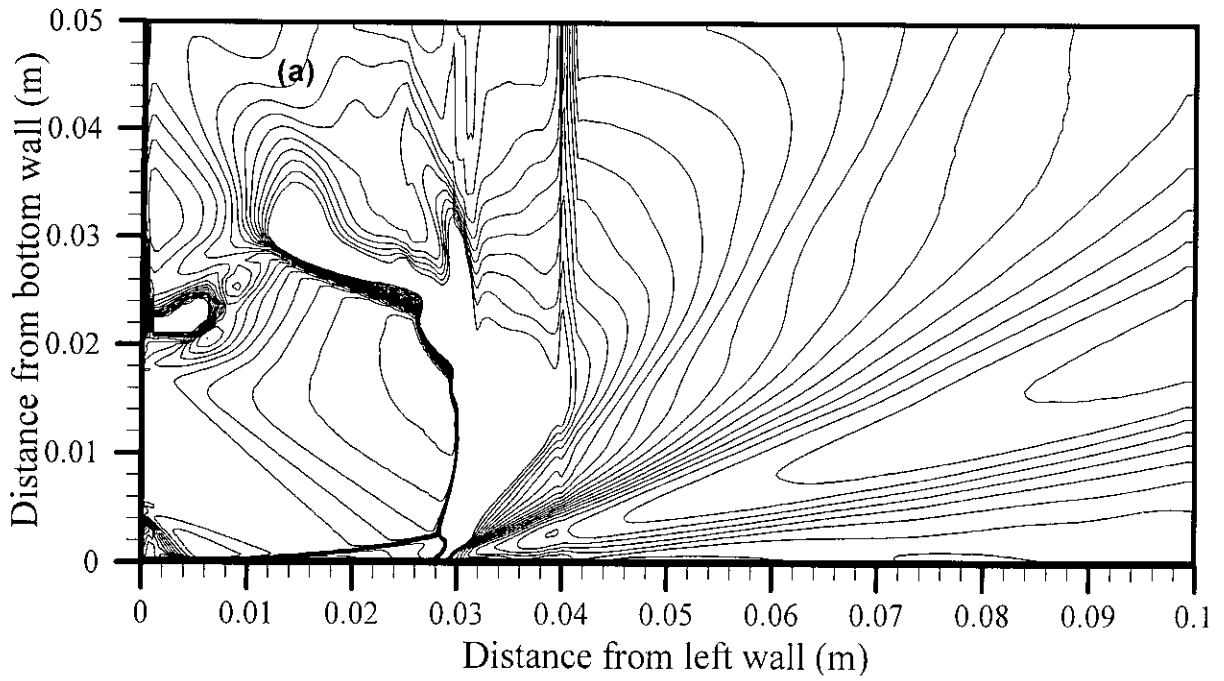


Fig. 3.22 (a) Temperature (K) contour, ϕ (250, 2550, 100); Case-11 ($\psi = 60^\circ$)

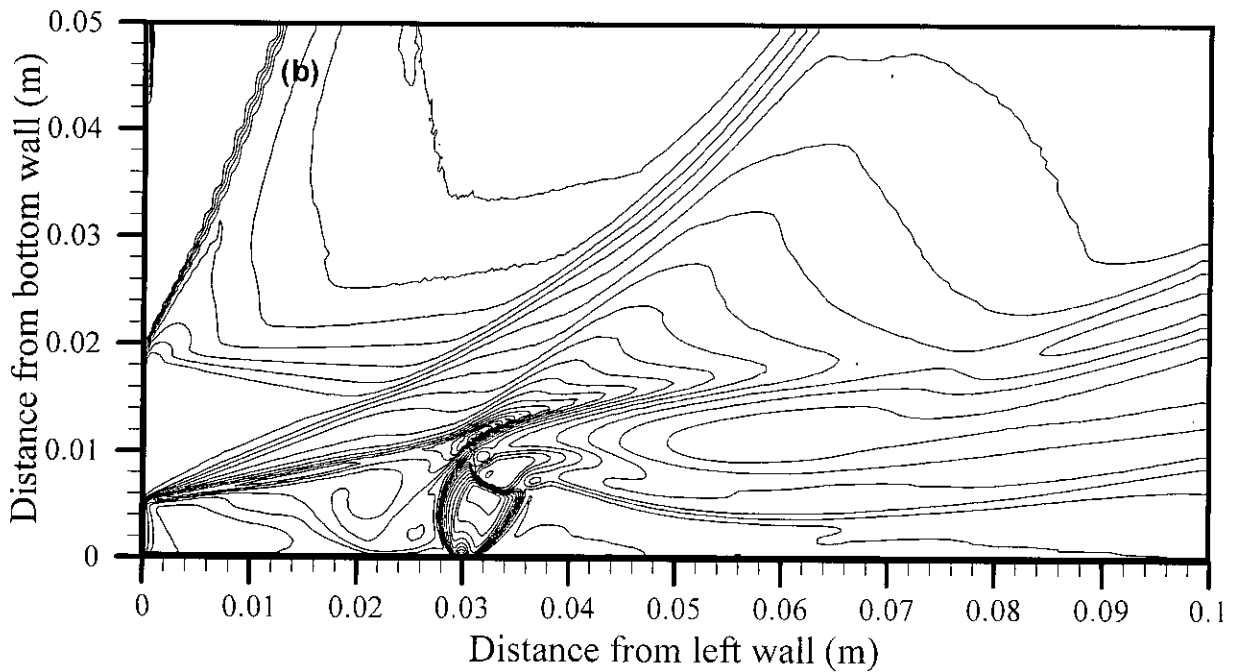


Fig. 3.22 (b) Temperature (K) contour, ϕ (250, 2550, 100); Case-12 ($\psi = 90^\circ$)

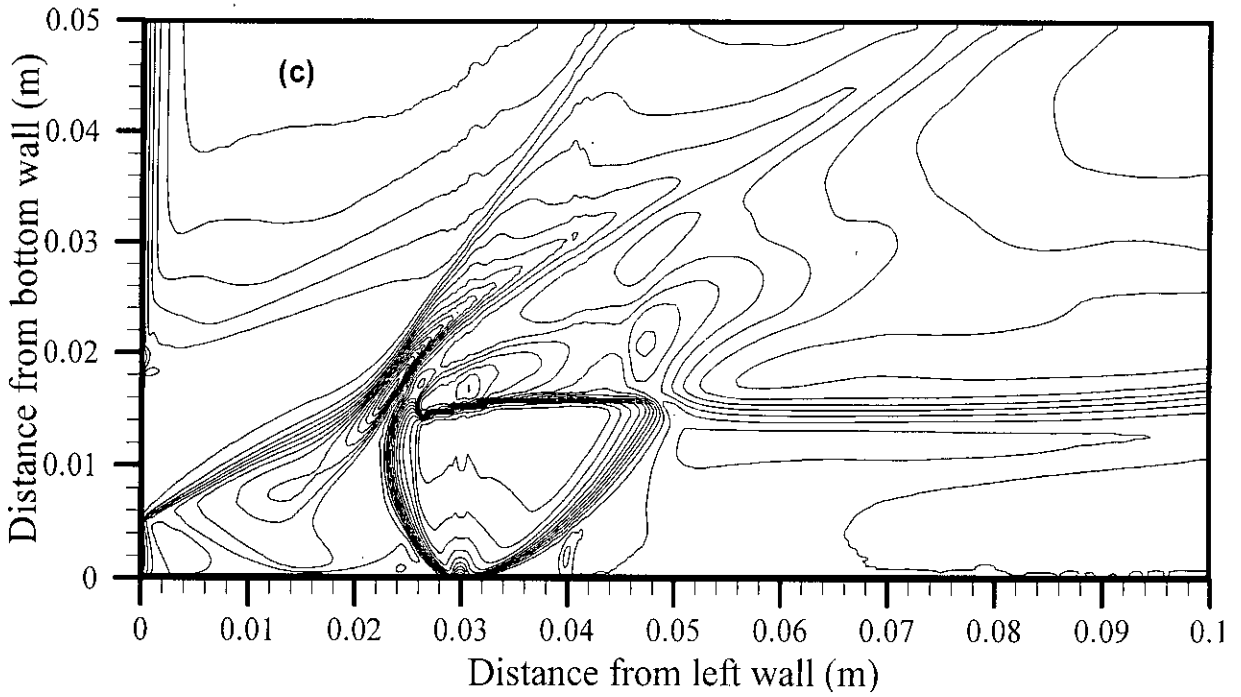


Fig. 3.22 (c) Temperature (K) contour, ϕ (250, 2550, 100); Case-13 ($\psi = 120^\circ$)

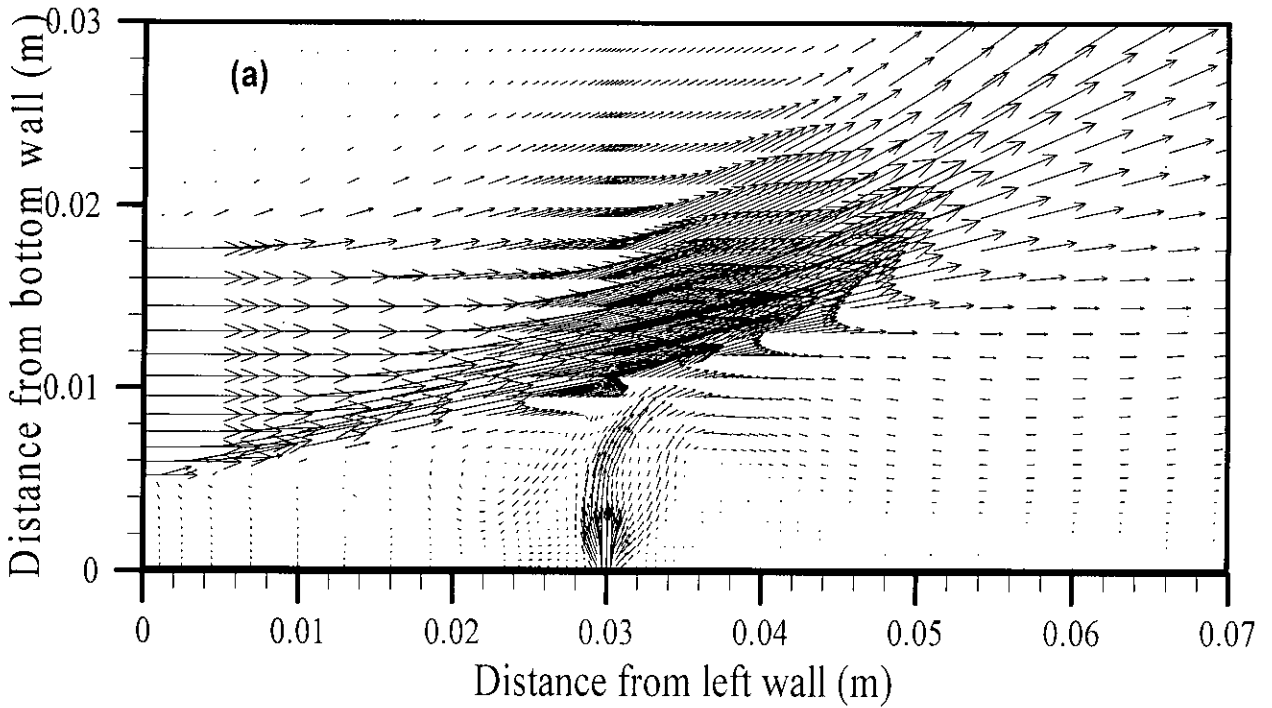


Fig. 3.23 (a) Velocity vector near injector; Case-14 ($M=0.7$)

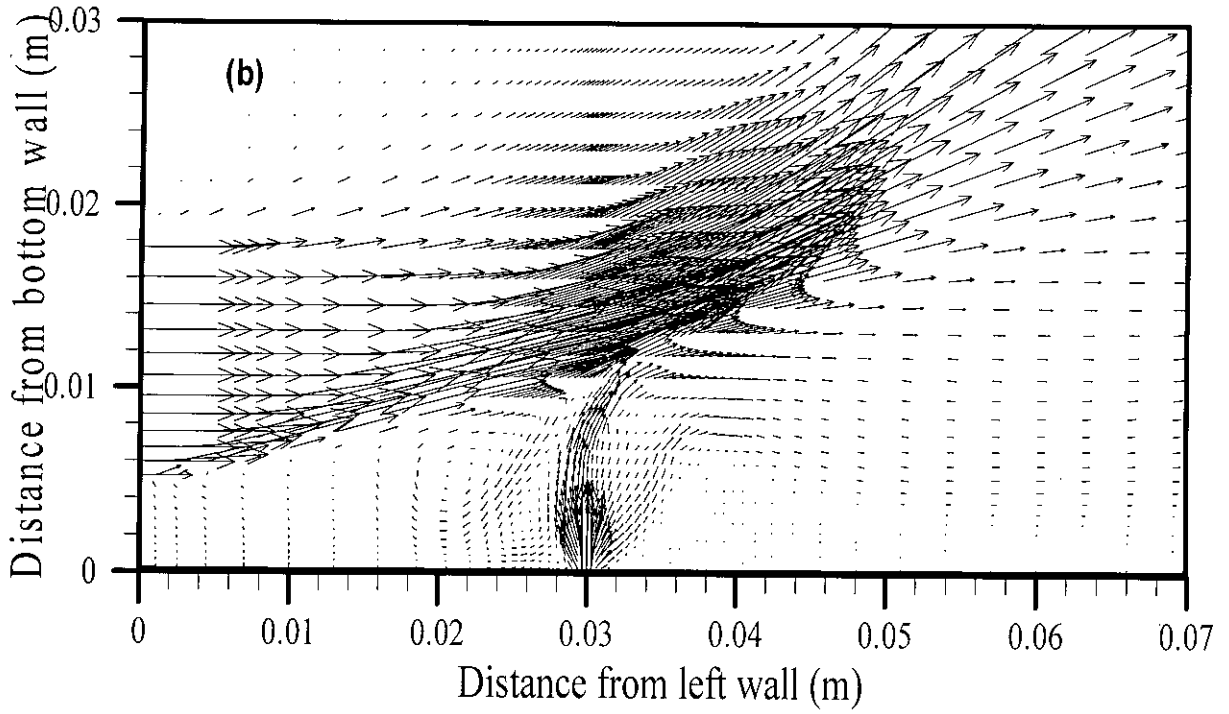


Fig. 3.23 (b) Velocity vector near injector; Case-15 ($M=1.0$)

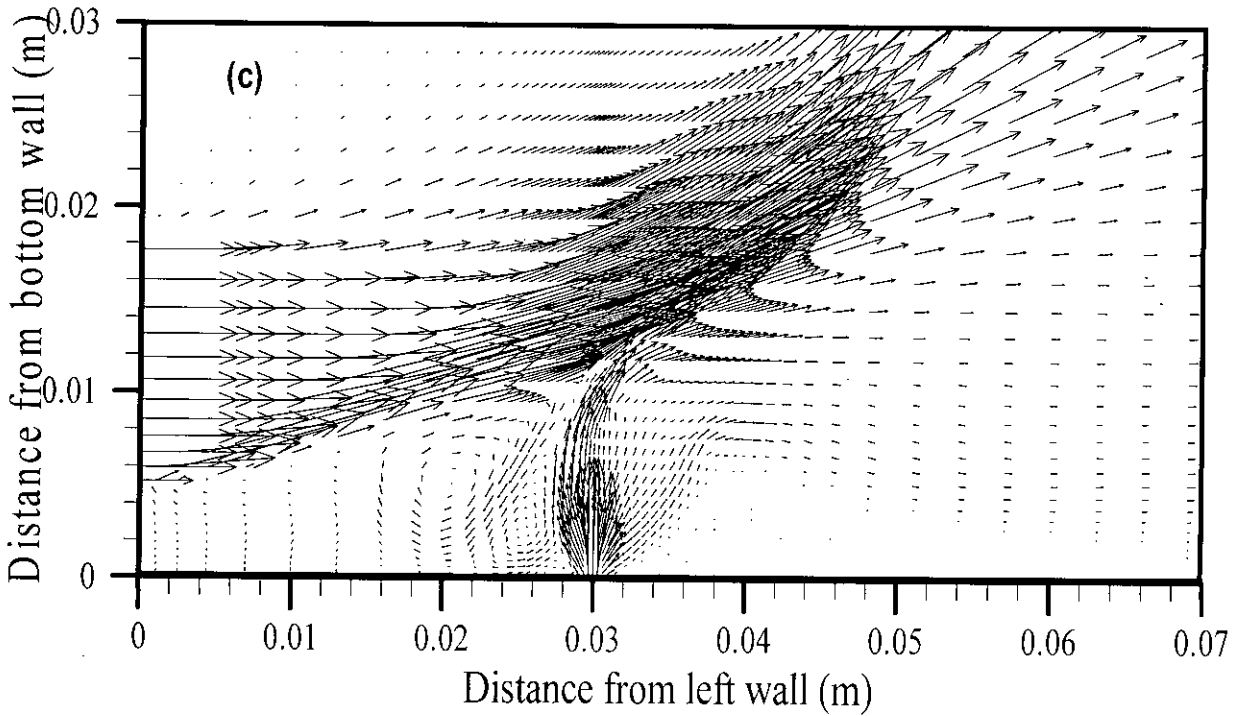


Fig. 3.23 (c) Velocity vector near injector; Case-16 ($M=1.3$)

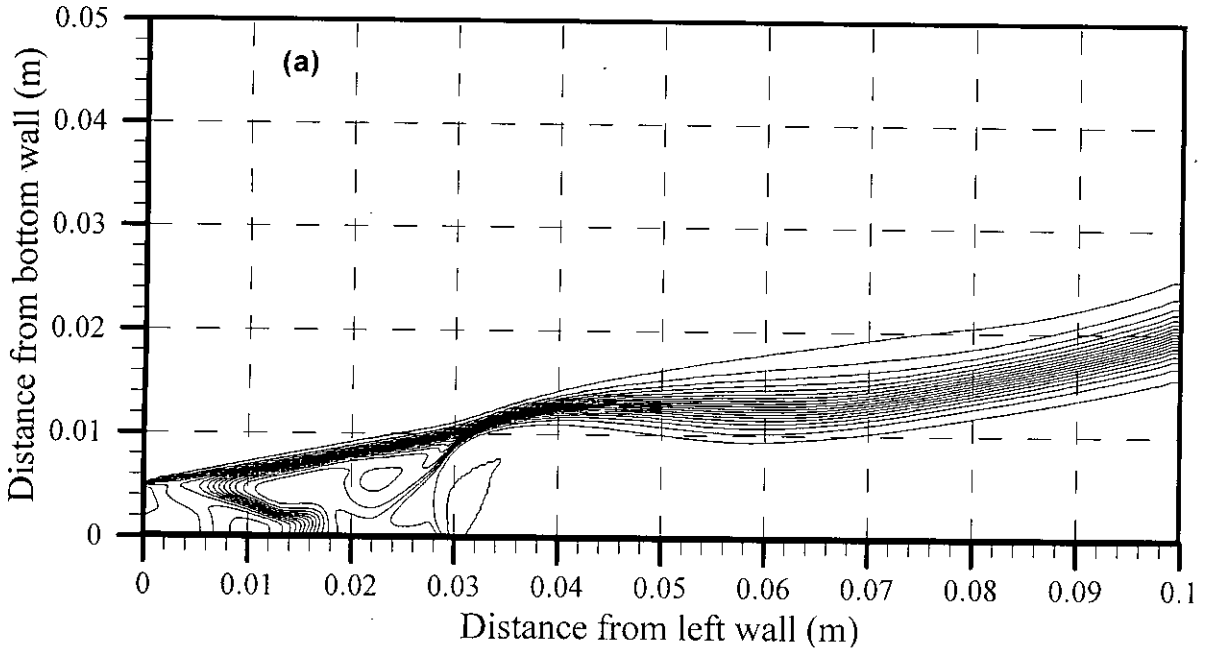


Fig. 3.24 (a) Mole fraction contour of Hydrogen, ϕ (0.05, 1.0, 0.05); Case-14 ($M=0.7$)

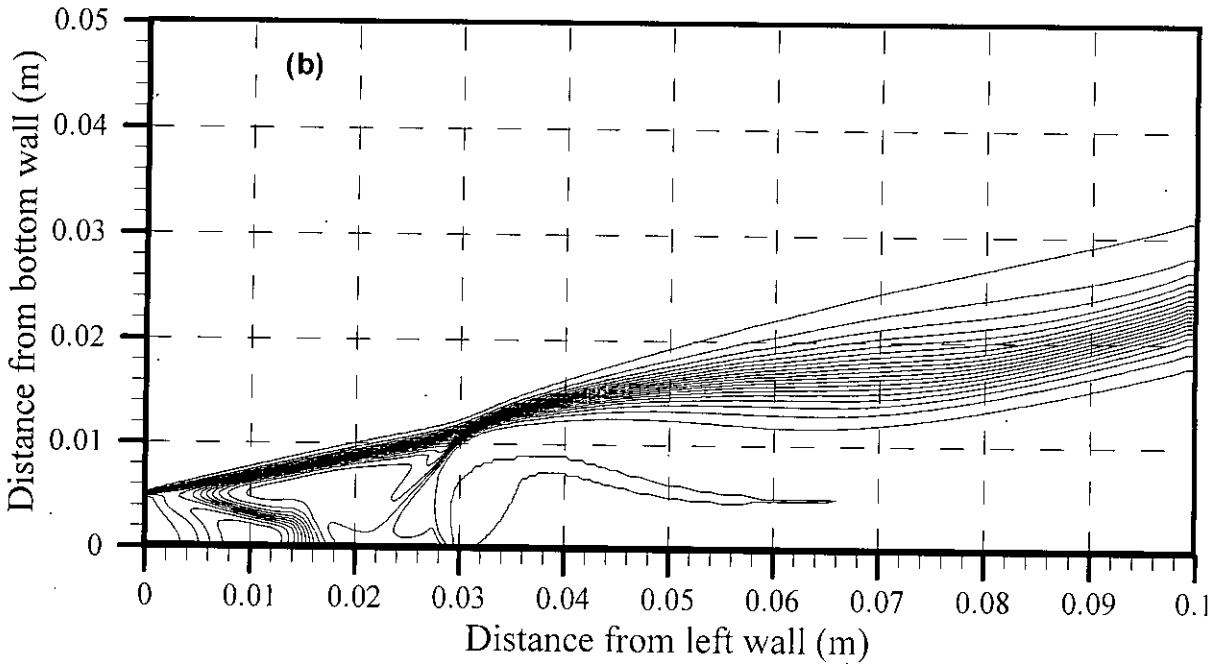


Fig. 3.24 (b) Mole fraction contour of Hydrogen, ϕ (0.05, 1.0, 0.05); Case-15 ($M=1.0$)

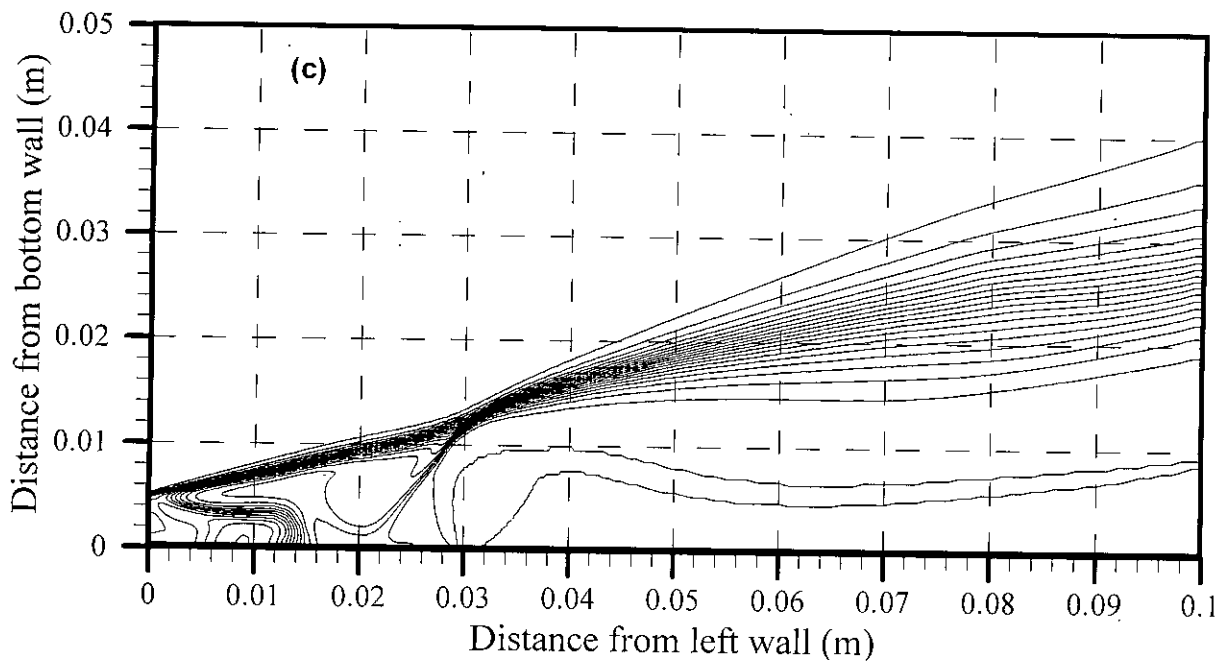


Fig. 3.24 (c) Mole fraction contour of Hydrogen, ϕ (0.05, 1.0, 0.05); Case-16 ($M=1.3$)

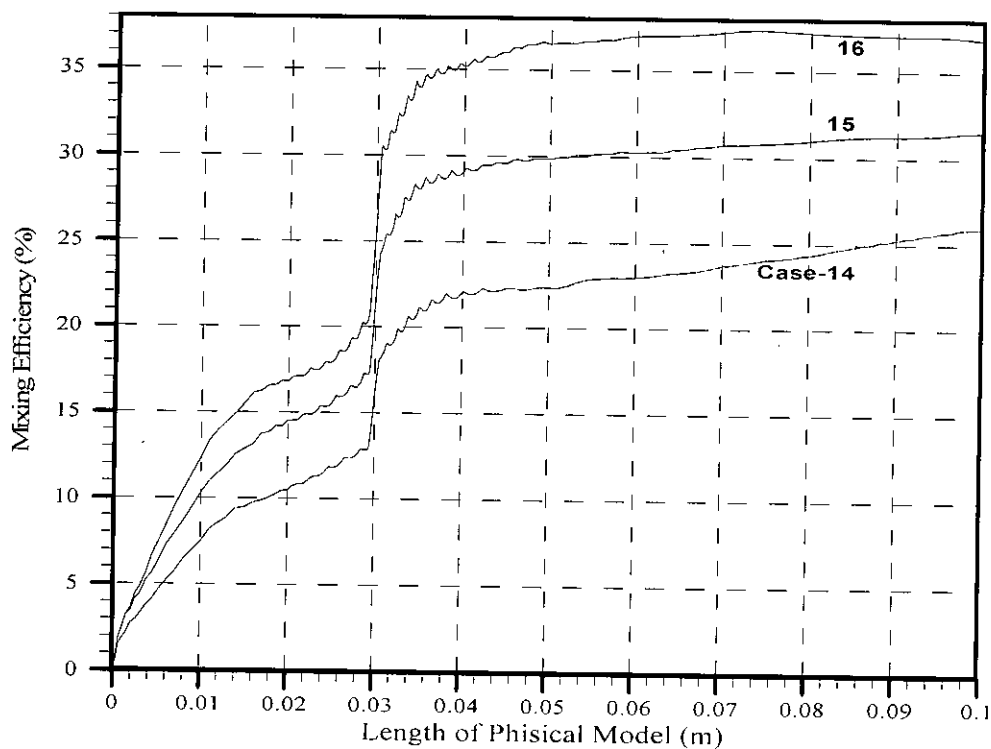


Fig. 3.25 Mixing efficiency along the length of physical model.

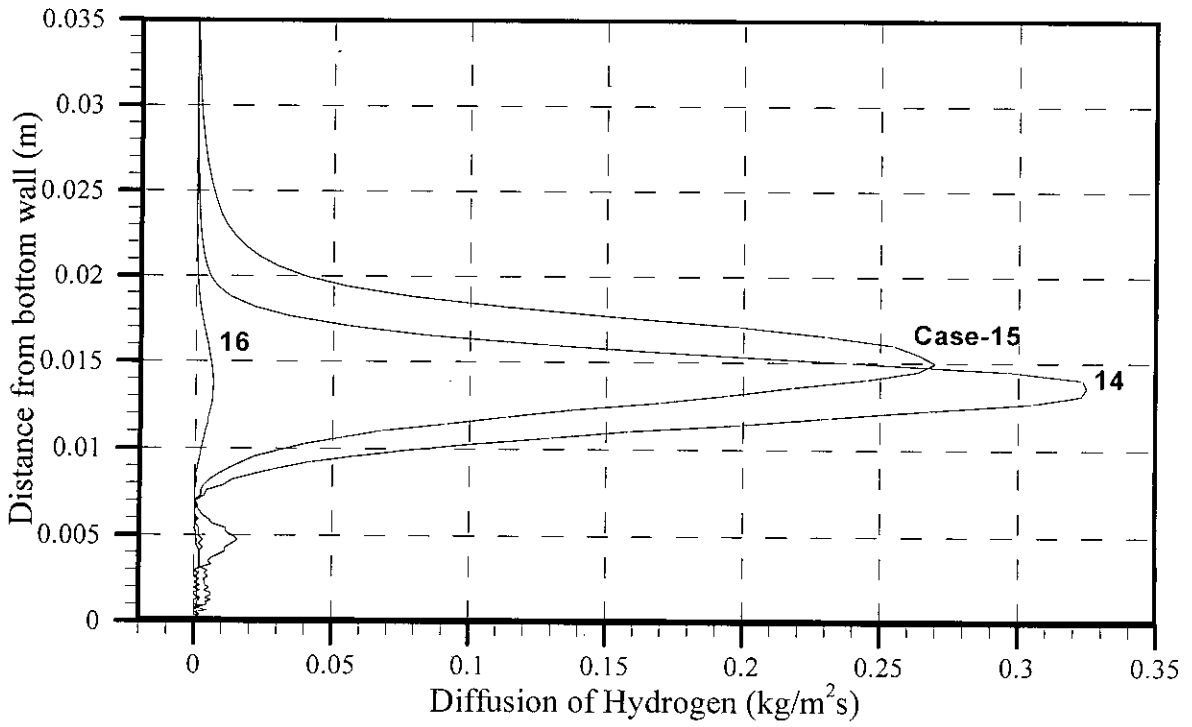


Fig. 3.26 Diffusion of Hydrogen at 0.08m from left wall

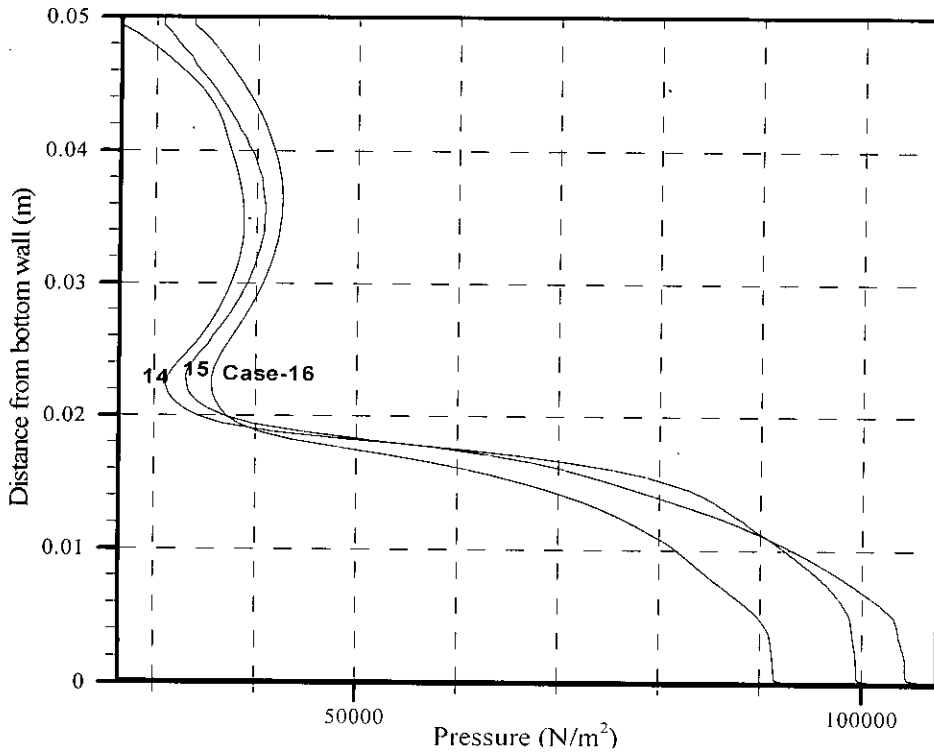


Fig. 3.27 Pressure distribution at 0.08m from left wall

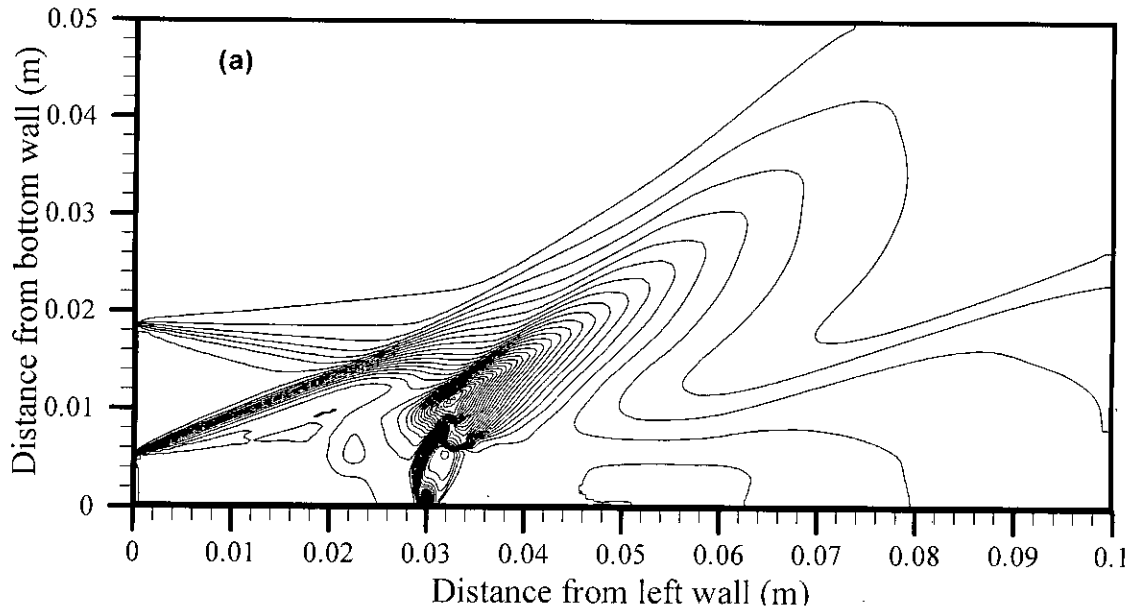


Fig. 3.28 (a) Pressure (Pa) contour, ϕ ($2 \cdot 10^4$, $2 \cdot 10^6$, $2 \cdot 10^4$); Case-14 ($M=0.7$)

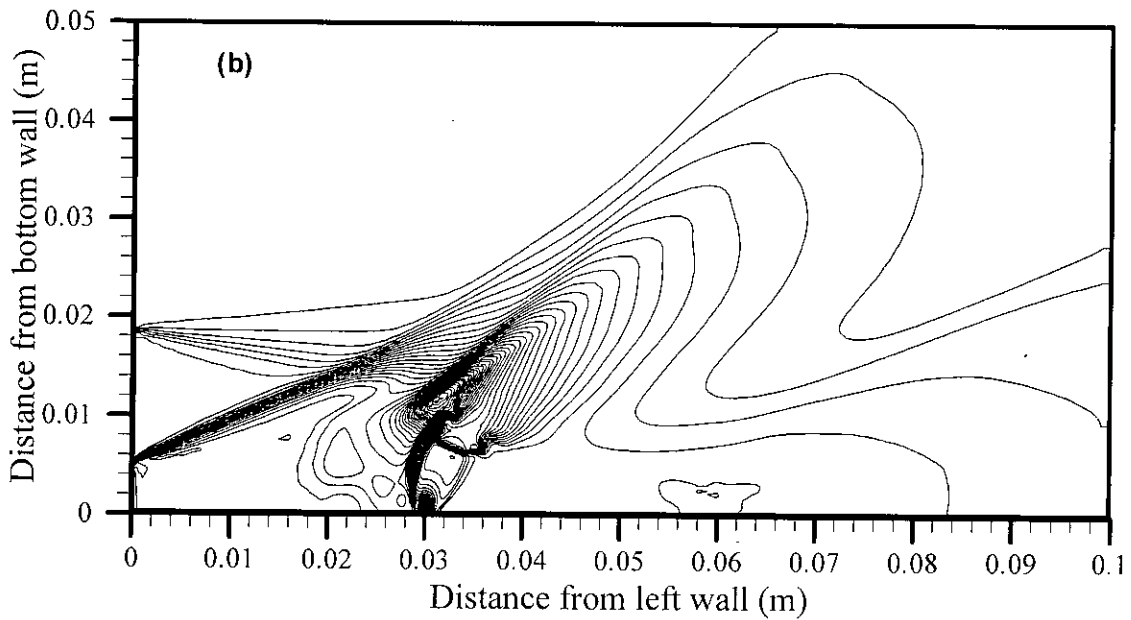


Fig. 3.28 (b) Pressure (Pa) contour, ϕ ($2 \cdot 10^4$, $2 \cdot 10^6$, $2 \cdot 10^4$); Case-15 ($M=1.0$)

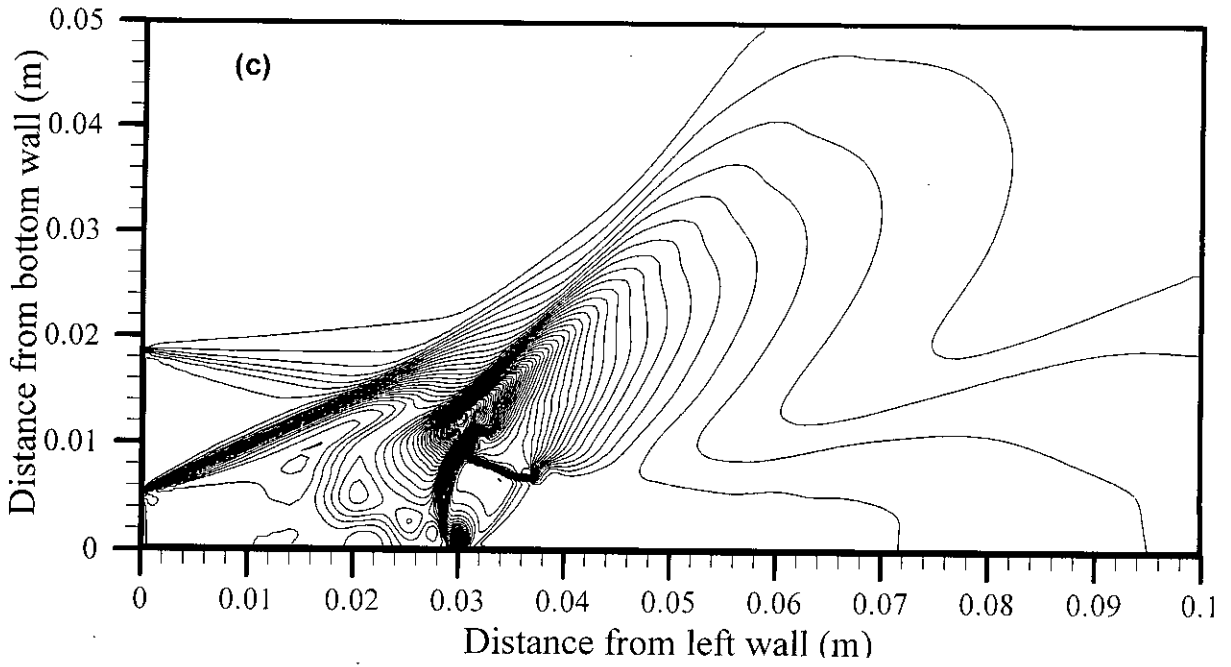


Fig. 3.28 (c) Pressure (Pa) contour, ϕ ($2 \cdot 10^4$, $2 \cdot 10^6$, $2 \cdot 10^4$); Case-16 ($M=1.3$)

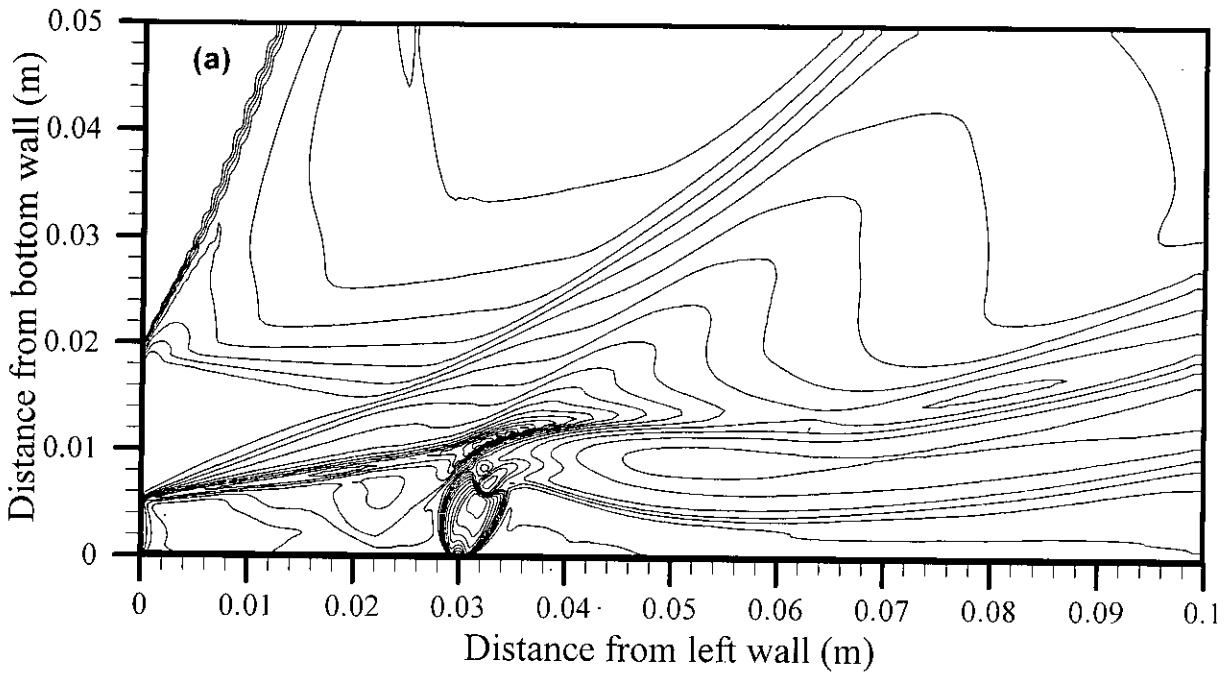


Fig. 3.29 (a) Temperature (K) contour, ϕ (250, 2550, 100); Case-14 ($M=0.7$)

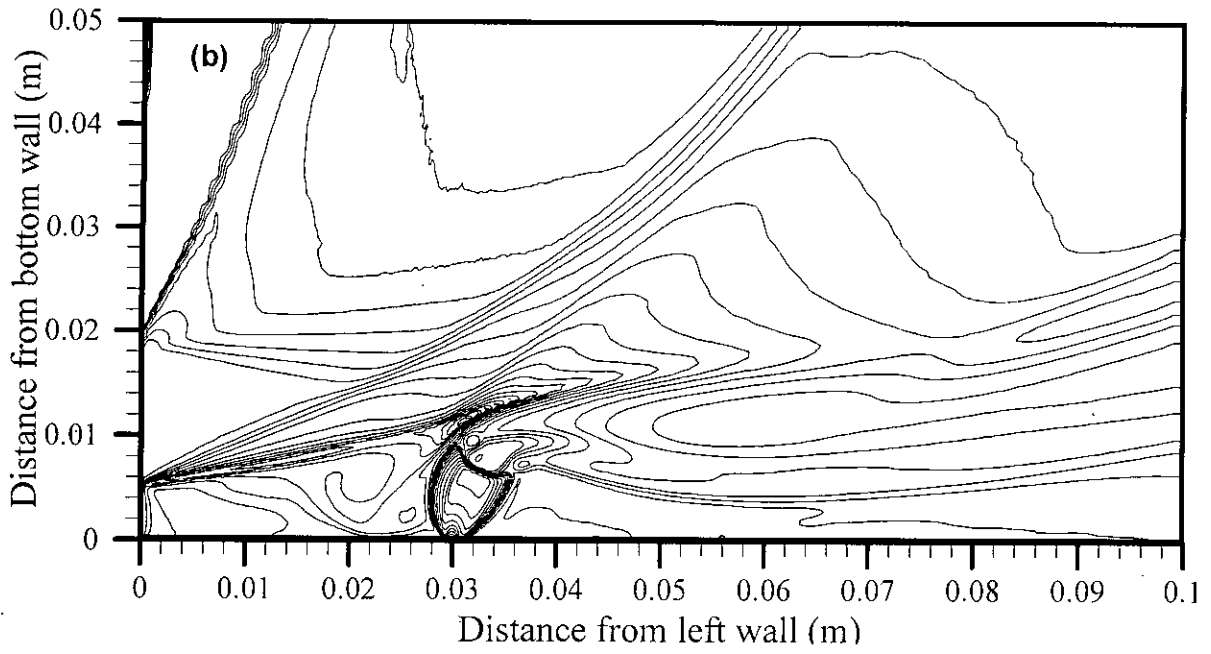


Fig. 3.29 (b) Temperature (K) contour, ϕ (250, 2550, 100); Case-15 (M=1.0)

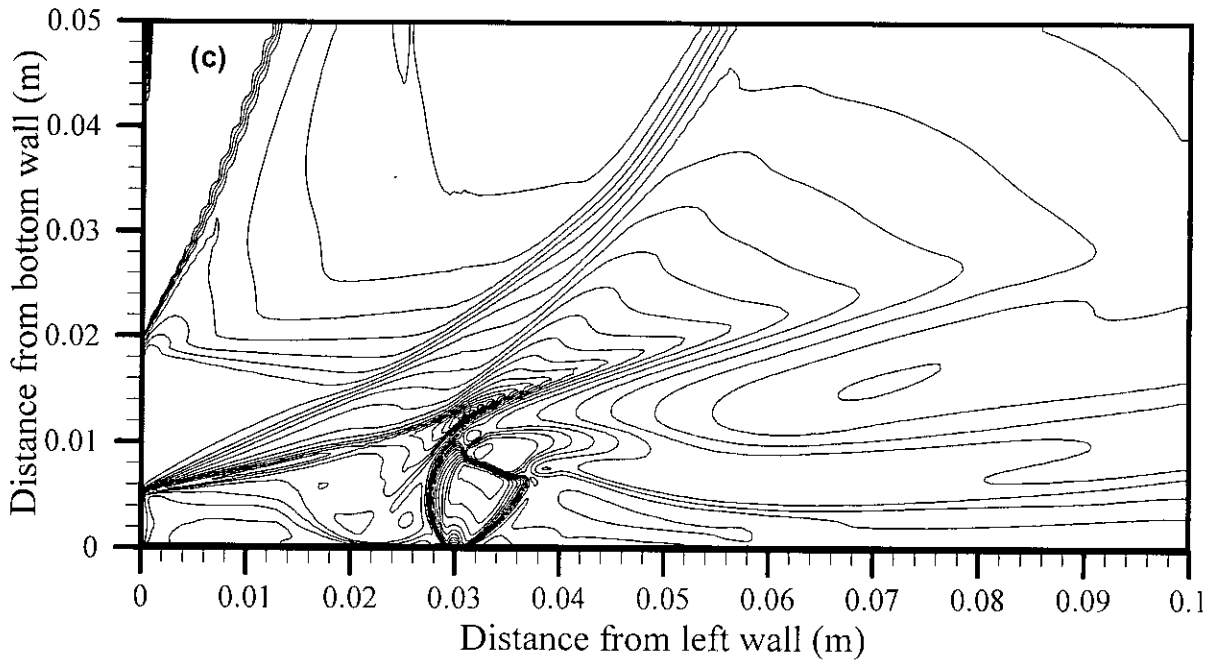


Fig. 3.29 (c) Temperature (K) contour, ϕ (250, 2550, 100); Case-16 (M=1.3)

Table 2.1 Coefficients of Thermodynamic Polynomials

Temperature range from 0 ~ 1000 K		
Coefficients	H ₂	N ₂
a ₁	0.33553514E+01	0.37044177E+01
a ₂	0.50136144E-03	-0.14218753E-02
a ₃	-0.23006908E-06	0.28670392E-05
a ₄	-0.47905324E-09	-0.12028885E-08
a ₅	0.48522585E-12	-0.13954677E-13
a ₆	-0.10191626E+04	-0.10640795E+04
Temperature range from 1000 ~ 5000 K		
Coefficients	H ₂	N ₂
a ₁	0.30667095E+01	0.28532899E+01
a ₂	0.57473755E-03	0.16022128E-02
a ₃	0.13938319E-07	-0.62936893E-06
a ₄	-0.25483518E-10	0.11441022E-09
a ₅	0.29098574E-14	-0.78057465E-14
a ₆	-0.86547412E+03	-0.89008093E+04

Table 2.2 Constants used in Transport Equations

Species	T _{i0} (K)	Viscosity		Thermal conductivity		Molecular Diffusion		
		$\mu_{i0} \times 10^6$ kg/(m.s)	S _i (K)	k _{i0} W/(m.K)	S _i '(K)	W gm/mol	σ_i (A)	T _{ei} (K)
H ₂	273	8.41	96.67	0.16273	166.67	2.0159	2.827	59.7
Air	273	17.16	110.06	0.02415	194.44	28.996	3.711	78.6

Table 3.1 Calculation Summary

Calculation Parameters	Computational Runs				
	Injector distance	10mm Case-1	20mm Case-2	30mm Case-3	40mm Case-4
Injecting angle	30 ⁰ Case-6	60 ⁰ Case-7	90 ⁰ Case-8	120 ⁰ Case-9	150 ⁰ Case-10
Air stream angle	–	60 ⁰ Case-11	90 ⁰ Case-12	120 ⁰ Case-13	–
Mach No.	0.7 Case-14	1.0 Case-15	1.3 Case-16	–	–

REFERENCES

- [1] Brown, G. L. and Roshko, A.: On Density Effects and Large Structure in Turbulent Mixing Layer, *J. Fluid Mechanics*, Vol. 64, No. 4, pp.775-816, (1974).
- [2] Papamoschou, D. and Roshko, A.: Observation of Supersonic Free Shear Layers, *AIAA Paper 86-0162*, January (1986).
- [3] Ragab, S. A. and Wu, J.L.: Instabilities in the Free Shear Layer Formed by Two Supersonic Streams, *AIAA Paper 88-0038*, January, 1988.
- [4] Rogers, R. C.: A Study of the Mixing of Hydrogen Injected Normal to a Supersonic Airstream, *NASA TN D-6114*, (1971).
- [5] Kraemer, G. O. and Tiwari, S. N.: Interaction of Two-Dimensional Transverse Jet with a Supersonic Mainstream, *NASA CR 175446*, (1983).
- [6] Holdeman, J. D. and Walker, R. E.: Mixing of a Row of Jets with a Confined Crossflow, *AIAA Journal*, Vol. 5, no. 2, pp. 243-249, (1977).
- [7] Thayer III, W. J. and Corlett, R. C.: Gas Dynamic and Transport Phenomena in the Two-Dimensional Jet Interaction Flowfield, *AIAA Journal*, Vol. 10, pp. 488-493, (1972).
- [8] Heister, S. D., Nguyen, T. T. and Karagozian, A. R.: Modeling of Liquid Jets Injected Transversely into a Supersonic Crossflow, *AIAA Journal*, Vol. 27, no. 12, pp. 1727-1734, (1989).
- [9] Catalano, G. D., Chang, K. S. and Mathis, J. A.: Investigation of Turbulent Jet Impingement in a Confined Crossflow, *AIAA Journal*, Vol. 27, No. 11, 1989, pp. 1530-1535.
- [10] Zakkay, V., Calarese, W. and Sakell, L.: An Experimental Investigation of the Interaction between a Transverse Sonic Jet and a Hypersonic Stream, *AIAA Journal*, Vol. 9, No. 4, pp. 674-682, 1971.
- [11] Thayer III, W.J.: New Information on the Two-Dimensional Jet Interaction Problem, *AIAA Journal*, Vol. 9, No. 3, pp. 539-541, 1971.
- [12] Torrence, M.G.: Effect of Injectant Molecular Weight on Mixing of a Normal Jet in a Mach 4 Airstream, *NASA TN D-6061*, January, 1971.

- [13] Rodriguez, G., Galametz, I., Thorembe, M.H., Rayer, C. & Haas, J.F.: Visualization of shocked mixing zones using differential interferometry and X-rays, *Proceedings of the 20th Int. Symp. on Shock Waves*, California, USA, 1995, pp. 647-652.
- [14] Zukoshi, E. E. : Turbulent Boundary Layer Separation in Front of a Forward-Facing Step, *AIAA Journal*, Vol. 5, No. 10, pp. 1746-1753, 1967.
- [15] Zukoshi, E. E. and Spaid, F.W.: Secondary Injection of Gases into a Supersonic Flow, *AIAA Journal*, Vol. 2, No. 10, 1964, pp. 1689-1696.
- [16] Weidner, E.H. and Drummond, J.P.: A Parametric Study of Staged Fuel Injector Configurations for Scramjet Applications, *AIAA Paper 81-11468*, (1981).
- [17] Takahashi, M. and Hayashi, A.K.: Numerical Study on Mixing and Ignition of Injecting Jet into a Supersonic Flow, *Proc. of Int. Symp. on Comp. Fluid Dynamics*, Nagoya, pp. 465-470, August, 1989.
- [18] Spaid, F. W. and Zukoshi, E. E.: A Study of the Interaction of Gaseous Jets from Traverse Slots with Supersonic External Flows, *AIAA Journal*, Vol. 6, No. 2, pp. 205-212, 1968.
- [19] Yokota, K. and Kajii, S.: The Three-Dimensional Supersonic Flow and Mixing Fields with a Perpendicular Air Injection from a Finite Length Slit, *Trans. Japan Soc. Aero. Space Sci.*, Vol. 39, no. 124, pp. 173-183, (1996).
- [20] Yokota, K. and Kajii, S.: The Effects of Aspect Ratio of a Finite Length Slit on the Mixing in the Three-Dimensional Supersonic Flow, *Trans. Japan Soc. Aero. Space Sci.*, Vol. 39, no. 124, pp. 199-210, (1996).
- [21] Yokota, K. and Kajii, S.: The Injection Methods and Mixing Characteristics in the Two-Dimensional Supersonic Free Stream, *Trans. Japan Soc. Aero. Space Sci.*, Vol. 38, no. 122, pp. 383-393, (1996).
- [22] Yokota, K. and Kaji, S.: The Two Dimensional Supersonic Flow and Mixing Field with a Perpendicular Injection, *Trans. Japan Soc. Aero. Space Sci.*, Vol. 39, No. 123, pp. 28-42, 1996.
- [23] Yoshida, A. and Tsuji, H.: Supersonic Combustion of Hydrogen in a Vitiated Airstream Using Traverse Injection, *AIAA Journal*, Vol. 15, No. 4, pp. 463-464, 1977.

- [24] Crabb, D., Durao, D.F.G. and Whitelaw, J.H.: A Round Jet Normal to a Crossflow, *J. Fluids Engg.*, Vol. 103, pp. 142-153, 1981.
- [25] Drummond, J.P. and Weidner, E.H.: Numerical Study of a Scramjet Engine Flow Field, *AIAA Paper 81-0186*, January, 1981.
- [26] Nakae, T., Teramoto, S. and Nagashima, T.: DSMC Method for Transverse Gas Ignition into a Supersonic Air Flow, Air Flow, *Eleventh International Symposium on Air Breathing Engines*, Tokyo, Japan, pp. 728-733, September 1993.
- [27] Obata, S. and Nagashima, T.: Direct Simulation of Reacting Fuel Gas Flows in a Supersonic Mixing Layer, *Eleventh International Symposium on Air Breathing Engines*, Tokyo, Japan, pp. 739-745, September, 1993.
- [28] Kumar, A. Bushnell, D. M. and Hussaini, M.Y.: A Mixing Augmentation Technique for Hypervelocity Scramjets, *AIAA Paper 87-1882*, June, 1987.
- [29] Guirguis, R.H.: Mixing Enhancement in Supersonic Shear Layers: Effect of Convective Mach Number, *AIAA Paper 88-0701*, January, 1988.
- [30] Orth, R.C., Schetz, J.A. and Billig, F.S.: The Interaction and Penetration of Gaseous Jets in Supersonic Flow, *NASA CR-1386*.
- [31] Moussa, Z. M., Trischka, J.W. and Eskinazi, S.: The Near Field in the Mixing of a Round Jet with a Cross-Stream, *J. Fluid Mechanics*, Vol. 80, Par-1, pp. 49-80, 1977.
- [32] Andreopoulos, J. and Rodi, W.: Experimental Investigation of Jets in a Crossflow, *J. Fluid Mechanics*, Vol. 138, pp. 93-127, 1984.
- [33] Andreopoulos, J.: On the Structure of Jets in a Crossflow, *J. Fluid Mechanics*, Vol. 157, pp. 163-197, 1985.
- [34] Anderson, Jr. J. D.: Hypersonic and High Temperature Gas Dynamics, McGraw-Hill Book Company, New York, pp. 592-605, 1989.
- [35] Moss, J. N.: Reacting Viscous-Shock-Layer Solutions with Multicomponent Diffusion and Mass Injection, *NASA TR-411*, June 1974.
- [36] White, F.M.: *Viscous Fluid Flow*, McGraw-Hill, New York, (1974).
- [37] Brokaw, R.S.: Alignment Charts for Transport Properties Viscosity, Thermal Conductivity, and Diffusion Coefficients for Nonpolar Gases and Gas Mixtures at Low Density, *NASA TR R-81*, 1961.

- [38] Reid, R.C. and Sherwood, T.K.: *The Properties of Gases and Liquids*, Second Edition, McGraw-Hill, New York, pp. 520-543, (1966).
- [39] Yee, H.C.: A Class of High-Resolution Explicit and Implicit Shock Capturing Methods, *NASA, TM 101088*, (1989).
- [40] Hishida, M.: *Turbulent Flow and Flame Structure Generated by Interaction between Nonsteady Multi-dimensional Flame and Flowfield*, Ph.D. Dissertation, Department of Aerospace Engineering, Nagoya University, Japan, 1997.
- [41] Ali, M., Fujwara, T. and Leblance J. E.: "The Effects of Backward-facing step on Mixing and Flame holding in Supersonic Combustor", Submitted to *Int. Journal of Engineering Science*.
- [42] Rausch, V.L., McClinton, C.R. and Hicks, J.W.: Scramjet Breath New Life into Hypersonics, *Aerospace America*, July (1997).
- [43] Ali, M. and Islam, A.K.M.S.: Effect of Mainflow Inlet Width on Penetration and Mixing of Hydrogen in Scramjet Combustor, *Proceedings of the Eighth Asian Congress of Fluid Mechanics*, pp. 647-650, December 6-10, Shenzhen, China, (1999).
- [44] Tabejamaat, S. JU. Y. and Niioka, T.: Numerical Simulation of Secondary Combustion of Hydrogen Injected from Preburner into Supersonic Airflow, *AIAA Journal*, Vol.35, no.9, September, (1997).

List of Publications

(Related to this Thesis)

1. S. Ahmed, M. Ali, A.K.M. Sadrul Islam, "A Numerical Study on Mixing and Flame Holding in Supersonic Combustor". Proc. of Millennium International Symposium on Thermal And Fluid Science, Xi'an, China, September 18-22, 2000.
2. S. Ahmed, M. Ali, A.K.M. Sadrul Islam, "Effect of Injector Distance from Backward-Facing step on Mixing in Supersonic Stream". Accepted for the presentation in the first M.I.T. conference on Computational Fluid and Solid Mechanics that will be held on June 12-14,2001 at the Massachusetts Institute of Technology, Cambridge, MA02139 U.S.A.



2